AN EFFICIENT CARRIER FREQUENCY OFFSET COMPENSATION TECHNIQUE USING SUPERIMPOSED TRAINING SEQUENCE FOR NEXT GENERATION (5G) WIRELESS NETWORKS

A Thesis submitted to the
UPES

For the Award of
Doctor of Philosophy
In
Electronics Engineering

By
Rajarao Manda
(500057719)

SUPERVISOR(S):
Dr. Adesh Kumar
Dr. R. Gowri

Department of Electrical and Electronics Engineering,
School of Advanced Engineering (SoAE)
UPES
Dehradun - 248007, Uttarakhand, India

June 2023

AN EFFICIENT CARRIER FREQUENCY OFFSET COMPENSATION TECHNIQUE USING SUPERIMPOSED TRAINING SEQUENCE FOR NEXT GENERATION (5G) WIRELESS NETWORKS

A thesis submitted to the
UPES

For the Award of
Doctor of Philosophy
In
Electronics and Communications Engineering

By
Rajarao Manda
(500057719)

Internal Supervisor
Dr. Adesh Kumar
Sr. Associate Professor
Department of Electrical and Electronics Engineering
UPES, Dehradun

External Supervisor
Dr. R Gowri
Professor
Department of Electronics and Communication Engineering
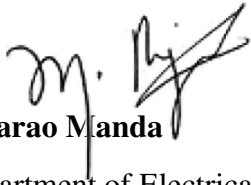Graphic Era Hill University, Dehradun

UPES
UNIVERSITY OF TOMORROW

Department of Electrical and Electronics Engineering,
School of Advanced Engineering (SoAE)
UPES
Dehradun - 248007, Uttarakhand, India

June 2023

DECLARATION

I declare that the thesis entitled "An Efficient Carrier Frequency Offset Compensation Technique using Superimposed Training Sequence for Next generation (5G) Wireless Networks" has been prepared by me under the guidance of Dr. Adesh Kumar, Senior Associative Professor, Dept. of Electrical and Electronics Engineering, School of Advanced Engineering, UPES, Dehradun and Dr.R Gowri, Professor, Graphic Era Hill University, Dehradun. No part of this thesis has formed the basis for the award of any degree or fellowship previously.

Rajarao Manda

Department of Electrical and Electronics Engineering,

School of Advanced Engineering, UPES,

Dehradun -248007, Uttarakhand, India.

Date:

CERTIFICATE

I certify that **Rajarao Manda** has prepared his thesis entitled "**An Efficient Carrier Frequency Offset Compensation Technique using Superimposed Training Sequence for Next generation (5G) Wireless Networks**", for the award of Ph.D degree of the UPES, under my guidance. He has carried out the work at the Department of Electrical and Electronics Engineering, School of Advanced Engineering, UPES.

Internal Supervisor:

Dr. Adesh Kumar

Sr. Associate Professor

Department of Electrical and Electronics Engineering

School of Advanced Engineering, UPES

Dehradun -248007, Uttarakhand, India.

Date:

Acres: Bidholi Via Prem Nagar, Dehradun - 248 007 (Uttarakhand), India, T: +91 135 2770137, 2776053/54/91, 2776201, M: 9997799474, F: +91 135 2776090/95

ge Acres: Kandoli Via Prem Nagar, Dehradun - 248 007 (Uttarakhand), India, M: +91 8171979021/2/3, 7060111775

CED ENGINEERING I COMPUTER SCIENCE I DESIGN I BUSINESS I LAW I HEALTH SCIENCES AND TECHNOLOGY I MODERN MEDIA I LIBERAL STUDIES

CERTIFICATE

I certify that **Rajarao Manda** has prepared his thesis entitled "**An Efficient Carrier Frequency Offset Compensation Technique using Superimposed Training Sequence for Next generation (5G) Wireless Networks**", for the award of Ph.D degree of the University of Petroleum and Enegry Studies, under my guidance. He has carried out the work at the Department of Electrical and Electronics Engineering, School of Advanced Engineering, University of Petroleum & Energy Studies.

External Supervisor:

Dr. R Gowri

Professor

Department of Electronics and Communication Engineering

Graphic Era Hill University, Dehradun

Uttarakhnad, India.

Date:

ABSTRACT

The process of decoding data in cellular systems necessitates the synchronization of the user's device with the base station (BS) of the network. The synchronization ensures that the transmitter and receiver are properly aligned in terms of time and frequency. Time synchronization ensures that the receiver can correctly sample the received signal at the appropriate time intervals. In digital wireless systems, timing synchronization is crucial for symbol detection and demodulation. Frequency synchronization ensures that the transmitter and receiver are operating at the same frequency. Any difference in carrier frequency between the two is known as carrier frequency offset (CFO) can cause distortion and interference in the received signal.

The occurrence of CFO is primarily attributed to the discrepancies between local oscillators and the Doppler shift. This CFO causes non-orthogonality between the sub-carriers in multi-carrier modulation systems and hence inter-carrier interference (ICI). The Universal Filtered Multi-carrier (UFMC) technology is a highly promising solution for forthcoming wireless communication systems, owing to its exceptional spectral efficiency and resilience to interference that may arise from synchronization errors. However, when CFO is non-negligible, the UFMC suffers from severe performance degradation, even though it is more immune to CFO than the OFDM. Hence, it is imperative for the UFMC receiver to obtain a precise estimation of CFO prior to signal detection. These estimation algorithms may introduces more computational complexity. The UFMC exhibits greater system complexity due to the inclusion of a FFT block at the receiver and filtering operation in the transmitter. Thus, it is necessary to decrease the complexity of the system.

The research was conducted in two distinct phases. In the preliminary stage, our principal goal is to construct a UFMC transceiver system model with the intention of reducing its overall complexity. This achieved by simplification of the transceiver architecture's structure at the baseband signal processing level result in a decrease in system complexity. Further, the study conducted

an analysis of the interference caused by non-orthogonality resulting from the filtering process on the transmitter end. According to this analysis the length of sub-band filter was adjusted in relation to the sub-band size to reduce the interference. The second phase of the study involved an analysis of the influence of the CFO in the UFMC system through the utilization of the closed-form of ICI expression. The estimation of the CFO in the UFMC system was carried out using the Superimposed Training (SIT) sequence. The SIT sequence was algebraically added to the data, with a predetermined power allocation ratio that defined the power distribution between the training and data sequences.

The estimation approach uses the auto-correlation property of the received symbols and SIT sequence. However, the power distribution between the training and data sequences effect the accuracy of CFO estimator. That is, the CFO estimation accuracy decrease with an increase in power allocation to data. Another hand if the power allocation is more for the training sequence, the estimation accuracy is better, but the interference in the data sequence might be more due to the SIT sequence, which degrades the bit error rate (BER) performance. So, there is a trade-off between the power allocation ratio and estimated accuracy. To overcome this issue, the power allocation ratio is optimized to minimize the training sequence interference on data in terms of BER and mean square error (MSE). In terms of spectral efficiency and BER, this proposed method performs better than the traditional methods, but at the expense of greater computational complexity. With the proposed model and method, the system performance is better than the conventional methods and improves the spectral efficiency up to 4.76%.

ACKNOWLEDGMENT

This thesis would not be possible without the support and encouragement of many people. First and foremost, I express my profound gratitude and sincere thanks to my supervisors Dr. R. Gowri and Dr. Adesh Kumar for giving me all their support, advice, inspiration and motivation in carrying out this work. Their technical expertise and approach of tackling problems have been of great help to me. Besides, their constant motivation, encouragement, personal guidance and understanding helped me to carry out this work with great zeal and enthusiasm. I thank them for taking me under their wings and providing numerous inputs in the work.

I convey my special thanks to my ex-department head Dr. Sushabhan Chowdhary, Cluster head Dr. Piyush Kuchal, all faculty and staff members of Electrical and Electronics Engineering department for providing an excellent academic environment.

I am grateful to Dr. Gurvinder Singh Virk, Dean, School of Engineering and for his constant and continuous encouragement to carry out the work.

Ultimately, I would like to convey my perpetual appreciation and acknowledgment to my parents (Chenchaiah, Akkamma), spouse Mrs. Koteswari, and my family members for their affection and assistance throughout my existence. The unwavering support and steadfast belief in my capabilities have served as a significant source of inspiration. Merely expressing gratitude may not be adequate for the assistance that has been provided to me.

Rajarao Manda

Contents

List of Figures

List of Tables

List of Abbreviations

1G	First Generation
2G	Second Generation
3G	Third Generation
3GPP	Third Generation Partnership Project
4G	Fourth Generation
5G	Fifth Generation
6G	Sixth Generation
AI	Artificial Intelligence
AMPS	Advanced Mobile Phone System
AWGN	Additive White Gaussian noise
B5G	Beyond 5G
BER	Bit Error Rate
CCRR	Computational Complexity Reduction Ratio
CFO	Carrier Frequency Offset
CGRV	Complex Gaussian random vector
CIR	Channel Impulse Response
CMOS	Complementary Metal Oxide Semiconductor
CP	Cyclic Prefix
CP-OFDM	Cyclic Prefix- Orthogonal Frequency Division multiplexing
CSI	Channel state information
D2D	Device to Device
DFT	Discrete Fourier transform
DIT	Decimation In Time
DL	Down Link
EDGE	Enhanced data rate for global evolution

eMBB	enhanced Mobile Broadband
EPC	Evolved Packet Core
ESPRIT	Estimation of Signal Parameters via Rotational Invariance Technique
FBMC	Filter Bank Multi-Carrier
FDD	Frequency division duplex
FFT	Fast Fourier transform
FIR	Finite Impulse Response
FO	Frequency Offset
F-OFDM	Filtered OFDM
GFDM	Generalized Frequency Division Multiplexing
GPRS	General packet radio services
GSM	Global system for mobile communications
HD	High Definition
HSDPA	High-Speed Downlink Packet Access
HSPA	High-Speed Packet Access
HSUPA	High-Speed Uplink Packet Access
ICI	Inter-carrier interference
IDFT	Inverse Discrete Fourier transform
IFFT	Inverse Fast Fourier Transform
IIoT	Industrial Internet of Things
IMT	International Mobile Telecommunications
IoE	Internet of Everything
IoT	Internet of Things
IP	Internet Protocol
IS	Interim Standard
ISBI	Inter Subband Interference
ISI	Inter Symbol Interference
ITU	International Telecommunication Union
LoS	Line-of-Sight
LS	Least Squares

LTE	long term evolution
M2M	Machine to Machine
MCM	multi-carrier Modulation
MIMO	multi-input multi-output
ML	Machine Learning
MLE	Maximum Likelihood Estimation
MMFGR	Maximum-to-Minimum Filter Gain Ratio
MMSE	Minimum Mean Square Error
MTC	Machine Type Communications
MUSIC	MUltiple SIgnal Classification
NGWN	Next-generation Wireless Networks
NMT	Nordic Mobile Telephone
NR	New Radio
OBE	Out-off Band Emission
OFDM	Orthogonal Frequency Division Multiplexing
OFDMA	Orthogonal Frequency Division Multiple Access
OQAM	Offset Quadrature Amplitude Modulation
OTFS	Orthogonal Time Frequency Space Modulation
PAPR	Peak to Average Power Ratio
PDF	Probability Density Function
PN	Pseudo Noise
PRB	Physical resource blocks
PS	Pilot Symbols
PSK	Phase Shift Keying
QAM	Quadrature Amplitude Modulation
QoE	Quality of Experience
QPSK	Quadrature Phase Shift Keying
RB	Resource Block
RF	Radio Frequency
SIR	Signal to Interference Ratio
SIT	Superimposed Training

SMS	Short Message Service
SNR	Signal to Noise Ratio
SUI	Stanford University Interim
TACS	Total Access Communication System
TDL	Tapped Delay Line
TDD	Time Division Duplex
TDMA	Time Division Multiple Access
TO	Timing Offset
TS	Training Symbols
TTI	Transmission Time Interval
UAV	Unmanned Aerial Vehicle
UFMC	Universal Filtered Multi-carrier
UL	Up Link
UMTS	Universal Mobile Telecommunications System
URLLC	Ultra-Reliable Low Latency Communications
V2X	Vehicle-to-Everything
WCDMA	Wideband Code Division Multiple Access
WiMAX	Worldwide interoperability for Microwave Access
ZC	Zadoff-Chu

Units

μs	Micro Second
bps/Hz	Bits per second per Hertz
kbps	Kilo bits per Second
kHz	Kilohertz
kmphr	Kilometer per hour
mm	Millimeter
ms	Millisecond
mW	Milliwatt
nm	Nanometer
ns	Nanosecond
Gbps	Gigabit per Second
Mbps	Megabits per Second
MHz	Megahertz
Tbps	Tera bits per second
THz	Terahertz

NOMENCLATURE

β	The normalized CFO value
Δf	The subcarrier spacing between the successive subcarriers
$\mathcal{X}$	The Toeplitz matrix of the corresponding vector X
$f(l)$	The impulse response of a desired/prototype filter
f_D	The maximum Doppler shift
$f_p(l)$	The impulse response of pth sub-band filter
$f_{c,t}$	The local oscillator frequency at the transmitter
$f_{c,r}$	The local oscillator frequency at the receiver
f_{os}	The offset frequency
$h(l)$	The impulse response of a wireless channel
$x(n)$ or $x_i(n)$	The time-domain i^{th} UFMC signal/symbol
$x_p(n)$ or $x_{ip}(n)$	The time-domain p^{th} subband filtered signal of ith UFMC signal
y_i	The received i^{th} time-domain UFMC symbol
$y_{i,zp}$	The received i^{th} UFMC symbol after zeros padded to y_i
$z(n)$	The AWGN vector
$d_p(n)$ or $d_{ip}(n)$	The IFFT of pth subband data for i^{th} UFMC signal
B	The Number of subbands
$D_p(k)$ or $D_{ip}(k)$	The input data (QAM modulated) samples of pth subband data for i^{th} UFMC signal
E_{ICI}	The energy of the UFMC symbol due ICI
E_{ISBI}	The energy of the UFMC symbol due ISBI
E_{SC}	The energy on data subcarriers within the UFMC symbol

K_0	The initial subcarrier index of the lowest subband of a UFMC signal
L_f	The Subband filter length/order
L_h	The length of the wireless channel
M	The order of the modulator
N	IFFT/FFT size
N_D	The Number of data subcarriers
N_T	The total received UFMC symbol length
Q or Q_p	The Number of subcarriers per subband
R_{x_1,x_2}	The correlation of two sequences x_1 and x_2
Y_{2N}	The 2N-point DFT of y(n)
$X_{p,2N}$	The 2N-point DFT of pth subband filtered signal
Y_{2N}^{even}	The even numbered samples of 2N-point DFT of y(n)
Y_{2N}^{odd}	The odd numbered samples of 2N-point DFT of y(n)
$E\left[.\right]$	The Expected value of the corresponding function
$(.)^H$	The Hermitian matrix of the corresponding matrix
$^j X$	The value(s) X computed at j^{th} iteration of the method

Chapter 1

Introduction

The present chapter provides a concise discourse on the progression of mobile wireless communications, candidate modulation waveform approaches for upcoming wireless networks and the contribution of this work. Here we will first discuss the standards and development cycle of wireless networks, then a description of 5G and future iterations. The organisation of the thesis is ultimately addressed.

1.1 Evolution Towards 5G Networks

At present, there are five distinct generations of mobile networks, each characterized by its unique standards, techniques, and capabilities [5] shown in Fig. 1.1. The first-generation (1G) wireless networks like Advanced Mobile Phone System (AMPS) changed the world by communicating with each other through voice services between 1980 and 1990. The 1G communication technologies were mostly analog, built largely for voice communications and uses frequency division multiple access (FDMA). It suffered issues like poor capacity, unreliable transmission, and a poor security. In response to the aforementioned challenges, the telecommunications industry introduced second-generation (2G) cellular networks like Global System for Mobile communications (GSM), IS-95/CDMA, and Pacific Digital Cellular (PDC) in the 1990s. These networks were founded on digital technologies and aimed to enhance the performance, reliability, and roaming capabilities of conventional voice services. Additionally, they were designed to support short message services (SMS). The primary access technologies Time division multiple access(TDMA) and Code division multiple access(CDMA) are used

in 2G cellular networks. These technologies has been around since the 1980s, and a large percentage of mobile customers are still connected to the 2G mobile communication networks and it is believed that 2G will remain in use for at least a few more years before becoming obsolete. Certain initial systems have undergone improvements to facilitate packet data services and these expansions (EDGE and GPRS) are often referred to as 2.5G to imply that they are based on 2G technologies but have many more capabilities than the original technology. The GSM/EDGE is still widely used in cell phones, but it is also widely utilised in machine-to-machine communication applications, including but not limited to alarm systems, banking systems, and commercial property monitoring.
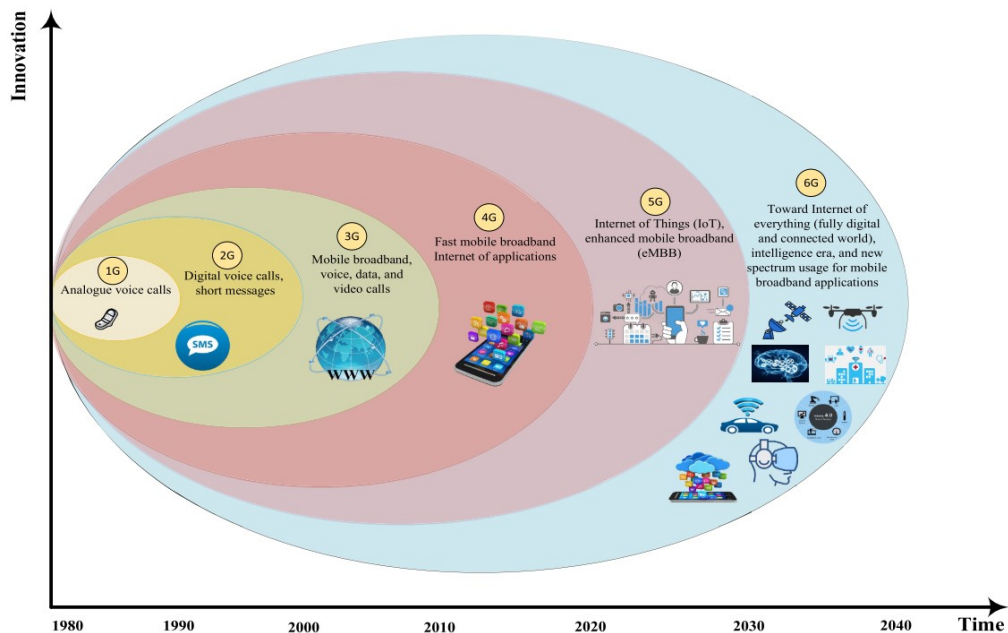
Figure 1.1: Evolution of wireless networks [1]

The third generation (3G) wireless systems emerged in the late 1990s and early 2000s. These systems provided significant advancements over the previous 2G networks in terms of throughput, network capabilities, and capacity. The ITU has designated a frequency spectrum at 2 GHz range on global scale and has requested recommendations for IMT-2000 in order to ensure the worldwide interoperability of mobile networks. Key features of 3G wireless systems include:

- Faster Data Transfer Rates to allow for faster and more efficient

communication. They provided maximum throughput of up to 384 Kbps for users in moving vehicles and 2 Mbps for pedestrians.

- Multimedia Support: 3G networks were designed to support multimedia services, including video calling, video streaming, and mobile internet access. These systems offered improved voice quality and facilitated the transmission of various types of data.

- Broadband Internet Access: With 3G, users gained access to broadband-like internet connectivity on their mobile devices. This allowed for web browsing, email access, and the use of various internet-based applications.

- Global Roaming: 3G systems aimed to provide global roaming capabilities, enabling users to access their services while traveling internationally. This was made possible through international standards and roaming agreements between different network operators.

- Enhanced Security: 3G networks introduced improved security mechanisms compared to their predecessors. They incorporated stronger encryption algorithms and authentication protocols to ensure the privacy and integrity of user data.

- Support for Advanced Applications: 3G systems were designed to support advanced applications such as mobile video conferencing, location-based services, mobile gaming, and multimedia messaging.

The ITU approved two proposals, namely the Universal Mobile Telecommunications System (UMTS) under the 3GPP standard, referred to Wideband CDMA (WCDMA), and CDMA-2000. In 1998, NTT Docomo initiated the launch of the inaugural pre-commercial 3G network, which was succeeded by the introduction of the initial commercial 3G network in Japan in October 2001, which was based on WCDMA technology. In South Korea SK Telecom successfully launched the first commercial 3G in January 2002 which was based on CDMA-2000 technology. The WCDMA's first version

(release 99), which enables data services using circuit and packet-switched bearers; voice and video services using circuit-switching bearers. 3G wireless communication networks have undergone significant evolution since their initial deployment. Here's an overview of the key stages in the evolution of 3G networks:

- 3G Release 99 (Rel-99) (2000): The first commercial 3G network deployments were based on the Rel 99 standard, which introduced the UMTS technology. The UMTS offered data rates of up to 2 Mbps and supported basic multimedia services like video calling and mobile internet access.

- 3.5G: Which employed with High-Speed Packet Access (HSPA) technology, that was implemented as a means of enhancing upgrade to 3G networks, provided faster transfer rates with good spectral efficiency. It consisted of two main standards: Rel-5 referred as High-Speed Downlink Packet Access (HSDPA) and High-Speed Uplink Packet Access (HSUPA) also known as Rel-6 [6, 7]. HSPA networks offered peak data rates of several Mbps (megabits per second), enabling advanced services like faster web browsing, online gaming and video streaming.

- 3.9G (HSPA+ or Rel-7): The Rel-7, further enhanced the capabilities of 3G networks using multiple-input multiple-output(MIMO) antenna technology and advanced modulation methods. The enhancement resulted in a notable improvement in data rates (maximum download speeds reaching 42 Mbps) and network capacity. HSPA+ enabled better support for high-bandwidth applications and served as a precursor for the shift towards 4G.

- 3GPP Long Term Evolution (LTE): LTE marked the beginning of true 4G technology, although it is often considered a transitional step between 3G and 4G. LTE introduced all-IP (Internet Protocol) based networks with significantly higher data rates, improved spectral efficiency and lower latency than the preceding 3G technologies [8, 9]. LTE networks

offered peak download speeds of up to 100 Mbps and supported advanced services like real-time online gaming and high-definition (HD) video streaming.

- 3GPP LTE-Advanced(LTE-A): This standard is an additional enhancements evolved in the LTE by incorporating advanced functionalities like carrier aggregation, enhanced MIMO, and higher-order modulation schemes. These advancements enabled the maximum data speed up to 1 Gbps, making LTE-A a true 4G technology. LTE-A also provided better network capacity and improved performance in densely populated areas.

It's worth noting that the term "3G" is often used broadly to refer to all the aforementioned generations of wireless communication networks, even though some of the later stages like LTE and LTE-A are technically considered 4G due to marketing and historical reasons.

The 4G-LTE networks prioritized mobile broadband services and placed emphasis on meeting rigorous standards for rapid data transfer speeds, minimal delay, and large capacity. Additional significant requirements encompassed the adaptability of the spectrum and the optimal harmonization of Time Division Duplexing (TDD) and Frequency Division Duplexing (FDD). The development of Evolved Packet Core (EPC) was aimed at substituting the existing architecture utilized by GSM and WCDMA/HSPA for core network purposes. The first commercial deployment of LTE (3GPP Rel-8) occurred in late 2009. Around 2010, we had the 4G-LTE network called as a mobile broadband system. Figure 1.2 demonstrate the overall trajectory of 3GPP evolution from LTE in Rel-8 through LTE-Advanced Pro in Rel-14. The LTE technology has made notable progress in various aspects such as data transfer rates, capacity, spectrum utilization, deployment adaptability, and application diversity. It has achieved the maximum data speeds up to 300 Mbps in 20 MHz of spectrum and 1Gbps over a 100 MHz aggregated bandwidth with 4x4 MIMO

system.

Here are some key features and characteristics of 4G networks:

- Data Rates: Offers a maximum download speeds of up to 100 Mbps for users with high mobility (moving in vehicle) and up to 1 Gbps for pedestrians.

- Internet Protocol (IP)-Based Architecture: Employs fully IP based frame work, which facilitates the smooth assimilation with other IP-based networks and services. This facilitates the convergence of various communication technologies, such as voice, video, and data, over a single network infrastructure.

- Advanced Modulation Techniques: 4G networks make use of sophisticated modulation techniques such as OFDM in conjunction with MIMO technology to improve spectral utilization and enhance the overall capacity of the network. These techniques allow for better data transmission and reception, even in challenging environments.

- Low Latency: 4G networks aim to provide low latency that refers to the minimal delay required to receiving the data correctly from the transmitter. This reduced latency is particularly beneficial for real-time applications including online gaming, video conferencing, and interactive services.

- Enhanced Multimedia Support: 4G networks offer enhanced support for multimedia services, including high-definition video streaming, online gaming, and high-quality voice and video calls. The increased bandwidth and improved network capacity enable smoother and more reliable multimedia experiences.

- Backward Compatibility: These networks are designed to possess the capability of accommodating the functionality of preceding generations of networks. This means that 4G-enabled devices can still connect to and use 3G or 2G networks when 4G coverage is not available.

- Mobile Broadband: 4G networks enable fast and reliable mobile broadband internet access, allowing users to access the internet, browse websites, use online applications, and download/upload data on their smartphones, tablets, or other connected devices

| Release 8 (2008) • LTE • EPC/SAE | Release 9 (2009) • LTE Home NodeB • Location Services • MBMS support • Multi-standard BS | Release 10 (2011) • *LTE-Advanced* • Carrier aggregation • Enhanced downlink MIMO • Uplink MIMO • Enhanced ICIC • Relays | Release 11 (2012) • Carrier aggregation enhancements • Enhanced heterogeneous deployments • CoMP | Release 12 (2014) • Small cell enhancements • Lean carrier • Multi-antenna enhancements • D2D | Release 13 (2015) *LTE-Advanced Pro"* • MTC enhancements • License Assisted Access • Narrowband IoT • FD-MIMO • Dual connectivity | Release 14 (2017) *LTE-Advanced Pro"* • Mission critical enhancements • Vehicle to Everything (V2X • IoT |

Figure 1.2: Evolution of 3GPP LTE Releases

1.2 5G Wireless Networks

The earlier generations when it moved from 2G to 4G, the primarily goal of it was about data rates. Most of the technologies of previous generations on air interface that are designed to provide higher data rate. However, when we look at fifth generation (5G), we find a number of different technologies that must integrate at different levels, including the physical, access, and network layers, in order for it to be function. There are different scenarios, an immense variety of requirements and applications needed to be handled concurrently by one single network, which is radically different from what happened in all prior generations. The development of 5G networks have been driven by the rapid expansion of wireless data services supported by smart devices and mobile Internet. Moreover, it is anticipated that there will be a significant increase in the quantity of individuals utilizing the Internet, mobile subscribers, Internet of Things (IoT) devices and machine type communication (MTC) connections in the forthcoming years [10, 11]. To enable these seamless smart applications, the 5G focused on tactile network which is accessed through several methods, including the simultaneous usage of both licensed and unlicensed spectra, intelligent spectrum management, and the implementation 5G New Radio (NR) [12].

7

1.2.1 Requirements and Technical Challenges of 5G and Beyond 5G (B5G)

The 3GPP has established specific objectives to fulfill the demands of 5G wireless networks [13, 14]:

- Wider bandwidth transmission -100MHz (millimeter wave (mmWave) bands- 30 to 60 GHz).

- High data rates- 1000 times of throughput improvement over 4G (10 Gbps) in mobile environment

- High spectral efficiency - 30 bps/Hz in the downlink, 15 bps/Hz in the uplink.

- Support massive MIMO

- Support communication with user mobility at speed of up to 400km/hr

- Low latency (less than 1 ms)

- The concept of network densification pertains to the deployment of heterogeneous and multi-tier networks.

- The enhancement of energy efficiency: wireless charging and energy harvesting techniques.

- Support advanced services and applications such as smart city, IoT

The year 2018 marked the finalization of the initial release of 5G mobile network by the 3GPP in its Rel-15. This laying the groundwork for the commercial 5G networks on a global scale [15]. Subsequent to that, 3GPP has been trying to increase performance and solve new use cases by upgrading 5G technology in Re-16 and Rel-17 [16]. Figure 1.3 gives the brief specifications of Rel-15 to Rel-18. The approval of the work package pertaining to 3GPP Rel-18 marks the commencement of the evolution towards 5G Advanced as per the source [17]. The 3GPP has introduced NR as a novel 5G air interface in Rel-15, aims to meet a number of usage situations like enhanced
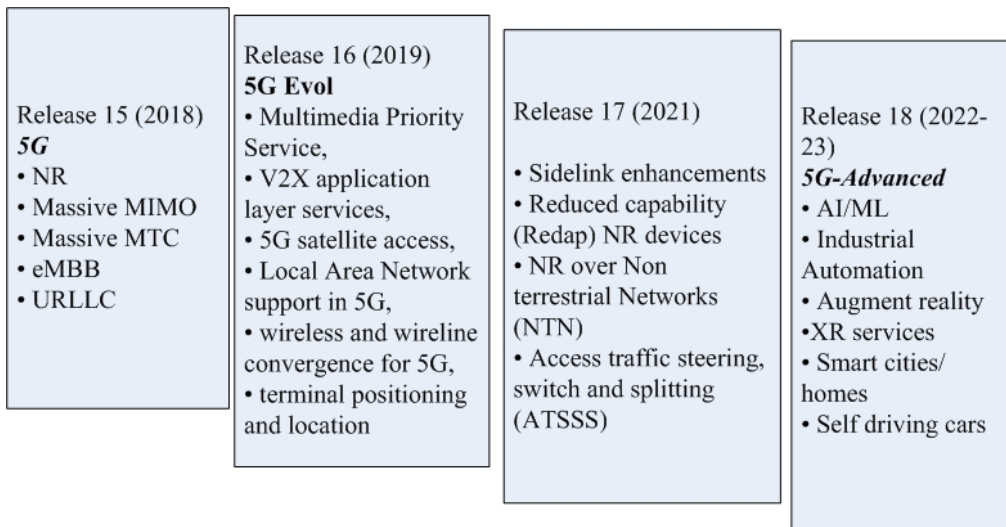
Figure 1.3: Evolution of 3GPP LTE Releases for 5G

mobile broadband (eMBB), massive MTC, and ultra-reliable low-latency communications(URLLC). At the Rel-16 initial stage (i.e., the evolution of 5G) incorporates several noteworthy modifications that enhance current functionalities and cater to novel use cases and deployment scenarios including industrial IoT (IIoT) and vehicle-to-Everything (V2X) communications. The MIMO and beam forming technology advancements, increased support for dynamic spectrum sharing, reductions in latency and carrier aggregation, and power savings in user equipment (UE) are some of the key improvements to existing capabilities for 5G Evolution. Recently, the 3GPP Rel-17 introduces enhancements not only for established applications such as enhanced mobile broadband, industrial automation, and V2X, but also for emerging use cases like non-terrestrial and public safety networks [18]. Preliminary findings from Rel-18 suggest that it will significantly enhance the capabilities of 5G technology in the domains of Artificial intelligence (AI) and extended reality. The last one is still in progress

1.3 Evolution of 5G towards 6G

At present, there is a widespread implementation of 5G wireless communication networks on a global scale. These networks have been standardized to facilitate

large-scale connectivity, ensure high levels of reliability, and guarantee low latency. Despite its potential, 5G technology is faced with several inherent limitations and challenges that have impeded its complete realization. The proliferation of Internet of Everything (IoE) networks has been facilitated by the progressions in intelligent devices and software applications. These networks comprise a diverse range of applications that are time-sensitive in nature, such as autonomous and aerial vehicles, medical applications, and intelligent services. Also, the deployment of IoE networks would necessitate extensive computing and sensing capabilities that may surpass those of 5G networks. Different data-centric, automated procedures are proven to be more capable than the capabilities described by 5G key performance metrics. Numerous applications, including haptics, telemedicine, and networked autonomous vehicles, necessitate extended packets that exhibit extreme levels of reliability. These applications are not in line with the 5G principle of utilizing small packets for URLLC. The forthcoming applications based on augmented and virtual reality necessitate μs level latency and high data rates at Tbps level [19]. These requirements appear to be challenging for 5G networks to meet. Furthermore, the 5G connectivity density ($10^6/km^2$) may not be sufficient to fulfill the rising demands of next-generation smart sectors. Thus, it has been projected that the 5G technology will not be fully capable of fulfilling all the demands of the future beyond the year 2030.

The 6G wireless networks are anticipated to facilitate a wide range of capabilities such as global coverage, enhanced efficiency in terms of spectral utilization, energy consumption, cost-effectiveness, heightened intelligence quotient, and improved security measures. To meet the aforementioned requirements, the development of 6G depends on novel technologies that enable new air interface and transmission methodologies, as well as advanced network architecture [20]. These technologies encompass the design of new modulation waveform, multiple access techniques, MIMO technologies, cell-free architecture, network slicing, and edge computing techniques. In addition, the AI is positioned to assume a crucial function in the development

of the 6G, as it possesses the capacity to effectively tackle a diverse array of wireless network challenges [21].

According to our perspective, the 6G of wireless communication technology is expected to exhibit four novel paradigm shifts [20].

- In order to meet the global coverage mandate, the forthcoming 6G technology won't be restricted to ground-based networks and it has to support non-terrestrial networks. Thereby establishing an integrated communication network that spans space, air, ground, and sea.

- A comprehensive investigation of all spectra will be conducted to enhance the connection density and data speeds.

- To enable the development of intelligent applications through the utilization of AI and big data analytics, in response to the challenges posed by the vast datasets produced by highly heterogeneous networks, diverse communication scenarios, massive MIMO, broad bandwidths, and emerging service demands.

- The enhancement of network security

Here are some key features of 5G and 6G technology:

5G

- Faster speeds: The theoretical download speed up to 20 Gbps.

- Lower latency: Typically lower than that of 4G networks, that is less than 1 ms

- More connected devices: 5G is designed to handle a larger number of connected devices than 4G, which is important for the growing number of IoT devices.

- New spectrum: 5G uses higher frequency spectrum than previous generations, which allows for faster speeds and more bandwidth.

- Greater energy efficiency: 5G is designed to be more energy-efficient than 4G, which could lead to longer battery life for connected devices.

6G

- Even faster speeds: Anticipated to surpass the speed of its predecessor 5G, with theoretical download speeds of up to 1 Tbps.

- More advanced technologies: 6G is expected to incorporate new technologies like holographic communication, which could enable more immersive virtual and augmented reality experiences.

- Smarter networks: Expected to apply AI and machine learning to improve efficiency and optimize network performance.

- Increased security: 6G is expected to have more advanced security features to protect against cyber attacks.

- More environmentally friendly: 6G is expected to be designed with environmental sustainability in mind, with a focus on reducing energy consumption and carbon emissions.

Overall, both 5G and 6G are expected to be a key enabler for the use cases including the IoT, AI, and smart cities. Also these future generation wireless networks are expected to bring significant improvements to wireless connectivity, enabling new applications and experiences that were not possible before. However, the deployment of 5G and 6G networks will require substantial investment in infrastructure, including the installation of new e-NodeB and fiber cables, as well as research and development into new technologies and standards.

1.4 Frequency Spectrum for 5G and B5G

The limited availability of spectrum in traditional cellular mobile bands has led to increased interest in the utilization of new frequency bands ranging from 30 to 300 GHz for the development of next-generation cellular wireless networks. These frequency bands offer significantly wider bandwidths compared to current cellular networks, as evidenced by recent research studies [22, 23]. That means, the frequency spectrum for 5G and B5G networks spans a wide range of

frequencies, including both traditional cellular frequency bands and new bands specifically allocated for these advanced networks.

For 5G, the ITU has identified three frequency ranges namely low band (below 1 GHz), mid band (between 1 and 6 GHz), and high band (above 6 GHz), as illustrated in the table 1.1. The low band provides good coverage and penetration, while the mid-band offers an appropriate trade-off between coverage and capacity. The high band, commonly referred to as mmWave, provides extremely high data speeds but with limited coverage and high attenuation. However, finally, the 5G bands are divided into two categories according to the 3GPP release 17 [18]: Frequency Range 1 (FR1) (sub-7 GHz frequency bands from 410 MHz to 7.125 GHz); Frequency Range 2 (FR2) (24.25 to 71.0 GHz). However, the researchers are exploring to use terahertz (THz) frequencies, which offer even higher data rates but with even more limited coverage and greater attenuation. This particular range of frequencies has certain special characteristics which has some disadvantages, and advantages. The deployment of mmW communication is particularly appropriate for situations involving limited distance small cell access and direct line-of-sight (LoS) within mobile networks [24]. In addition, the diminutive wavelengths of millimeter-wave (mmW) signals, in conjunction with progressions in low-power complementary metal oxide semiconductor (CMOS) radio frequency (RF) circuits, facilitate the installation of a substantial quantity (32 elements) of reduced-size antennas within limited spatial parameters. Multiple antenna systems have the potential to create electrically steerable arrays with high gain. These arrays can be manufactured at the base station, integrated into the structure of a mobile, or even embedded within a microchip [25].

5G technologies have been commercially deployed in a number of regions throughout the world [26]. Nevertheless, the 5G mmWave technology is currently in its nascent phase of advancement. It's important to note that the specific frequency bands and their availability may vary by region and regulatory environment. Different countries and organizations allocate and manage the spectrum differently, so the frequency bands used for 5G and B5G

deployments may differ from one location to another.

Table 1.1: Spectrum for 5G and B5G

Name of the band	Description	Commonly used bands
Sub 6/7 GHz bands	These frequency bands provide wide coverage and better penetration through buildings. The specific frequency ranges vary by country and regulatory bodies, but they typically fall between 600 MHz and 6 GHz. Sub-6 GHz bands are often referred to as low- and mid-band frequencies.	600 MHz; 700 MHz; 850 MHz; 900 MHz; 1.8 GHz; 2.1 GHz; 2.3 GHz; 2.6 GHz; 3.5 GHz; 4.5 GHz; 6.425 GHz, 7.125 GHz
mmWave Bands	These bands are situated within the realm of extremely high frequencies, typically above 24 GHz. They offer extreme high data rates but have shorter range and are more susceptible to signal blockage. These high-frequency bands are typically used for high-speed, short-range communications in dense urban areas.	24-28 GHz; 37-40 GHz; 26 GHz (24.25 – 27.5 GHz) (in Europe/ India); 42 GHz (in Japan); 60 GHz (unlicensed band)
Terahertz (THz) Bands	Beyond 5G, researchers and industry are exploring to use at higher frequencies in range of THz (100 GHz to 10 THz). These bands offer enormous data rates but face significant technical obstacles in relation to signal propagation and device design.	–

1.5 Modulation Waveform Techniques for 5G and B5G

To accomplish the goals outlined above regarding the system performance metrics, next-generation wireless networks (NGWN) will make extensive use of a wide variety of innovative enabling technologies. The subsequent sections will discuss about the new modulation waveform technologies that are recommended for the NGWN.

The eMBB, massive MTC, and URLLC are the three service types that will generally be supported by 5G and beyond. To efficiently support these amenities and their corresponding deployment scenarios, a versatile air interface is necessary. In order to make such an adaptability, it is necessary to construct

an appropriately functioning new waveform, which serves as the defining characteristic of any air interface. So, the most important decision at the physical layer is the selection of a flexible radio waveform. The development of a versatile waveform necessitates the consideration of various parameters such as localization in time/frequency slots, resilience to time/frequency dispersion, spectrum utilization, latency, peak to average power ratio (PAPR) and out-of-band emission (OBE) [27, 28]. The paper [29], provides an overview of waveform development, the challenges and requirements of waveform design for 5G and B5G, and the future directions of waveform design. The authors also discuss the impact of waveform design on the system's performance and energy efficiency. [30], gives an overview of waveform design for 5GNR, including the basic waveform structure, the candidate waveforms, and the performance evaluation criteria. The authors also discuss the challenges and opportunities of waveform design for 5GNR.

Modulation waveform is one of the essential element of wireless networks, including 5G and 6G networks. This determine how data is transmitted over the air and affect the system's capacity, spectral efficiency, and reliability. Nowadays, there have been various proposals of waveform methodologies for 5G and 6G networks, aiming to fulfill the increasing requirements for enormous rates of data transfer, reduced latency, extensive connectivity, and energy efficiency. As the investigation progresses, certain waveforms that were suggested are expeditiously dismissed due to their ineffectiveness in practical applications, while others remain under active consideration. Here, we will discuss some of the modulation waveforms that have been suggested for 5G and B5G networks.

1.5.1 Orthogonal Frequency Division Multiplexing (OFDM)

The OFDM technique is a widely used multi-carrier modulation (MCM) technique that is presently being implemented in a different standards, including the IEEE 802.11 family and the DL of 4G LTE [31]. The MIMO technologies and wide bandwidth operations can both benefit from OFDM's

low implementation complexity and low cost. The OFDM scheme involves the partitioning a high-speed data stream into a large number of parallel data sub-streams of lower speed, each transmitted simultaneously on different orthogonal subcarriers. It enables robustness against frequency-selective fading channels. Here are some key points about OFDM:

- Subcarrier Division: OFDM splits the available frequency spectrum into multiple orthogonal subcarriers. These subcarriers are closely spaced and overlap, but their orthogonality ensures that they do not interfere with each other.

- Orthogonal Subcarriers: The orthogonality between the subcarriers allows to be packed closely together without causing interference as shown in Figure 1.4. By utilizing closely spaced subcarriers, OFDM maximizes spectral efficiency.

- Robustness to Multipath Fading: OFDM is particularly well-suited for wireless communication because it is highly resistant to multipath fading. Since the subcarriers are spaced apart in frequency, they experience fading independently, and the receiver can effectively mitigate the effects of fading through equalization.

- Guard Interval/ Cyclic prefix (CP): OFDM includes a guard interval or CP between each symbol to mitigate the effects of intersymbol interference (ISI) that arise as result of the phenomenon of multi-path propagation. The cyclic property of CP enables the conversion of the linear convolution into a circular convolution, thereby facilitating the implementation a single tap equalizer in the OFDM system.

Figure 1.5a displays the OFDM's system block diagram. The transmission process involves the synchronous and independent transmission of data symbols, which are typically modulated using some form of digital modulation, such as M-ary QAM or M-ary PSK, on closely spaced orthogonal subcarriers. The orthogonal overlapped subcarriers of OFDM systems, as seen in Fig. 1.4, enable flexible frequency assignment and yields in a very effective utilization
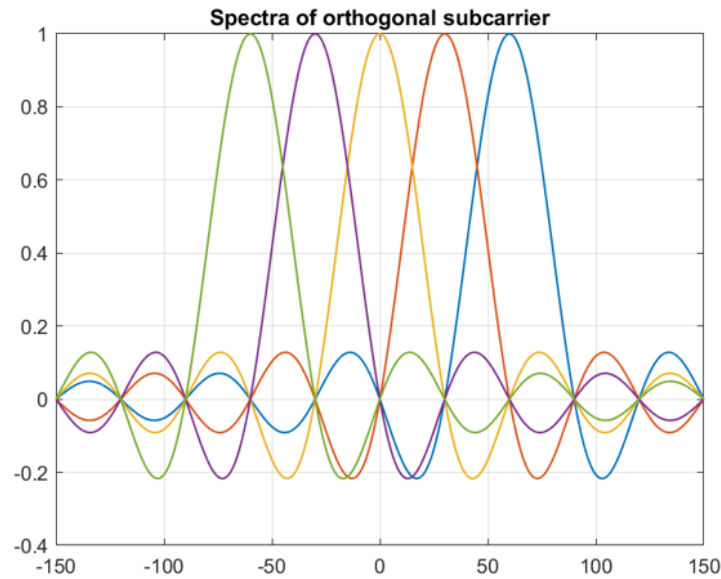
Figure 1.4: Spectra of OFDM subcarriers

of the available spectrum. The subcarrier's bandwidth refers to the frequency spacing between adjacent subcarriers used for data transmission and is set to a value that is lesser than the channel's coherence bandwidth. It's important to note that the specific value for the subcarrier spacing can vary depending on the standard or implementation. For example, in 5GNR, the subcarrier spacing is defined as the integer multiple of 15 kHz (i.e., $2^\mu \Delta f$; where $\Delta f = 15kHz$ and $\mu = 0, 1, 2, 3, 4$), depending on the deployment scenario and the operating frequency band.

To generate an OFDM signal, you need to follow a series of steps that illustrated in the Figure 1.5a:

- Determine the system parameters: Define the required bandwidth, subcarrier spacing, the number of subcarriers, CP length, and modulation scheme. These parameters depend on the specific application and the communication standard being used.

- Generate the data symbols: Convert the input data into symbols according to the chosen modulation scheme as discussed above.

- Subcarrier allocation/Mapping: Divide the available frequency spectrum

17
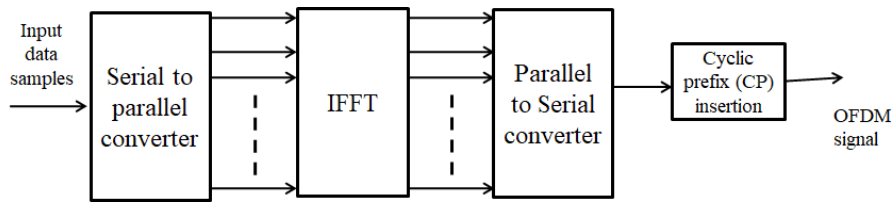
(a) The block diagrammatic representation of the OFDM transmitter
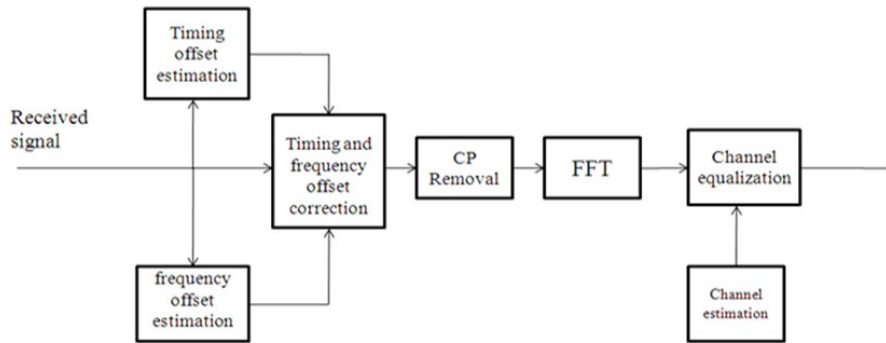
(b) The block diagrammatic representation of the OFDM receiver

Figure 1.5: The OFDM wireless system adapted from [2]

into multiple subcarriers. Assign the generated data symbols to these subcarriers to achieve the maximum spectral efficiency and the minimum ICI.

- Perform Inverse Fast Fourier Transform (IFFT): Apply an IFFT operation to convert the data symbols in the frequency domain to the time domain.

- Add CP: Insert a CP at the start of every OFDM symbol. The CP is a replicated version of the latter part of the symbol and it's length depends on the configuration listed in Table 1.2.

Now, the digital OFDM symbol convert into an analog signal then up-convert this analog signal to the desired carrier frequency and transmit it over the wireless channel.

Table 1.2: Length of CP

Configuration	Number of OFDM symbols	Guard period (in μs)	CP length
Normal CP	7	5.21/4.69	160/144
Extended CP	6	16.67	512

At the receiver of OFDM, the transmitted OFDM signal captures and then the

following steps are typically implemented using digital signal processing (DSP) algorithms and techniques.

- Timing Synchronization: The receiver performs timing synchronization by computing timing offset (TO) to determine the correct starting point of each symbol within the received signal. This helps in separating the different subcarriers.

- Frequency Offset (FO) Compensation: The receiver compensates for any FO that occurs between the transmitter's and receiver's oscillators. This is usually done by applying a frequency correction to each subcarrier.

- Perform FFT: The receiver removes the CP from received signal after the correction of TO and FO, then performs the FFT to convert into frequency-domain symbols. These frequency-domain received OFDM symbols are used for channel estimation and single-tap frequency domain equalization.

- Channel Estimation: The receiver estimates the channel characteristics, including it's frequency response and impulse response from the signal obtained at the output of FFT processor. This information is necessary for equalization and demodulation.

- Equalization: The receiver applies equalization techniques to counteract the effects of channel distortion. This helps in reduction of the ISI resulting from the effects of multi-path propagation.

Nevertheless, this technology exhibits certain limitations, including a high PAPR, increased OBE, and greater susceptibility to frequency dispersion. The large signal peaks poses challenges for the power amplifier at the transmitter to handle these peaks without spectral spreading and distortion. For OFDM based system, minimizing the side lobes of the sincs at the edge carriers is crucial in mitigating interference from adjacent channels.

- High PAPR: Which implies that there can be large variations in the signal's amplitude, leading to large signal peaks. This high PAPR poses

19

challenges for power amplifiers, as they must handle these peaks without distortion or efficiency loss. Techniques such as peak power reduction algorithms and crest factor reduction can be employed to mitigate this limitation.

- Sensitivity to CFO: OFDM relies on maintaining precise orthogonality between subcarriers. Any FO between the transmitter and receiver can cause ICI and result in a degradation of performance. Frequency synchronization techniques are needed to compensate for these offsets and maintain orthogonality.

In order to comply with the spectral mask specifications of different standards, OBE is commonly decreased through the implementation of diverse windowing and filtering methods, in addition to the allocation of guard bands. To address this issue, the 3GPP LTE standard allocates 7-10 % of the available bandwidth as guard bands. The spectrum utilization is diminished due to the fixed allocation of the guard band. For instance, the leakage from other subcarriers results in ICI when the orthogonality is lost as a result of frequency offset, Doppler spread, or phase noise. Similar to this, when the TO happens outside of the guard interval, it results in ISI or ICI.

The aforementioned limitations render it inappropriate for upcoming radio systems. Several types of OFDM waveform schemes that employ filtering operations are currently under investigation for the 5G standard, with the aim of mitigating some of the limitations of OFDM, such as reducing OBE.

1.5.2 Generalized Frequency Division Multiplexing (GFDM)

The GFDM is a new physical layer waveform approach for 5G systems that aims to address the major broadband and real-time issues [32, 33]. The GFDM uses a more flexible approach by using overlapping subcarriers with non-orthogonal waveforms while OFDM divides the available spectrum into orthogonal subcarriers. This allows GFDM to achieve an improved spectral

efficiency than the OFDM. The key characteristics of GFDM include:

- Waveform flexibility: GFDM supports the use of different waveforms for each subcarrier, enabling adaptation to specific channel conditions and requirements.

- Low OBE: By using overlapping subcarriers, GFDM reduces the OBE, allowing more efficient use of the available spectrum.

- Low latency: GFDM has low latency characteristics, making it suitable for applications that require real-time communication, like wireless video streaming and virtual reality.

- Frequency localization: GFDM allows for frequency localization, which means that it can concentrate the transmitted energy on specific frequency regions, enhancing the robustness of the signal against frequency-selective fading and interference.

- Improved coexistence: GFDM exhibits better coexistence capabilities in the presence of other wireless systems due to its waveform flexibility and reduced OBE.

The fulfilment of low latency demand in the tactile Internet scenario poses a significant challenge. However, GFDM's flexibility and block structure, which can be likened to a datagram, make it a suitable solution for this challenge. Given the limited amount of information to be conveyed, it is feasible to devise a GFDM frame that conforms to the 100 ms temporal constraint. In the event that a higher throughput is required, it is possible to employ irregular subcarrier allocation or non-uniform subcarrier spacing to accommodate the additional data rate. The block structure of GFDM confers a significant advantage in the context of the random access channel scenario. Its features make it suitable for various applications, such as multimedia streaming, IoT devices, and M2M communication. GFDM is considered a prominent contender for the physical layer of the forthcoming cellular system, which is expected to cater to diverse communication requirements envisaged for the 5G networks [34]. However, it is

noteworthy that GFDM is a technology that is still in the process of development and has not yet been widely adopted in commercial wireless systems

1.5.3   Filter Bank Multi-carrier (FBMC)

The FBMC is a modulation technique that bears resemblance to OFDM and involves the application of a filtering function to individual sub-carriers [35–37]. The FBMC is designed to address some of the limitations of OFDM, especially in scenarios where spectral efficiency and frequency localization are important. In OFDM, each subcarrier's frequency spectrum has a rectangular shape, leading to high sidelobes and spectral leakage. On the other hand, the FBMC uses more sophisticated filtering techniques to shape the subcarriers and minimize the interference between them, resulting in a better frequency spectrum utilization and lower out-of-band radiation. At the transmitter, the data is passed through a prototype filter, that shapes the data into multiple subcarriers with overlapping frequency spectra. These subcarriers are then modulated with the input data using techniques such as QAM. At the receiver, a filter bank with filters matching the transmitter's prototype filters is used to separate the subcarriers. The received signals from each subcarrier are then demodulated, and the data is extracted. Since the subcarriers in FBMC overlap, the receiver filters need to have good frequency selectivity to separate the individual subcarriers accurately. Thus, it can be inferred that FBMC operates as a "synthesis" filter bank during transmission and as an "analysis" filter bank during reception. These filter banks execute suitable filtering procedures at the subcarrier level.

In FBMC, the subcarriers can be better localized with the availability of advanced prototype filter design through over sampled coefficients in frequency domain. The subcarrier filters exhibit a high degree of selectivity and necessitate extended filter time constant that is commonly fourfold of the fundamental symbol length, leading to temporal overlap of individual symbols. For example, if the oversampling factor K equal to four, i.e. the separation between the adjacent coefficients is one fourth of the subcarrier spacing and hence each

FBMC symbol duration is equivalent to K (four) times of subcarrier spacing. To optimize spectrum utilization, multiple FBMC symbols are superimposed and combined in the time domain, with a T offset between adjacent symbols. This gives rise to the apprehension of ISI or ICI at the demodulation stage. In order to eliminate the ISI or ICI that may arise between the actual components (either real or imaginary) of two neighbouring sub-channels, it is necessary to apply an offset of T/2. The aforementioned observation motivates "Offset-QAM" (O-QAM) FBMC modulator. In order to attain orthogonality, the utilization of O-QAM is employed as the modulation technique, thereby rendering FBMC non-orthogonal in relation to the complex plane. The filter length of this particular system renders it unsuitable for supporting low latency services within the context of 5G technology.

One of the key advantages of FBMC is its ability to handle frequency-selective channels more efficiently. It can reduce the effects of multi-path fading and interference with the filter banks that can adapt to the channel conditions. This makes FBMC particularly useful in scenarios where there are significant variations in the channel characteristics. Another advantage of FBMC is its lower OBE compared to OFDM. The use of prototype filters with better spectral containment properties helps reduce the ICI, allowing to utilize the available spectrum more efficiently. In recent years, the FBMC is attracting a significant attention due its potential advantages in various wireless communication applications. It offers benefits in scenarios with stringent spectral efficiency requirements, mMTC, and IoT applications. Despite its advantages, FBMC also has some challenges. It requires more complex signal processing algorithms compared to OFDM, which can increase the computational complexity of the receiver. Additionally, FBMC is not as widely adopted as OFDM, which means it may have limited interoperability with existing communication systems.

1.5.4 Universal Filtered Multi-carrier (UFMC)

The UFMC is a new MCM approach that introduced the sub-band filters in comparison to OFDM [38] to mitigate the levels of spectral side-lobe. This

enhances the flexibility to accommodate fragmented spectrum and enhances the resilience against various forms of ICI. Therefore, UFMC is consider a contender for the 5G wireless communication system and replaces OFDM with superior performance [39]. The fundamental concept of UFMC symbol generation is illustrated in figure 1.6. The following operations are implemented to generate UFMC symbols:

- Determine the number of subcarriers: UFMC divides the available bandwidth into subbands consist of multiple number of subcarriers. This number depends on the system requirements and the available bandwidth.

- Apply subcarrier mapping: Assign the data symbols to the subcarriers based on the specific mapping scheme used in UFMC. This mapping determines how the data symbols are distributed across the subcarriers of each subband. The input data is typically modulated onto each subcarrier using some form of digital modulation, such as M-ary QAM. The modulation scheme and parameters (e.g., constellation size, modulation order M) depend on the communication system requirements.

- Perform IFFT: Each subband data symbol is subjected to IFFT to obtain time-domain subband symbol.

- Subband Filtering: UFMC uses a prototype filter to shape the spectrum of each suband. The prototype filter should have good frequency selectivity properties to minimize interference between adjacent subcarriers. After processing through IFFT, each subband symbol is passed through an individual filter that shapes the frequency response of the suband. The purpose of these filters is to limit the out-of-band emissions and improve spectral efficiency.

- Once all subbands have been filtered, integrated to form a unified composite signal. That is sum up of all the shaped suband signals to obtain the UFMC symbol.

The composite UFMC signal is then amplified and transmitted over the wireless

medium using an appropriate antenna configuration.
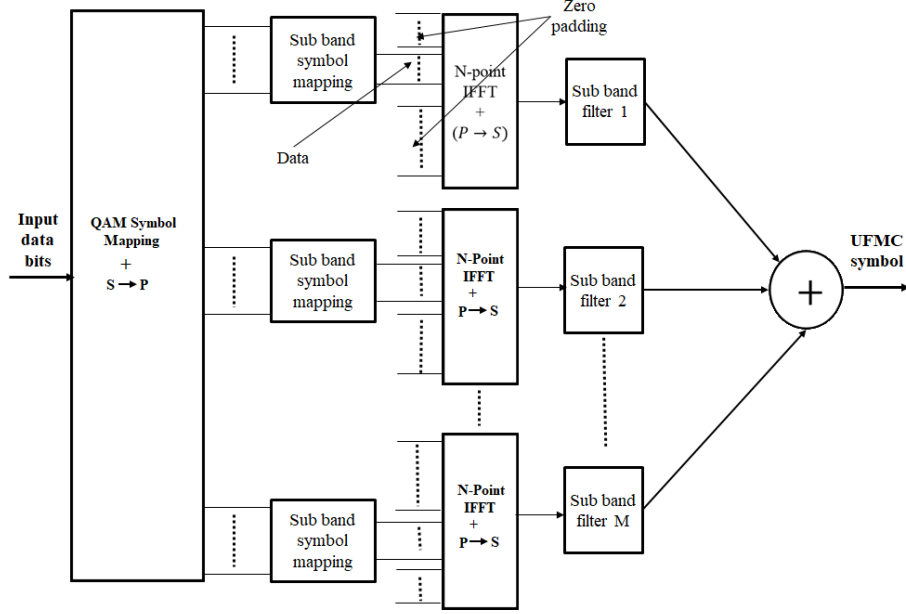
Figure 1.6: The UFMC transmitter block diagram adapted from [3]
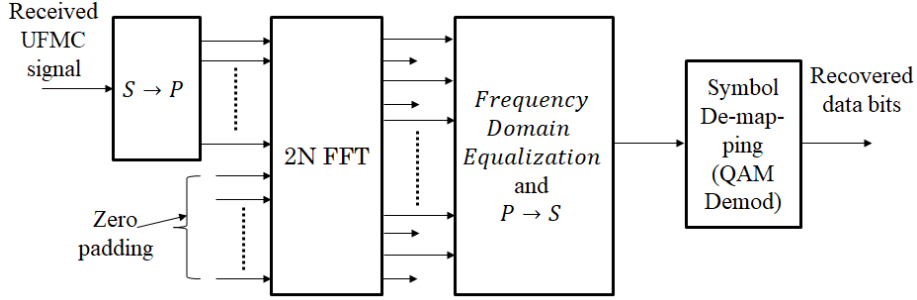
Figure 1.7: The UFMC receiver block diagram adapted from [3]

Consider a scenario of the UFMC system that divides the available spectrum into B subbands, and each subband is responsible for carrying Q subcarriers i.e., $N_D = BQ$. These subbands are processed through IFFT and subband filter with length of L_f to generate the UFMC signal. The final UFMC signal having a length of N+L_f-1 is

$$x\left(n\right) = \sum_{p=0}^{B-1} x_p\left(n\right) \tag{1.1}$$

Where n = 0,1,2,....N+L_f-2, $x_p\left(n\right)$ denotes the pth subband filter output, which is the linear convolution of d_p represents the data vector related p^{th} subband and

f_p represents the pth subband filter coefficients.

$$x_p(n) = \sum_{l=0}^{L_f-1} f_p(l)\, d_p(n-l) \tag{1.2}$$

where $f_p(n)$ is the center frequency shifted of the prototype filter impulse response $f(l)$ corresponding to the subband. That is given by

$$f_p(l) = f(l)\, e^{\frac{j2\pi}{N}(K_0+(p-1/2)Q)l} \tag{1.3}$$

Where $K_0 = (N - N_D)/2$ is the initial subcarrier index of the lowest subband of the UFMC signal. The $d_p(n)$ represents the N-point IFFT of pth sub-band written as

$$d_p(n) = \frac{1}{N} \sum_{k=0}^{Q-1} D_p(k)\, e^{\frac{j2\pi}{N}(K_0+(p-1)Q+k)n} \tag{1.4}$$

Where the sequence $D_p(k_p)$ represents the pth sub-band data samples. The pth sub-band data symbols in frequency-domain are given as

$$D_p(k_p) = \begin{cases} D((p-1)Q + k_p); & \text{for } k_p \in [0, Q-1] \\ 0; & Otherwise \end{cases} \tag{1.5}$$

Where $D(k)\,; k \in [0, N_D - 1]$ are the input data symbols in frequency-domain (QAM samples) The final UFMC symbol having the length $N + L_f - 1$, propagate through the transmission medium. The zeroes are padded to the received symbol at the receiver to performed 2N-point FFT. After 2N-point FFT transformation, only needs the even-numbered samples are extracted to estimate the data symbols on each subcarrier individually as shown in Fig 1.7 because the odd-numbered samples consist of interference component (proof of this given in chapter 3).

In comparison to OFDM, the CP duration is dropped and this extra duration required per symbol is implement by subband filters. The UFMC filtering scheme is characterized by the OFDM CP order that is comparatively shorter than the FBMC system. When compared to FBMC, this feature enhances the

26

suitability for short bursts transmission [3].

In summary, the UFMC is designed to address some of the limitations of traditional OFDM, like high OBE and poor spectral efficiency. It achieves this by using a sophisticated filtering technique that allows for better control over the spectral characteristics of the transmitted signal. Another benefit of UFMC is the flexible subcarrier spacing. Unlike OFDM, which has fixed subcarrier spacing, UFMC allows for non-uniform subcarrier spacing. This flexibility can be useful in scenarios where different subcarriers require different levels of robustness or where a more efficient utilization of the available bandwidth is desired. Therefore, the UFMC has been considered as a potential modulation technique for NGWN, such as 5G and B5G.

1.6 Contributions

The main findings of this thesis can be succinctly outlined as follows:

- **Modeling of the UFMC transceiver:** The final UFMC transmitted symbol is simplified and implemented it in frequency domain without filtering operation. In addition, the 2N-point FFT and decimation parts in the receiver systems are replaced with a single N-point FFT to process UFMC received symbol for the data detection.

- **Interference analysis in the UFMC due to filtering operation:** The variation of interference in the UFMC signal due to subband filter is analyzed and accordingly the optimal filter length is determined to minimize the interference. .

- **Impact of CFO in the UFMC system:** The effect on system performance is formulated and analyzed in the presence of CFO.

- **CFO estimation using SIT sequence:** Finally, the CFO estimated using SIT sequence with iterative process to improve the estimation accuracy for proposed system model.

1.7 Organization of the Thesis

The thesis is organized in the following manner:

Chapter 1 describes the technical evolution of the wireless systems towards the next generation and the contribution of this work.

Chapter 2 discusses the literature review on various methods of frequency offset estimation in the OFDM and UFMC systems.

Chapter 3 mainly focus on the proposed UFMC transceiver system model to reduce the computational and hardware complexity.

Chapter 4 covers the interference analysis due to filtering operation and the selection of optimal filter length to minimize the ICI and ISBI.

Chapter 5 presents the impact of CFO in UFMC system and the proposed CFO estimation method using superimposed training sequence.

Chapter 6 provides a conclusion of the thesis and outlines possible directions for future research.

1.8 Summary

The evolution of wireless networks has been trans-formative, reshaping how people connect, businesses operate, and technologies advance. The journey is ongoing, with future developments promising even greater connectivity and opportunities, but also requiring responsible and sustainable management of resources and security. In order to accommodate a diverse range of services, both 5G and B5G networks necessitate enhanced flexibility in their air interface. The Filtered waveforms play a crucial role in the design of a versatile air interface, as they facilitate the implementation of flexible numerology settings, asynchronous transmission, and the mitigation of OBE. There existed two distinct classifications of waveforms, namely sub-band-wise filtering and subcarrier-wise filtering. The filtered multicarrier waveforms typically exhibit superior spectrum confinement and enhanced resilience against time or frequency distortions. The utilization of sub-band filtering techniques, such as UFMC, proves to be appropriate in situations where the bandwidth remains

constant and wide-ranging. Conversely, subcarrier-wise filtering methods, like FBMC, are more suitable for scenarios that require adaptability in bandwidth and are limited to narrower ranges.

Chapter 2

Literature Survey

From early discussion, the NGWN such as 5G and 6G networks are expected to provide faster data rates, lower latency, increased spectral efficiency, more reliable, and more advanced wireless connectivity. 5G operates on high-frequency bands provide faster and more reliable wireless communication, and uses advanced technologies like massive MIMO, beam forming, and network slicing to increase network capacity and reduce latency. 5G also enables new use cases like autonomous vehicles, virtual reality, and smart cities. 6G networks are still in the early stages of development, and it's not clear yet what exactly they will offer. However, experts predict that 6G will be even faster, more reliable, and more intelligent than 5G. 6G is expected to use a combination of technologies, including the AI, IoT, and quantum computing, to enable new applications and services that we can't even imagine today.

To achieve these goals or to establish such a network, several design strategies must be incorporated at the level of diverse network layers. The modulation waveform technique and its multiple access methods at the physical layer level are defined the network transfer function that enables services of 5G and B5G. In this literature review, first we will discuss the various modulation waveforms that have been proposed for NGWN with system complexity and then we will discuss some of the recent studies on CFO estimation algorithms in UFMC.

2.1 Review on Modulation Waveforms

Modulation waveforms are key components of wireless communication systems, including 5G and 6G networks. They determine how data is

transmitted over the air and affect the system's capacity, spectral efficiency, and reliability. In recent years, various modulation waveforms have been proposed for 5G and 6G networks, aiming to meet massive connectivity with higher data speeds, low latency and energy efficient.

- **OFDM** is a well-known MCM waveform that has been used in many past and present wireless systems. In this the available frequency spectrum divided into many subcarriers and each subcarrier is carrying a portion of data. Because of its ability to support high data rates, adaptive modulation and coding, and its resilience to multi-path fading the OFDM has been proposed for the NGWN [31].

- **Filtered OFDM (F-OFDM)** is a modification of traditional OFDM that uses a variable-length filter to reduce spectral leakage and improve spectral efficiency. It also facilitates a higher degree of adaptability in the distribution of subcarriers, thereby mitigating interference and enhancing the overall system's performance [40].

- **FBMC** waveform has emerged as a prospective candidate for 5G and 6G networks that offers several advantages over the traditional OFDM waveform. It is also a MCM scheme that uses a bank of filters to divide the frequency band into smaller sub-bands. This helps in reducing the interference between the sub-carriers and also enables more flexible resource allocation. Several studies have shown that FBMC can achieve higher spectral efficiency and better performance in multi-path channels compared to OFDM [35, 37].

- **GFDM** is a modulation waveform that uses a combination of filter banks and pulse shaping to achieve a more flexible frequency and time domain resource allocation [33]. GFDM offers several advantages over OFDM, including lower out-of-band radiation and a higher degree of frequency selectivity. However, GFDM is more complex to implement compared to OFDM.

- **UFMC** is another multi-carrier modulation scheme that partition the

31

frequency spectrum into smaller subbands and then employs filters to reduce OBE. However, unlike FBMC, UFMC uses a single filter that is designed to have a frequency response that matches the desired sub-band [38]. This makes UFMC simpler to implement and more power-efficient compared to FBMC. The UFMC has been shown to offer better performance in doubly-selective wireless channels compared to OFDM.

The OFDM is currently the most widely used modulation waveform, but FBMC, GFDM and UFMC are all potential candidates for NGWN. The choice of modulation waveform will depend on various factors, such as system requirements, complexity, and cost. In recent years, UFMC modulation has garnered increasing attention as a potential solution for future wireless communication systems owing to its superior spectral efficiency and improved flexibility compared to other multi-carrier systems. Furthermore, the UFMC is highly suitable for short packet transmission and outperforming compared to OFDM and FBMC [3, 39]. However, the computational complexity increases because of its sub-band filtering and FFT processing in the UFMC transceiver model compared to the OFDM transceiver model. This complexity directly effects the cost of the system implementation, speed and power consumption. Therefore, it required to simplify or restructure the UFMC transceiver model without degrading the system performance to reduce the system complexity.

2.2 Review on System Complexity of UFMC

In general, the implementation complexity of UFMC is higher than the conventional CP-OFDM, due to the need for a more complex filtering operation. The complexity of a UFMC system can be assessed from various perspectives, including hardware implementation, signal processing algorithms, and computational requirements. Despite its higher complexity, UFMC has some advantages over OFDM, such as better spectral containment, higher flexibility in spectrum usage, and better performance in frequency-selective channels. Here are a few factors that contribute to the complexity of a UFMC

system:

- **Frequency domain processing**: UFMC involves frequency domain processing to achieve orthogonality between subcarriers. This requires performing DFT operations and matrix manipulations, which can be computationally demanding. These computations scales with the number of subcarriers.

- **Filtering and equalization**: UFMC relies on sophisticated filtering techniques to remove out-of-band emissions. The design and implementation of these filters may entail significant computational demands and necessitate intricate algorithms like FIR or IIR method. The level of complexity escalates proportionally with the quantity of subcarriers and the desired filtering characteristics.

- **PAPR reduction**: UFMC systems often employ techniques to reduce the PAPR, like clipping, filtering, or coding can introduce additional complexity due to the need for additional signal processing operations.

- **Channel/CFO estimation and equalization**: To combat the effects of channel impairments and frequency offset errors, UFMC typically requires channel/CFO estimation and equalization. This involves estimating the channel response/CFO and compensating for the channel distortions due these factors. The complexity depends on the channel model, the estimation algorithms used, and the desired level of equalization accuracy.

- **Implementation considerations**: The complexity of a UFMC system also depends on implementation factors including but not limited to hardware constraints, power usage, and real-time processing requirements. Efficient implementation techniques like FFT algorithms and parallel processing architectures can help mitigate complexity.

It's noted that the complexity of a UFMC system can vary depending on the specific design choices, performance requirements, and implementation

constraints. Therefore, a precise quantification of the overall complexity is challenging without specific details about the system configuration and constraints. The complexity of UFMC can be reduced by using efficient implementation methods, such as fast filtering algorithms, parallel processing, and optimized hardware architectures. Different research papers and standards have been proposed variations of UFMC with varying complexity trade-offs [41–47].

In [41], the transmitter complexity reduced by approximating the frequency domain UFMC signal. The fundamental concept underlying the suggested methodology is to exploit the inherent redundancy in the transmitted signal by employing a sparse FFT algorithm. By carefully selecting specific subcarriers and using the sparse FFT algorithm, the authors have successfully decreased the necessary operations for the transmitter processing. When an oversampling factor of 2 is employed, the overall complexity of UF-OFDM, as measured in terms of multiplications and additions, is found to be within a range of 2.4 to 10 times higher than that of CP-OFDM.

The proposed time-domain transmitter in [42], simplifies the implementation of UF-OFDM by using a reduced complexity filtering structure, and reduces the number of taps required in the filter. The authors also show that the proposed transmitter can be used with different filter designs and can provide flexibility in terms of the choice of filter length and number of subcarriers.

The paper [43], aims to execute computations pertaining to the three fundamental components of UFMC transmitter, when taking into account the requisite adaptability criteria such as size of the IFFT, filter length, and parameters linked to spectrum shifting. Therefore, initially, a simplified mechanism for computing the IFFT is suggested, which eliminates unnecessary radix-2 decimation in time (DIT) butterflies. Subsequently, a simplified hardware architecture for the filtering system is suggested to cut down on the multipliers. Ultimately, this paper presented for the production of a substantial quantity of intricate coefficients necessary for the purpose of spectrum shifting.

The proposed methodology in the study conducted by [44] involved the division of the resource blocks (RB) into two different classifications named as odd and even. In which the filtering operation is applied to only these two groups, instead of applying to each RB in the standard UFMC system. As a result, there are fewer IFFT and filtering operations, which results in a significantly reduced level of complexity.

The number of computations at the UFMC transmitter and receiver can be reduced through the implementation of the FFT pruning approach, which involves the removal of operations associated with zero inputs [45]. By this approach, an observed reduction of approximately 50% in both UFMC transmitter and receiver complexity has been noted, with no accompanying degradation in performance. The utilization of the FFT pruning technique in UFMC receivers results in reduced computational requirements in comparison to the traditional model. However, it necessitates extensive reprogramming efforts due to the dynamic variation of non-zero inputs.

In [46], the authors introduce a technique called composite pulse shaping, which combines multiple pulse shapes to achieve efficient spectral shaping while reducing hardware requirements. That means, first, they introduce a simplified pulse shaping technique that eliminates the need for a large number of complex filter structures. Secondly, by exploiting the specific characteristics of the UFMC signal, they are able to achieve efficient spectral shaping with reduced hardware requirements. This approach involves the use of polyphase filter banks to achieve efficient signal processing in the frequency domain and enables the reduction of hardware complexity by eliminating the need for multiple filters required in conventional UFMC transmitters.

Recently, a re-configurable baseband UFMC transmitter architecture [47] was proposed, which offers the ability to select the quantity of subcarriers per sub-band and the type of pulse-shaping filter to provide a high degree of flexibility. In [48], a proposal was put forth for an advanced receiver designed for the UFMC. This receiver utilises both odd and even numbered samples of

a 2N-point FFT in order to enhance performance during high computational demands. However, it should be noted that this approach does not alleviate the computational complexity burden associated with a 2N-point FFT.

2.3 Review on CFO Estimation Methods

One of the significant challenges in NGWN is CFO estimation, which refers to the deviation between the carrier frequency at the receiver and that at the transmitter. The CFO causes a reduction in the amplitude of subcarriers; non-orthogonality among the subcarriers results in ICI and loss in the system's BER performance [49, 50]. Accurate CFO estimation and compensation are crucial for achieving high performance in OFDM or UFMC systems. A simple implementation and robustness against synchronization errors have made UFMC as an emerging modulation scheme. Although UFMC is more immune to CFO than OFDM, it suffers severe degradation in performance when there is a significant CFO [51, 52]. The UFMC waveform is near to OFDM if there is no sub-band filtering operation in the UFMC. So, the estimation of CFO in UFMC systems can be achieved by utilizing the CFO estimation techniques employed in OFDM systems. The present literature survey will undertake a study of the algorithms for CFO estimation in OFDM systems and then we will discuss some of the recent studies on CFO estimation algorithms in UFMC.

Mainly there are two types of techniques used to estimate CFO:

Data-aided methods: In data-aided CFO estimation, the receiver exploits the pilot symbols (PS) or training symbols (TS) that are known and embedded within the transmitted signal to compute the frequency offset. These PS are typically inserted periodically into the data stream and carry known information. By comparing the received known symbols with their expected values, the receiver can estimate the CFO and correct it to recover the transmitted data accurately. The general steps involved in data-aided CFO estimation:

- Pilot Detection: The receiver detects and extracts the PS from the received signal. These PS are typically known and have a predefined pattern.

- Symbol Timing Recovery: Before CFO estimation, it is essential to recover the symbol timing accurately. This process involves estimating the start and end of each symbol in the received signal, which is typically done using techniques such as matched filtering or maximum likelihood estimation.

- CFO Estimation: With the known PS and accurate symbol timing, the receiver can estimate the CFO. The estimation can be performed through various algorithms, such as maximum likelihood estimation (MLE), least squares (LS) estimation, or correlation-based techniques.

  - In MLE-based method, in which first the likelihood function that represents the probability of observing the received signal for given CFO parameter is defined and then the receiver maximizes likelihood function to find the CFO value. This can be achieved by searching for the CFO value that yields the highest likelihood value. In practice, CFO estimation is often performed over a range of possible CFO values to ensure accurate estimation. One common approach is to perform a grid search over the CFO range of interest. The grid search involves evaluating the likelihood function for different CFO values within the range and selecting the CFO value that maximizes the likelihood.

  - LS-based method aims to minimize the mean square error (MSE) between the received signal and the reference signal which has been shifted by the CFO estimate. The CFO value that yields the minimum error is considered as the estimated CFO. The LS method is computationally efficient but requires many training symbols.

  - Correlation-based techniques exploit the periodicity of the PS to find the phase shift or frequency difference between consecutive PS, which corresponds to the CFO.

This approach compromised by the additional data transmitted in the form of pilots or training within/instead of the data symbols, resulting in sub-optimal

bandwidth utilization.

Blind methods: This estimation obviates the need for transmitting pilot or data symbols, and instead relies on the statistical characteristics of the received signal. Blind CFO estimation algorithms include the maximum entropy method, the cyclic statistics-based method, and the eigenvalue-based method.

In [53], the author introduced a novel frequency offset estimator utilizing the MLE approach, which relies on the deployment of two successive symbols that are the same. This method can handle frequency offsets up to half the subcarrier spacing. However, obtaining good performance requires a lot of symbols, which makes the use of bandwidth inefficient. Furthermore, this approach exhibits sensitivity to CFO fluctuations and exhibits sub-optimal performance when confronted with a substantial CFO magnitude. As a result, this method cannot guarantee the accuracy of the CFO estimation. The author also details a technique for increasing the detection range with shortened TS duration to identify the CFO. For example, the TS's length can be halved to extend the CFO acquisition range by a factor of two. While this methodology may be effective to a certain extent, it is essential to note that the accuracy of the estimations tends to deteriorate as the symbols become shorter. This is due to the fact that there are fewer samples available for averaging, and as a result, the training symbols must be retained for a longer duration than the guard interval. This is necessary to prevent distortion caused by the CIR during the frequency offset estimation process.

In [54], the CFO estimation technique explores the utilization of a pair of TS. The initial one is comprised of two indistinguishable halves and serves the purpose of approximating a frequency deviation that below the subcarrier spacing. Meanwhile, the second symbol encompasses a pseudo noise (PN) sequence that is utilized to expand the range of estimation. One limitation of this approach is its higher overhead, which is attributed to the utilization of two training symbols. The article referenced as [55] presents an expansion of the approach detailed in [54] that enhances the range of CFO estimation and eliminating the requirement for a second training symbol. This approach attains

38

superior precision with a subsequent rise in computational burden.

The paper [56] presents a novel scheme for estimating CFO in OFDM systems, which is a modified version of Moose's algorithm [53] . In this method, the procurement and monitoring of CFO are predicated through a TS block of fixed length that comprising multiple small, identical TS. The TS block's length is kept constant, so when the TS in a block is reduced in length, the number of TS should be increased in accordance. By reducing the length of each TS in a block and choosing the right estimator (single-h and multiple-h) at the same time, it is possible to reduce estimation errors even further and expand the CFO acquisition range.

In [57], a new approach for frequency synchronization, which exhibits a wider estimation range compared to the conventional method. This approach involves the implementation of a frequency offset estimation technique that comprises two distinct steps. The initial stage involves the correlation of the received signal with a local TS, thereby mitigating the impact of the TS. This approach ensures that the CFO's estimation range remains unaffected by the periodicity of the data in the TS. During the second stage, the received signal is subjected to correlation with its corresponding delay in order to get a precise estimation of the CFO. The conventional method relies on the period of the data in the TS to establish the CFO's estimation range. However, this method renders this factor irrelevant.

In [58], the suggested approach takes advantage of the envelop equalized processing, to transform the estimation of frequency offset into the estimation of the frequency of a complex tone.. Additionally, a new algorithm for calculating the frequency of complex tone is suggested. This method exhibits a significantly expanded estimation range while maintaining a comparable level of accuracy to that of methods presented in [55] and [54]. The performance of this approach remains unaffected by the characteristics of TS employed. Consequently, the TS intended for timing synchronisation or channel estimation can be utilized to gauge the frequency offset.

In [59–61] a pilot based method with different algorithms have proposed. In

pilot-based CFO estimation, a specific PS or tones are inserted within the transmitted data symbols at known positions. These PS are typically known to both the transmitter and the receiver. By examining the received PS within the received data symbols, the receiver can estimate the CFO. To estimate the CFO, the receiver correlates the received PS with the known PS. The correlation operation is performed by multiplying the received symbols with their conjugates and accumulating the results over a certain period. The resulting accumulated correlation provides an estimate of the CFO. But the bandwidth efficiency reduced due to transmission of PS and the power of the pilot is same as data, therefore lack of power efficiency. The accuracy of CFO estimation can be significantly improved by incorporating channel side information, as proposed in the methodology outlined in [62].

Some novel carrier offset estimators have been proposed in [63, 64], which make use of the CP redundancy in OFDM, without requiring any supplementary pilots. The efficiency of CP-based algorithms is contingent upon the presence of surplus CP, that is, the CP length selected beyond the extent of the fading channel. Furthermore, these schemes have the capability to solely approximate the frequency offset towards the nearest subcarrier. The efficacy of these methods is predominantly contingent upon the extent of the control period, and typically necessitates a control period duration that exceeds that of the channel response.

An algorithm for blind carrier offset estimation proposed in [65], that achieves high performance while maintaining low complexity. To accomplish this the intrinsic structural information of OFDM signals is used. The algorithm provides a level of precision comparable to that of the super-resolution subspace method, namely MUSIC (MUltiple SIgnal Classification), while avoiding the need for computationally demanding subspace decomposition. The null subcarriers were observed to exhibit minimal power in the CFO analysis. The MUSIC technique uses only one OFDM symbol to estimate the CFO and it's estimation accuracy could be impacted by noise. Consequently, it is necessary to employ a multiple OFDM symbols to mitigate the impact of noise during the

estimation of CFO.

In [66], introduces a new strategy for tackling the challenge of CFO estimation, which does not rely on the utilization of reference symbols, pilot carriers, or excess CP. This methodology offers a carrier offset estimation technique with high precision, by exploiting the intrinsic structure of OFDM signals. Despite potential distortion from an unspecified carrier offset, the OFDM symbol retains a discernible algebraic structure that can be utilized for blind carrier estimation. The estimator that has been suggested in an analytical format and does not impose any constraints on the acquisition range, unlike certain other algorithms. One noteworthy characteristic of the subspace-based algorithm under consideration is its ability to provide a level of performance comparable to that of a super-resolution subspace algorithm, specifically ESPRIT [67].

In [68], the proposed method which is based on a diagonality criterion and does not necessitate any priori information regarding the channel or transmitted data. When there is no CFO, the received signal's auto-correlation exhibits a diagonal pattern, where the off-diagonal components exhibit negligible values. The inclusion of a CFO results in the non-orthogonality between the sub-carriers, thereby causing a non-diagonal configuration. In accordance with this property,the calculation of CFO is performed by the process of power minimization in the non-diagonal elements.

According to the methodology proposed in [69], involves virtually dividing one OFDM symbol received at the receiver into two distinct OFDM symbols with a temporal disparity. This is achieved through the utilization of both the two-fold oversampling and the CP. A cost function that mathematically represented as a cosine function is established for the estimation of CFO through the utilization of these two distinct OFDM symbols and also closed-form expression for estimating CFO is obtained by utilizing the characteristic of this cosine function. The proposed approach in [70], involves the use of a cost function based on Kurtosis for blind CFO estimation. In order to minimize the cost function, it is necessary to collect a greater number of OFDM symbols. In contrast to training,

blind estimation typically necessitates a lengthy data record. Therefore, its applicability is restricted to channels that vary slowly over time and involves a high degree of complexity.

The paper [71], introduces a novel computationally efficient blind CFO estimator for MIMO-OFDM systems. A meticulously crafted cost function is formulated such that it can be precisely represented as the combination of a limited number of harmonically linked cosine waves, even in the presence of noise. By utilizing this particular characteristic, it has been determined that the process of minimizing the cost function that has been designed can be executed in a manner that is computationally efficient. This eliminates the need for a thorough and exhaustive grid search procedure. This approach aims to refine the estimator through the incorporation of an extra one-step adjustment, thereby enhancing the accuracy of estimation outcomes.

The paper [72], presents a comprehensive analysis of the impact of frequency-selective channels on the effectiveness and detect-ability of non-data aided techniques for the OFDM systems that incorporate null subcarriers. That is, this method uses the null sub-carriers, which are subcarriers that transmit zero, with unique spacing in order to address the problem of identification..

In [73], the authors introduces a sub-optimal approach for estimating the CFO by use of null subcarriers. The proposed methodology involves partitioning the CFO into its integer and fractional components, wherein the fractional CFO is initially estimated, then the estimation of the integer CFO. This methodology involves the imposition of null subcarriers on all odd subcarriers within the training OFDM symbol. The correlation operation can be applied to estimate the fractional part of the CFO within the range of two subcarrier spacing, resulting in the loss of orthogonality among subcarriers. The estimation of the integer component of the CFO, leading to a displacement of the subcarrier indices, is accomplished through the effective use of subcarriers positioned at even intervals.

Recently, CFO estimation for UFMC has been studied in some interesting ways,

where LS is one of the widely used solutions [74–79].

The paper [75] outlines the development of a resilient hybrid CFO estimation method that uses two identical TS, specifically designed for systems based on UFMC technology. This methodology involves the derivation of a CFO estimator using a LS criterion. This estimator is employed to obtain a preliminary estimation of the coarse CFO by utilizing a wide frequency searching grid. Subsequently, the residual CFO is precisely evaluated by means of the auto-correlation of the received signals that have undergone compensation. The algorithm exhibits characteristics of increased estimation range and improved estimation precision.

In [76], introduces a preamble configuration utilizing the Zadoff-Chu (ZC) sequence as the foundation for UFMC-based systems to estimating CFO. The aforementioned plan is primarily bifurcated into two distinct stages. Initially, a rudimentary technique for estimating the carrier frequency offset is elucidated using the MLE algorithm. The searching step of this approach is also examined, with emphasis on its computational simplicity. As per the preamble structure, the compensated preamble can be used for the purpose of finely estimating residual CFO through correlation. Nonetheless, this approach has a drawback of superfluous transmission, leading to a decrease in bandwidth efficiency, particularly for sporadic communications.

In [77], the authors suggest a straightforward technique for estimating CFO in UFMC systems. This method offers significant reduction in computational complexity while also ensuring exceptional performance. Initially, a selection criterion of low complexity is devised, which is based on the principle of the bisection method. This criterion is applied to gradually reduce the frequency range of concern through iterative processes. Subsequently, the estimation of CFO is accomplished through a closed-form expression that has been derived from the Taylor series expansion technique.

The paper [78], outlines a blind estimation method for estimating CFO in the UFMC system, and is designed to operate within the confines of a

43

predetermined carrier assignment. One UFMC symbol and a smaller number of complex multiplications that are required by this scheme to produce fractional CFO estimation, specifically by taking advantage of the characteristic of auto-correlation functions. Moreover, the CFO in integer form is chosen from the permissible contenders that minimize the frequency response of the CFO compensated signal that corresponds to the designated subcarriers with null values.

In the context of OFDM systems, conventional channel estimation methods typically involve the utilization of a pilot symbol assisted scheme. This scheme entails the insertion of pilot tones within the OFDM symbol to facilitate channel estimation. However, this approach necessitates additional bandwidth for transmitting pilot symbols, which results in a reduction in spectral efficiency and transmission rate.

The superimposed training (SIT) scheme was suggested as an alternative to the pilot-based method for the purpose of achieving more efficient transmission and offers the benefit of maintaining the data rate without any loss, thereby facilitating greater efficiency in terms of bandwidth utilization. The technique of SIT for channel estimation has been extensively researched in previous studies, as evidenced by sources [80–84]. In this approach, the interference of the data sequence is perceived during estimation, necessitating the use of an effective method to eliminate it. In order to mitigate interference, M. Ghogho devised a novel technique for single carrier block transmission systems, referred to as "Data Dependent Superimposed Training" as detailed in [82]. In order to prevent its interference, the periodic training is created based on the data sequence. The implementation of this technique has the potential to completely eradicate the impact of data sequence on channel estimation, resulting in a higher degree of precision in estimation. The limitations of some of the reviewed research papers or existing techniques that are proposed recently for complexity reduction in the UFMC system and for the CFO estimation are listed briefly in Table 2.1 and Table 2.2 respectively.

Table 2.1: Some of reviewed research papers on the UFMC complexity

Reference	Methodology	Limitations/gaps
T. Wild and F. Schaich, "A reduced complexity transmitter for UF-OFDM," IEEE Veh. Technol. Conf. (2015) [41]	Each sub-band is constructed with small IFFTs and FFTs ,the filtering is executed as multiplication in the frequency domain and the overlapping sub-bands with their side-lobes are superimposed in a large 2-N point IFFT.	Used two stage process: At stage 1, 64-IFFT's and at stage 2, 2N-point IFFTs. Still 10 times more complex than the conventional OFDM
Jafri etc., "Hardware Complexity Reduction in UFMC Transmitter Implementation" IEEE Access (2017) [43].	The system complexity was reduced in three aspects: IFFT complexity reduction, FIR filtering complexity reduction, and simplified spectrum shift coefficients generation	Filtering and spectrum shifting operation is still included
M. Saad"UFMC Transceiver Complexity Reduction", 25th Int. Conf. Telecommun. ICT (2018) [45]	The FFT pruning concept is applied to reduce the unnecessary computation at FFT/IFFT processing	Burden of sub-band filtering not removed
Z. Guo etc., "Low Complexity Implementation of Universal Filtered Multi-Carrier Transmitter", IEEE Access(2020) [46]	Introduce the FIR filter with poly-phase structure	Burden of subband filtering not removed

2.4 Motivation and Research Gaps

All the proposed methods might be inefficient in terms of either bandwidth or BER performance in high mobility scenarios and at high carrier frequency. Because the major computational complexity in the UFMC receiver system includes the 2N-point FFT processor, the channel estimation, and equalization algorithms. Therefore we motivated from this to improve the spectral efficiency and system performance at low cost of complexity. From this study, we found some of the gaps and those are

Table 2.2: Some of the reviewed research papers on CFO estimation for UFMC

Reference	Methodology	Limitations/gaps
X. Wang etc., "Pilot-Aided Channel Estimation for Universal Filtered Multi-Carrier", 2015 IEEE 82nd Vehicular Technology Conference (2015) [74]	Inserting pilot symbols at equi-spaced in frequency or time domain to estimate channel and CFO.	CFO estimation is not guaranteed when the pilot tones undergo deep fading Consume some bandwidth and power
Y. Li etc., "A Novel Hybrid CFO Estimation Scheme for UFMC-Based Systems," IEEE Commun. Lett., (2017) [75].	Two consecutive identical UFMC symbols are employed to estimate CFO	Low spectral efficiency
Q. Liu and G. Kai, "An Effective Preamble-based CFO Synchronization for UFMC Systems," in 10th International Conference on Communications, Circuits and Systems. (2018) [76]	Two consecutive and almost identical OFDM symbols are employed to estimate CFO	Low spectral efficiency
F.-H. Hwang, "Blind CFO Estimation in a UFMC System Aided with Virtual Carriers," IEEE Trans. Veh. Technol.s(2022) [78]	Uses virtual subcarriers (VSC) or inherent structure of UFMC symbol	largely dependent on the number of VSC and suffers the error floor effect in the presence of frequency-selective fading channels
T.-T. Lin and F.-H. Hwang, "Design of a Blind Estimation Technique of Carrier Frequency Offset for a Universal-Filtered Multi-carrier System over Rayleigh Fading," IEEE Wirel. Commun. Lett. (2022) [79]	Inserting zero-valued (null) pilot in regular intervals	Low spectral efficiency

- The UFMC system exhibits a higher level of transmitter and receiver complexity when compared to the CP-OFDM system. This is primarily due to the need for a more complex filtering operation at the transmitter and a 2N-point FFT processor at the receiver. Its require a simplified transceiver structure to reduce the system complexity.

- In data-aided estimators, training sequences/pilot symbols are inserted in the time domain or frequency domain to determine CFO. In this type of estimators, some part of data symbol used to send training sequence to get good accuracy. The main drawback of this approach is that the utilization bandwidth and power is not good.

- As to blind estimators for CFO estimation are good in terms of bandwidth efficiency, but computationally more complex. At high mobility scenarios and at high carrier frequency (mmWave) bands, these methods are not good due to the lack of knowledge of transmitted data and channel variability. The other two methods, cyclic prefix based and null subcarrier based also consume some bandwidth to get good accuracy in CFO estimation

2.5 Problem Statement

"An efficient carrier frequency offset compensation technique using superimposed training sequence in next generation wireless networks".

Here the term "efficient" is defined in terms of the system complexity, spectral efficiency and the system performance after applying the proposed method. The term "efficient" typically implies that a model is designed to perform well with minimal computational resources such as a smaller number of parameters, reduced memory and processing requirements, and faster training and inference times, to minimize energy usage where power consumption is a critical factor. Therefore, this thesis work contributes a simplified transceiver structure to generate the UFMC base band signal and the estimation algorithm to estimate CFO and channel impulse response.

2.5.1 Objectives

The objectives of this thesis can be enumerated as follows:

- To model the UFMC system for 5G and beyond 5G wireless systems to reduce system complexity in terms of computations. This objective aims to develop and enhance the UFMC transmitter and receiver systems, with a focus on various aspects including filter design, IFFT/FFT processing that minimize the computational load while maintaining its performance. Also, conducting trade-off analyses between complexity and performance metrics, such as BER, and power efficiency. This can help find the right balance in system design.

- Analyze the interference (ICI and ISBI) in the UFMC and optimal filter length design to minimize the interference.This objective of study is to investigate and develop interference mitigation techniques that can be applied in UFMC systems. These may include filtering, or adaptive signal processing methods. Also evaluate the SIR for UFMC signals in the presence of interference and calculate the SIR under different interference scenarios to determine the system's robustness and performance.

- The estimation and compensation of the CFO using superimposed training sequence for UFMC based systems
  Sub-objective-1: Investigate how the UFMC systems perform under varying CFO conditions. Assess the system's robustness and the maximum allowable CFO that can be tolerated without a significant degradation in performance. Measure and analyze the BER or symbol error rate (SER) in UFMC system with different CFO levels. Determine how CFO affects signal quality and quantify the performance degradation. Sub-objective-2: Develop method and algorithm to estimate and compensate for CFO in UFMC systems. Compare the BER performance, complexity and cost of implementing the proposed algorithm with conventional methods. Analyze the hardware requirements and implications for CFO compensation in UFMC systems.

48

2.6 Summary

In summary, 5G and beyong 5G utilizes a range of modulation waveforms, each tailored to specific use cases and scenarios. These waveforms aim to provide high data rates, low latency, improved spectral efficiency, and robust performance in diverse communication environments. The choice of waveform depends on factors such as channel conditions, mobility requirements, and the specific needs of the application or service being supported.While UFMC offers benefits in terms of spectral efficiency and performance in frequency-selective channels, it introduces complexities in filter design, receiver processing, and sophisticated signal processing algorithms. These complexities must be carefully addressed in the design and implementation of UFMC systems to realize their potential advantages in practical communication scenarios.

The accurate CFO estimation is vital for the performance of UFMC-based communication systems. Various algorithms, including the Schmidl-Cox algorithm, pilot-based methods, and maximum likelihood estimation, are employed to address the challenges associated with CFO in UFMC systems. The choice of CFO estimation technique depends on the specific system requirements and implementation considerations.

Chapter 3

Modeling of the UFMC Transceiver

In early chapter we have seen the conventional UFMC system model, that says the system complexity is more compared to the OFDM because of filtering and FFT operations in terms of computations and hardware requirement. In this chapter,we proposed an efficient UFMC transceiver model.

The term "efficient" typically implies that a model is designed to perform well with minimal computational resources such as a smaller number of parameters, reduced memory and processing requirements, and faster training and inference times, which can be crucial for various applications. Also the model is designed to minimize energy usage where power consumption is a critical factor. In hardware design, efficient models can refer to specialized hardware (e.g., ASICs or FPGAs) designed to provide high performance while minimizing power consumption. The efficiency in models can be measured in various ways, including FLOPs (floating-point operations per second), model size, inference speed, and memory usage. The choice of an efficient model depends on the specific use case and the trade-offs between model efficiency and task performance. Here, primarily we focuses on the evaluation of system complexity, and the base-band signal generation with less number of computations (FLOPs) at both the transmitter and receiver.

The UFMC transmitter model is designed to efficiently utilize the available spectrum while providing robust communication in the presence of interference and channel impairments. It is particularly well-suited for applications that require a high degree of spectral efficiency and resilience to interference, such as 5G and beyond.

3.1 The UFMC Transmitter

The UFMC system model's functional block diagram is depicted in Figure 3.1.

The UFMC transmitter divides the total available data subcarriers are into several sub-bands consist of finite consecutive subcarriers. After performing the sub-carrier mapping, each sub-band is processed through IFFT. These time-domain sub-band signals are filtered individually with an FIR filter and summed to generate the UFMC signal. In case of multi-service/user based communication system, multiple PRBs allocated to each user or service is considered as sub-band. Let consider the general UFMC system having B subbands and each one carries Q_p consecutive subcarriers i.e., $N_D = \sum_{p=0}^{B-1} Q_p$; p = 0,1,..., B-1. The final UFMC signal having a length of N+L_f-1 is

$$x(n) = \sum_{p=0}^{B-1} x_p(n) \tag{3.1}$$

Where n = 0,1,2,....N+L_f-2, L_f is the order of subband filter and $x_p(n)$ represents the pth subband filter output, which is the linear convolution of the time-domain representation of pth subband data and the corresponding subband filter's impulse response.

$$x_p(n) = \sum_{l=0}^{L_f-1} f_p(l) d_p(n-l) \tag{3.2}$$

where $f_p(n)$ represents the vector of pth subband filter coefficient, which are determined by shifting the impulse response of a prototype filter $(f(l))$ at its the center frequency of the corresponding to the sub-band. That is given by

$$f_p(l) = f(l) e^{\frac{j2\pi}{N}(K_0 + K_{pshift})l} \tag{3.3}$$

In the above expression 3.3, K_0 represents the index of the lowest subband of the UFMC signal's starting subcarrier and the frequency shift of $K_{pshift} = \sum_{b=0}^{p-1} Q_b + Q_p/2$ The time-domain signal $d_p(n)$ represents the N-point IFFT

51

of pth sub-band written as

$$d_p(n) = \frac{1}{N} \sum_{k=0}^{Q_p-1} D_p(k) e^{\frac{j2\pi}{N}(K_0+K_p+k)n}; n \in [0, N-1] \tag{3.4}$$

Where the sequence $D_p(k)$ represents the pth sub-band data samples and $K_p = \sum_{l=0}^{p-1} Q_b$. The pth sub-band data symbols in frequency-domain are given as

$$D_p(k) \begin{cases} D(K_{p-1}+k); & \text{for } k = 0, 1, ...Q_p - 1 \\ 0; & Otherwise \end{cases} \tag{3.5}$$

Where $D(k) = [D(0), D(1), \ldots, D(N_D - 1)]$ are the input data symbols in frequency-domain are typically modulated onto each subcarrier using some form of digital modulation, such as M-ary QAM. The final UFMC symbol having the length $N + L_f - 1$, transmitted through the wireless channel. The UFMC receiver model is shown figure 3.1. At the receiver, the zeros are padded to the received UFMC signal y(n) to process through 2N-point FFT. The UFMC signal after zeros padding is

$$y_{zp}(n) = \begin{cases} y(n) = x(n) * h(n) + z(n); & \text{for } 0 \leq n \leq N + L_f - 2 \\ 0; & \text{for } N + L_f - 1 \leq n \leq 2N - 1 \end{cases} \tag{3.6}$$

The term $z(n)$ denotes the complex valued AWGN samples. The output of 2N-point FFT is defined as

$$Y_{2N}(m) = \sum_{n=0}^{2N-1} y_{zp}(n) e^{\frac{-j2\pi}{2N}mn} \tag{3.7}$$

The output of 2N-point FFT is defined as

$$Y_{2N}(m) = \sum_{n=0}^{2N-1} y(n) e^{-j\frac{2\pi}{2N}mn} = X_{2N}(m) H_{2N}(m) + Z_{2N}(m) \tag{3.8}$$

Where $X_{2N}(m)$, $H_{2N}(m)$ and $Z_{2N}(m)$ are the 2N-point DFT of the signals
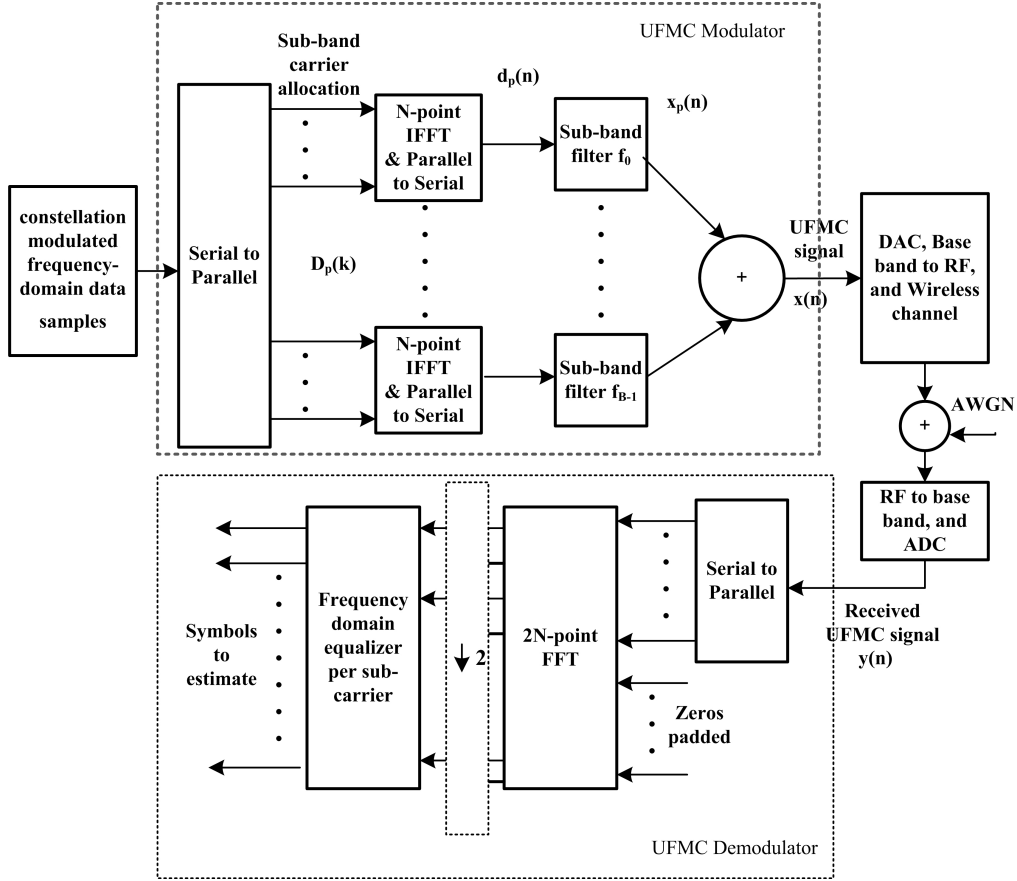
Figure 3.1: A schematic block diagram for UFMC system adapted from [3]

x(n), h(n) and z(n) respectively.

$$X_{2N}\left(k\right) = \sum_{n=0}^{2N-1}\sum_{p=0}^{P-1} x_p\left(n\right) e^{-j\frac{2\pi}{2N}kn} = \sum_{p=0}^{P-1} X_{p,2N}\left(m\right) \qquad (3.9)$$

The 2N-point DFT of $x_p\left(n\right)$ is denoted as $X_{p,2N}\left(m\right)$:

$$X_{p,2N}\left(m\right) = \sum_{n=0}^{2N-1}\sum_{l=0}^{L_f-1} f_p\left(l\right) d_p\left(n-l\right) e^{-j\frac{2\pi}{2N}mn} \qquad (3.10)$$

By substitute $d_p\left(n\right)$ that defined by equation 3.4 and perform the some mathematical operations, we will get

$$X_{p,2N}\left(m\right) = \frac{1}{N}\sum_{k=0}^{N-1} D_p\left(k\right) F_p\left(k\right) \sum_{n=0}^{2N-1} e^{-j\frac{2\pi}{N}\left(m/2-k\right)n} \qquad (3.11)$$

53

For even-numbered samples, m = 0, 2, ..., 2N-2 and k = m/2

$$X_{p,2N}{}^{even}(m) = 2D_p(m/2) F_p(m/2) \qquad (3.12)$$

Where S_p and F_p are the N-point FFT of s_p and f_p respectively. Similarly for odd-number samples m = 1,3,...,2N-1 or k $\neq$ m/2;

$$X_{p,2N}{}^{odd}(m) = \frac{1}{N} \sum_{k=0}^{N-1} D_p(k) F_p(k) \frac{1 - e^{-j\frac{2\pi}{N}(m/2-k)(N+L_f-1)}}{1 - e^{-j\frac{2\pi}{N}(m/2-k)}} \qquad (3.13)$$

$$X_{p,2N}{}^{odd}(m) = \frac{1}{N} \sum_{k=0}^{N-1} \left(D_p(k) F_p(k) e^{-j\frac{\pi}{N}(m/2-k)(N+L_f-2)} \right)$$
$$\left(\frac{\sin\left(\frac{\pi}{N}(m/2-k)(N+L_f-1)\right)}{\sin\left(\frac{\pi}{N}(m/2-k)\right)} \right) \qquad (3.14)$$

It is evident from equations 3.12 and 3.14 that the retrieval of data symbols can be achieved directly through even-numbered samples. However, the recovery of data symbols through odd-numbered samples is not feasible due to the interference component's presence. Hence, the receiver performs data detection on the even-numbered samples while discarding the odd-numbered samples. Therefore, from these 2N-subcarriers only the even subcarriers are extracted for data detection at receiver as they exclusively are composed of the data. Conversely, the odd numbered subcarriers are not utilized for data detection due to the presence of interference. The even subcarriers are

$$Y_{even}(k) = Y_{2N}(2k) = \sum_{n=0}^{2N-1} y_{zp}(n) e^{\frac{-j2\pi}{N}kn} \qquad (3.15)$$

The structure of the receiver is realized by making use of a 2N-point FFT and decimator components, which is depicted in Figure 3.1.

3.2   Proposed UFMC Transmitter Model

Mathematical models govern all facets of historical and contemporary wireless communication networks, that are derive from either theoretical principles or field measurement.   These models are employed in the preliminary stages of network planning and deployment, network resource management, to control network parameters and it's control.   Nevertheless, every model is inevitably distinguished by an intrinsic compromise between its precision and its feasibility.   From this perspective, the mathematical representation of the UFMC signal is simplified to reconfigure the UFMC transmitter and receiver for faster transmission. The simplification of the model as follows below:

From the equation (1.2), the pth sub-band filter output is written as

$$x_p(n) = \frac{1}{N} \sum_{k=0}^{Q-1} D_p(k) e^{\frac{j2\pi}{N}(K_0+pQ+k)n} \sum_{l=0}^{L_f-1} f(l) e^{\frac{-j2\pi}{N}(k-\frac{N+Q}{2})l} \qquad (3.16)$$

For simplicity, here assumed $Q_p = Q$; for $p = 0, 1, ..., B-1$, that is the total subcarriers are uniformly distributed among the all users/services.
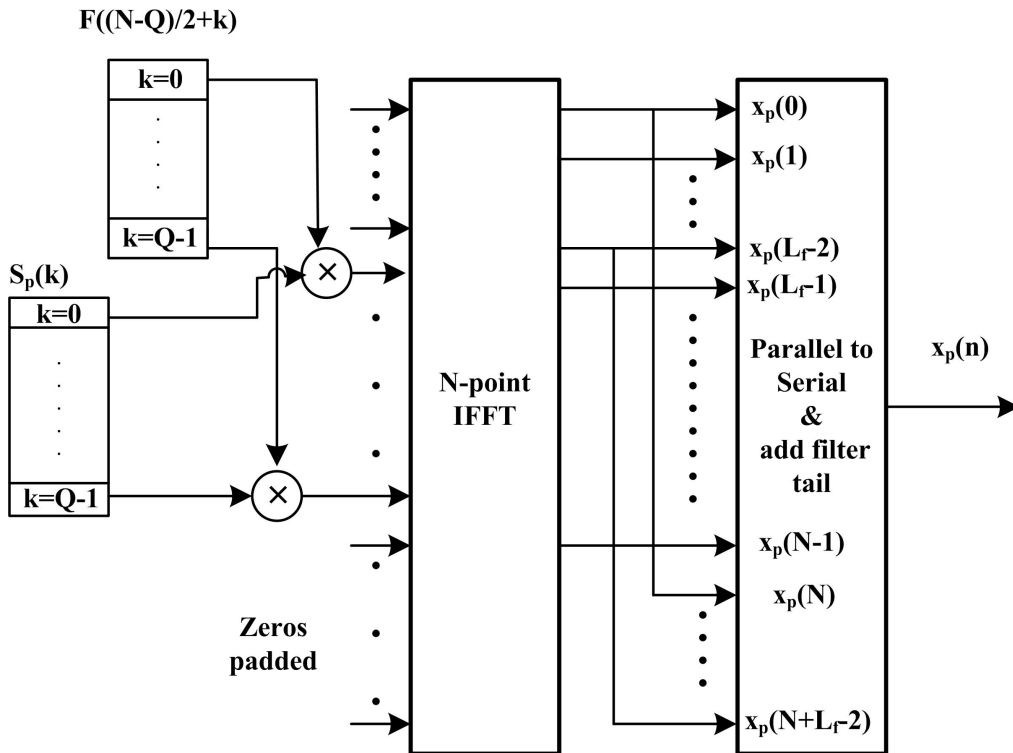

Figure 3.2: The proposed UFMC transmitter model

55

$$x_p(n) = \frac{1}{N} \sum_{k=0}^{Q-1} D_p(k) F\left(\langle k - \frac{N+Q}{2} \rangle_N\right) e^{\frac{j2\pi}{N}(K_0+pQ+k)n} \qquad (3.17)$$

Where F(k) is the N-point DFT of the proto-type filter f(l) and $\langle . \rangle_N$ represents the circular shift or modulo N operation.

$$F\left(\langle k - \frac{N+Q}{2} \rangle_N\right) = F\left(\frac{N-Q}{2} + k\right) = F_Q(k) \qquad (3.18)$$

$$x_p(n) = \frac{1}{N} \sum_{k=0}^{Q-1} D_p(k) F\left(\frac{N-Q}{2} + k\right) e^{\frac{j2\pi}{N}(K_0+pQ+k)n} \qquad (3.19)$$

From equation 3.19, it is observed that the first N-points of the sub-band filtered output are the N-point IDFT of the product of frequency-domain data samples of the sub-band and $F\left(\frac{N-Q}{2} + k\right); k = 0, 1, \ldots, Q-1$ and the last $L_f - 1$ points (filter tail) are equivalent to the first $L_f - 1$ point of N-point IDFT, which is implemented as shown in Figure 3.2.

Generally, the filtering operation gives linear convolution and the combination of FFT-IFFT operation produces the circular convolution output. In the proposed UFMC transmitter, the filter tails are the overlapped samples that are obtained from the addition of last samples $L_f - 1$ to the first of linear convolution, which results more interference (aliasing effect) on the adjacent sub-bands in the form of OBE. This interference effect can be reduced by computing the filter tails using the relationship between linear and circular convolution. From the basic computation methods, the circular convolution sequence can be obtained by wrapping around the last $L_f - 1$ samples of linear convolution and add to the first $L_f - 1$ samples of it. The sum of sequence is same for both linear and circular convolution. From these concepts, the we need to compute the filter tail in the UFMC signal and then compensate the aliasing effect in the first $L_f - 1$ samples of the UFMC signal. Alternatively, this can be reduce further by tracking the filter tail samples can be track using AI/ML algorithms. This is the future scope of this work.

3.2.1 Computational Complexity Analysis

The computational complexity associated with the conventional UFMC transmitter can be segregated into two distinct stages. The first stage involves the B IFFTs of size N, while the second stage pertains to the B linear convolution operations (filtering operation). Accordingly, the total number of computations required at the UFMC transmitter to generate the UFMC symbol is

$$CM_{UFMC,C} = B.\, CM_{IFFT}\,(N) + B.\, CM_{filter}\,(N + L_f - 1) \qquad (3.20)$$

Where $CM_{IFFT}\,(N)$ is the number of real multiplications and additions (arithmetic operations) required for computing N-point FFT is given by

$$CM_{FFT}\,(N) = \begin{cases} 5N\log_2 N; & \text{with radix-2 FFT [85]} \\ 4N\log_2 N - 6N + 8; & \text{with split radix FFT [86]} \end{cases} \qquad (3.21)$$

The computational complexity of a linear convolution operation with N and L_f as the input sequence lengths $CM_{filter}\,(N, L_f)$ is NL_f complex multiplications. The total number of arithmetic operations required for the linear convolution operation is

$$CM_{filter}\,(N, L_f) = 6NL_f \qquad (3.22)$$

It should be noted that every instance of complex multiplication necessitates four real multiplications and two real additions (6 real operations), while each instance of complex addition requires two real additions.

For the proposed UFMC transmitter model, the subband data processing is implemented by use of the N-point IFFT with input as a product of subband data samples and the corresponding frequency shifted values of subband filter response. According to this implementation, the number of arithmetic operations required to generate the UFMC symbol for the proposed model is

$$CM_{UFMC,P} = (B + 1)\,CM_{FFT}\,(N) + 6BQ + CM_{filtertail} \qquad (3.23)$$

The number of computations for conventional and proposed models is shown in Figure 3.3 according to the equations 3.20 and 3.23. The computational complexity reduction ratio (CCRR) can be defined as the ratio of computational complexity (arithmetic operations) of a conventional UFMC transmitter to the computational complexity of the proposed model. From these results, the computational complexity can be reduce approximately 8 times for N = 512 and 13.5 times for N = 1024.
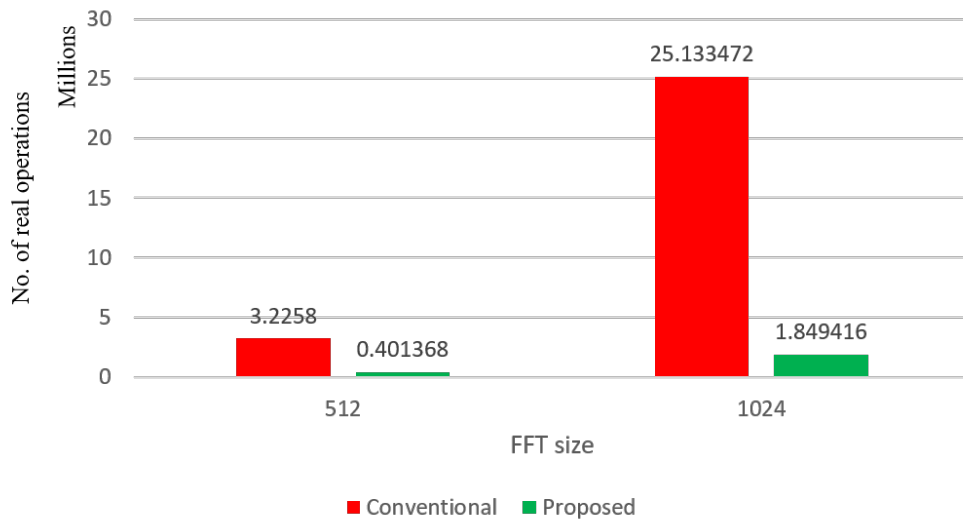
Figure 3.3: Number of computations comparison

3.2.2 Performance Analysis

Here, we simulate the both proposed and conventional UFMC transmitter system with the following parameters: FFT size of 1024, subband size of 12 SCs and the filter length of 73 to compare the power spectral density with CP-OFDM. Filter tails in the proposed UFMC transmitter are overlapped samples, leading to increased interference on neighboring sub-bands via OBE. This produced more emission in the adjacent subbands as shown in Figure 3.4.
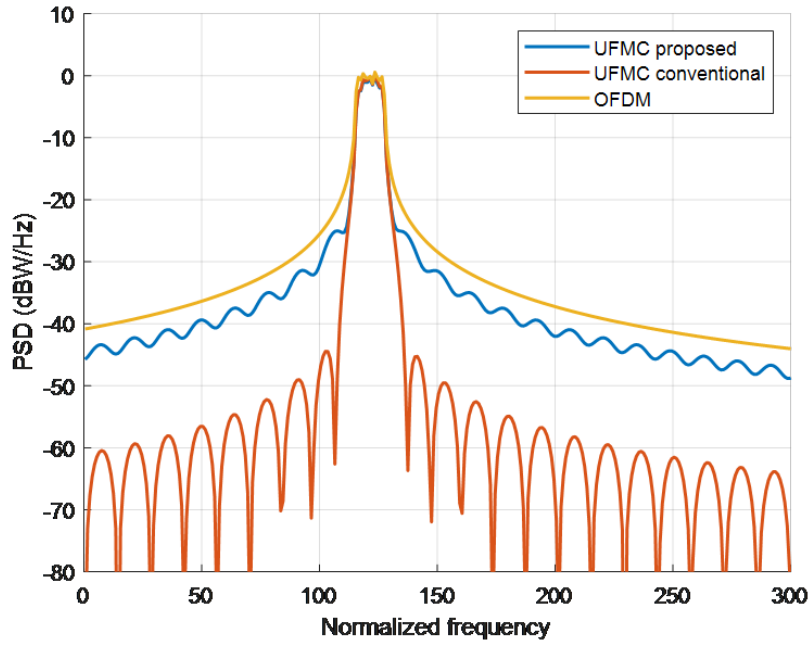
Figure 3.4: Power Spectral Density (PSD) comparison

Because of this high OBE, which may not suitable for the short burst data transmission. An alternative approach involves further reduction through the utilization of AI/ML algorithms to track the filter tail samples from the data obtained after IFFT processing. As shown in the Figure 3.5, the BER performance is almost closer to the conventional CP-OFDM since the proposed UFMC system is look like CP-UFMC.

3.3 Modeling of the Proposed UFMC Receiver

The even-numbered samples/sub-carriers of 2N-point FFT are defined as

$$Y_{even}(k) = Y_{2N}(2k) = \sum_{n=0}^{2N-1} y_{zp}(n) e^{\frac{-j2\pi}{N}kn} \tag{3.24}$$

We rewrite equation 3.24 as

$$Y_{even}(k) = \sum_{n=0}^{N-1} y_{zp}(n) e^{\frac{-j2\pi}{N}kn} + \sum_{n=N}^{2N-1} y_{zp}(n) e^{\frac{-j2\pi}{N}kn} \tag{3.25}$$

59
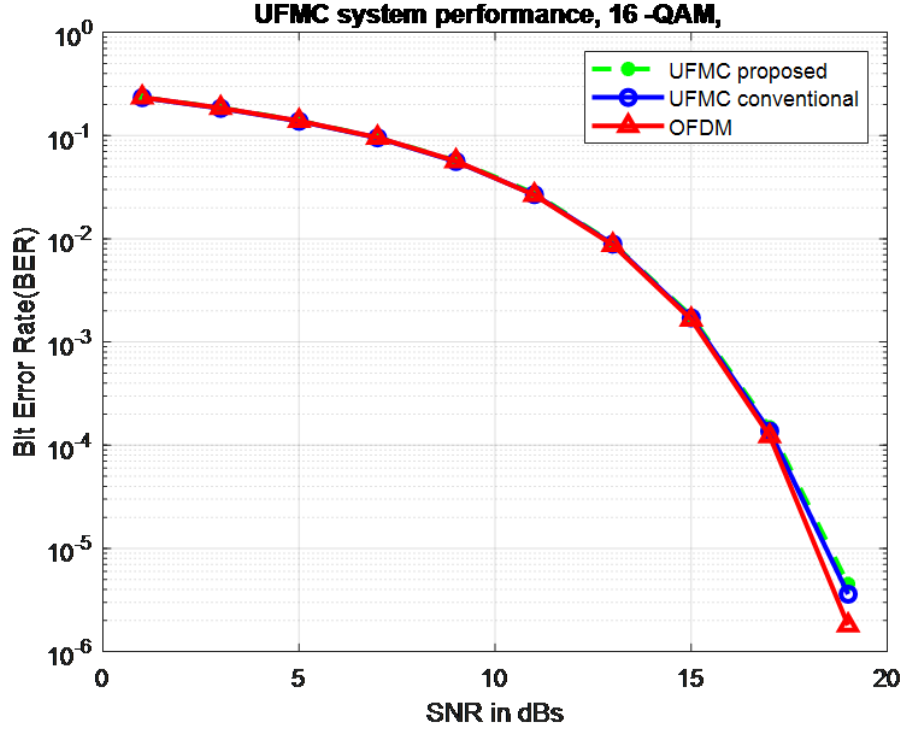
Figure 3.5: BER Performance

Let assume that m = n-N, then equation 3.25 can be rewritten as

$$Y_{even}(k) = \sum_{n=0}^{N-1} y_{zp}(n) e^{\frac{-j2\pi}{N}kn} + \sum_{m=0}^{N-1} y_{zp}(m+N) e^{\frac{-j2\pi}{N}k(m+N)} \qquad (3.26)$$

Since $e^{\frac{-j2\pi}{N}kN} = 1$, the above equation 3.26 rewrite as

$$Y_{even}(k) = \sum_{n=0}^{N-1} (y_{zp}(n) + y_{zp}(n+N)) e^{\frac{-j2\pi}{N}kn} \qquad (3.27)$$

Finally, the equation 3.27 can be written as

$$Y_{even}(k) = \sum_{n=0}^{N-1} y'(n) e^{\frac{-j2\pi}{N}kn} \qquad (3.28)$$

Where

$$y'(n) = \begin{cases} y(n) + y(n+N); & \text{for } 0 \leq n \leq L-3 \\ y(n); & \text{for } L-2 \leq n \leq N-1 \end{cases} \qquad (3.29)$$

Now, according to 3.28 the even-numbered subcarriers can be generated with
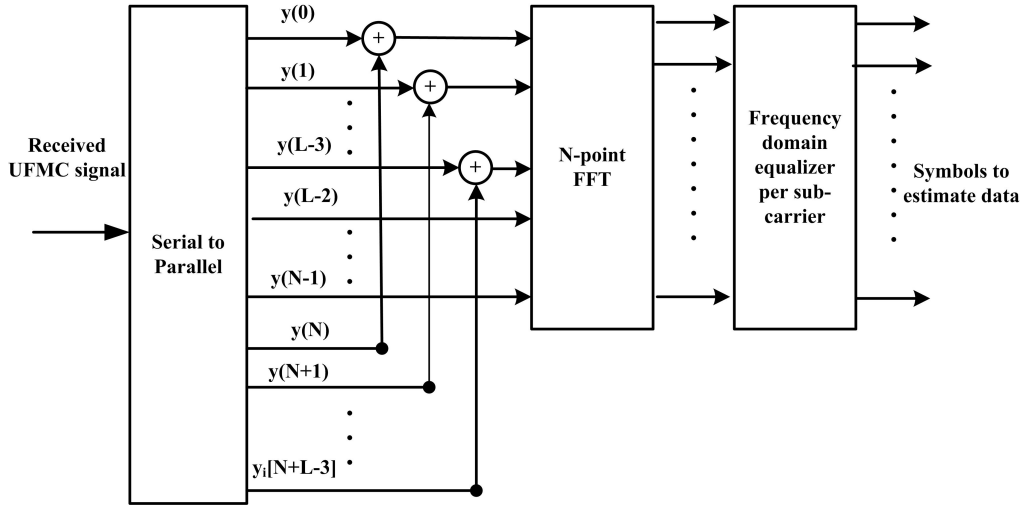
Figure 3.6: The Proposed Receiver model

a single N-point FFT having $y^{'}(n)$ as input, which is shown in Figure 3.6. Here, both the 2N-point DFT and decimator operations can be implemented with the single N-point DFT. The computational complexity can be reduced twice compared to the conventional UFMC receiver.

3.3.1 Complexity Analysis of the Proposed model

The major computational complexity in the UFMC receiver system includes the 2N-point FFT processor, the channel estimation, and equalization algorithms. The UFMC baseband signal model at the receiver is like the OFDM signal except for the filter equalization, so, the same algorithms can be applied in the UFMC system for channel estimation and equalization. Therefore, the UFMC receiver complexity is two times higher compared to the OFDM receiver. Furthermore, the additional memory or control overhead is one of the main disadvantages of the implementation. The N-point DFT is efficiently computed by the FFT algorithm [85], which requires the total number of arithmetic operations (real multiplications and additions) using radix-2 FFT algorithm is 5N $\log_2 N$ The split-radix FFT algorithm [86] has a lower number of arithmetic operations compared to the radix-2 FFT algorithm, which requires the total number of arithmetic operations to be 4N $\log_2 N - 6N + 8$. With the FFT

pruning algorithm, the number of real operations (additions and multiplications) required to process the UFMC base band received signal [45] is $5N \log_2 N - 2N + 4(L-2)$. Table 3.1 describes the computational complexity comparison between the conventional, FFT pruning approach and proposed receiver model. Which states that the proposed UFMC receiver model has a smaller number of arithmetic operations, it is simple and effective compared to conventional CP-OFDM and UFMC receivers.

Table 3.1: Computational complexity comparison

Receiver Model type	Number arithmetic operations	Required hardware blocks for the base band signal processing at the receiver
CP-OFDM receiver	$4N \log_2 N - 6N + 8$	CP remover, N-point FFT, FDE
Conventional UFMC receiver	$8N \log_2 N - 4N + 8$	Zeros padder, 2N-point FFT, Decimator, FDE
UFMC receiver with FFT pruning	$5N \log_2 N - 2N + 4(L-2)$	Zeros padder, 2N-point FFT, FDE
Proposed UFMC receiver	$4N \log_2 N - 6N + 8 + 2(L-2)$	N-point FFT, FDE

The complexity efficiency of the system can be measured by CCRR, which is defined as the ratio of the total number of computations required for the conventional model (CM_{conv}) to the total number of computations required for the proposed model (CM_{prop}).

$$CCRR = \frac{CM_{conv}}{CM_{prop}} = 2(1 + \frac{1}{\log_2 N}) \qquad (3.30)$$

From equation 3.30, the proposed model reduces the computational complexity more than two times as compared to the conventional UFMC receiver model. Also, in the proposed model, there are no zeros padding operations to process through 2N-point FFT. Therefore, the number of read/ write memory locations was reduced by two times approximately. However, the required storage space for read/ write operations is the same as the conventional OFDM receiver model. In proposed model, the adder blocks are used before N-point FFT which may

increase the connectivity complexity compared to the traditional model.

The power carried by odd-numbered frequency samples of 2N-point FFT is not utilized in the conventional UFMC receiver, hence the power efficiency is 50%. But in the proposed model, there is no 2N-point FFT and which uses all the samples processed by FFT. Therefore, the power efficiency can be improved to 100%. Finally, we can say that the proposed UFMC receiver model is more suitable for ultra-low latency and low energy consumption IoT uses cases as well as for next-generation cellular networks.

3.3.2 Simulation Results

The computational complexity of the receiver depends only on the size of the FFT. In this session, some computer simulation results are presented. The numerical analysis of computational complexity and its comparison is shown in Figure 3.7 for different bandwidth (BW) configurations mentioned in Table 3.2 under NR-TDL vehicular-A channel model with length of 24. These comparisons conclude that the proposed receiver model has a lesser number of arithmetic operations (i.e., two times lesser) at the base band FFT signal processing level compared conventional model and almost achieved the same computational complexity of the CP-OFDM receiver.
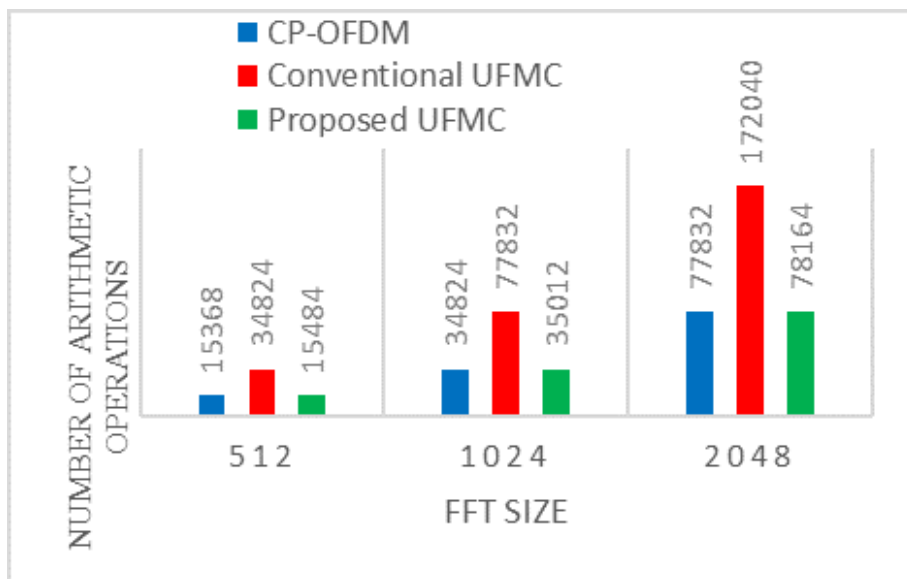
Figure 3.7: Comparison of computational complexity

Table 3.2: Bandwidth configuration for NR Frequency band Range (FR)-1 [4]

SCS kHz	Bandwidth/ specifications	5 MHz	10 MHz	20 MHz
	Number of subcarriers	333	666	1333
15	Number of data subcarrier	300	624	1272
	FFT size	512	1024	2048
	CP length	36	72	144

Furthermore, the complexity ratio (CR) of the UFMC receiver with respect to the OFDM receiver $\frac{CM_{ufmc}}{CM_{ofdm}}$ for different methods are shown in Figure 3.8. Consider the bandwidth of 20 MHz and N = 1024 for numerical comparison between the proposed and conventional models, in this case the CR values are 2.1904, 1.3881 and 1.0036 for the conventional, with FFT pruning algorithm and the proposed UFMC receiver model respectively. From these numerical analysis, the proposed model has less complexity ratio and more efficient in terms of computational complexity.
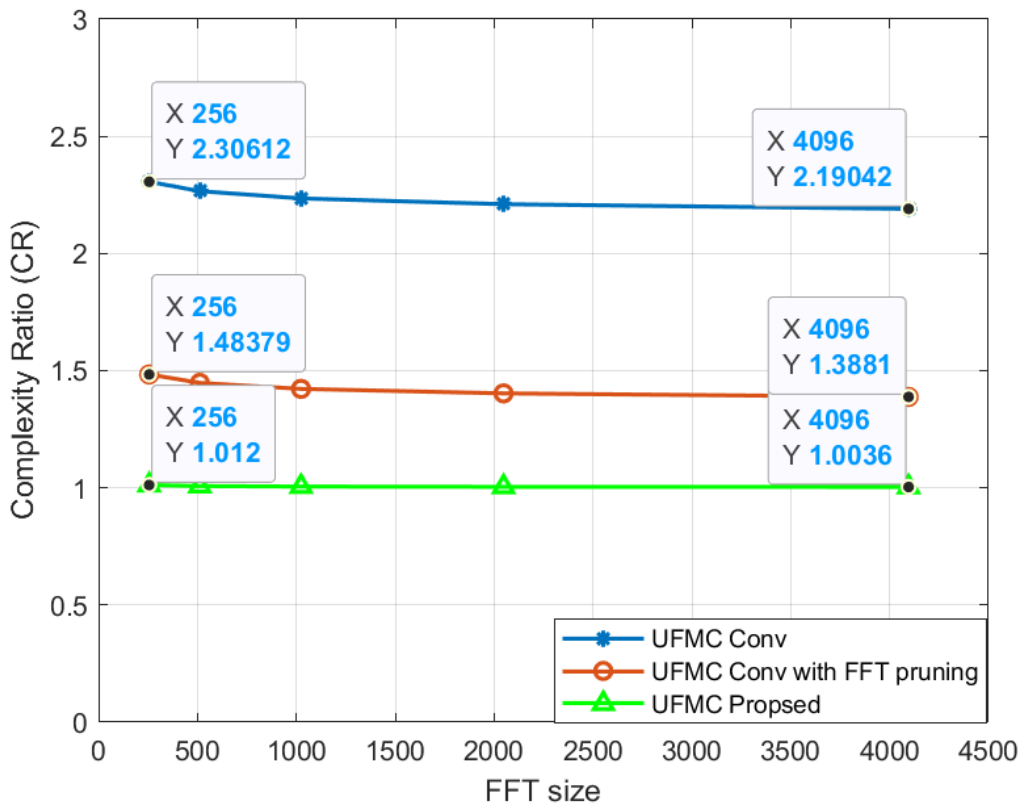
Figure 3.8: Complexity ratio (CR) of the UFMC receiver with respect to the OFDM receiver

Also, the FFT's per energy [87] can be improved, which is defined as

$$FFT's/Energy = \frac{Technology}{Power \times Executiontime \times 10^{-6}} \quad (3.31)$$

Where Technology is the CMOS process in micrometers, the power consumption is proportional to supply voltage, clock frequency, and load capacitance. The execution time depends on the number of operations/computations required to complete a particular task. From equation 3.31, the FFT's per energy is inversely proportional to the execution time, which means for the proposed model the FFT processor requires lesser execution time compared to the conventional one. Finally, we can say that the proposed UFMC receiver model is more suitable for ultra-low latency and low energy consumption uses cases of the next-generation cellular networks.
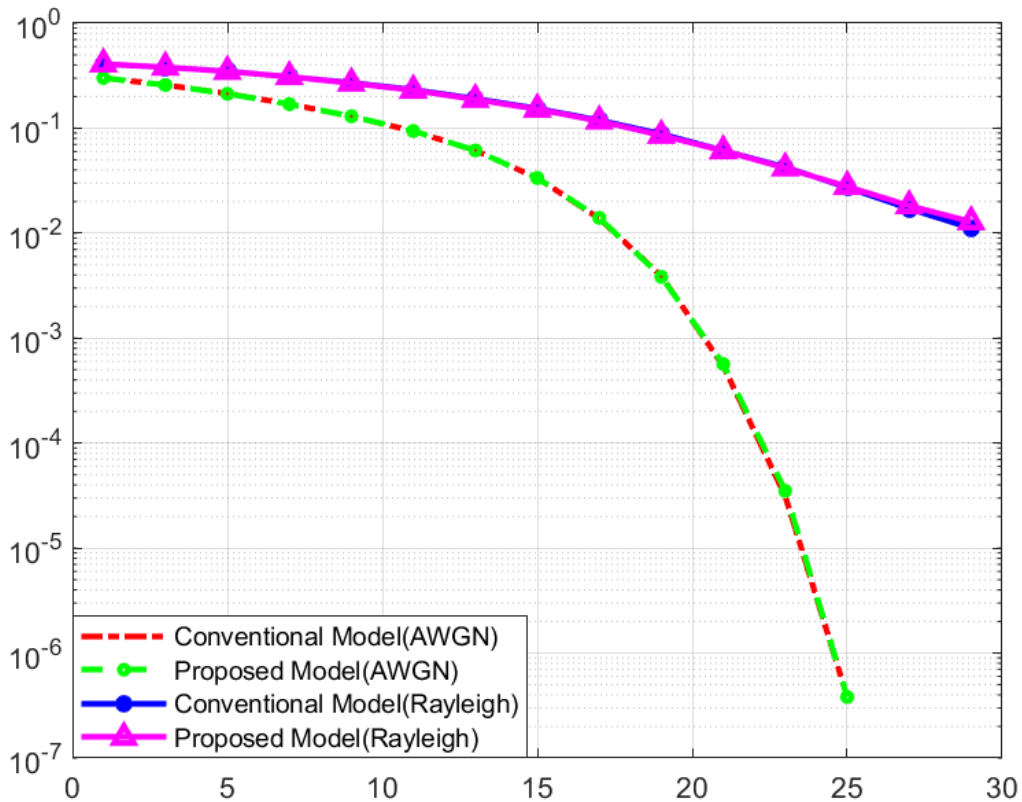
Figure 3.9: SNR versus BER for UFMC transceiver system

The proposed model is a simplified model of the conventional model. Therefore, it gives almost the same performance in terms of SNR versus BER at lower computational cost, which is shown in Figure 3.9 for the simulation parameters

Table 3.3: Simulation parameters for SNR versus BER performance

Parameter	Value
Channel bandwidth	10 MHz
Modulation type	16-QAM
FFT Size	1024
CP length	72
Number of UFMC symbols	7
Sub-band size	12
Stopband attenuation (As)	40
Channel type	AWGN/ Rayleigh fading

mentioned in Table 3. In practical cases due to the additional adders on the receiver side, the proposed model may increase the connectivity complexity and occurs small losses; hence small performance degradation shown in Figure 3.9. One of the minor drawback of the proposed model is that the hardware implementation needs to use $L_f + L_h - 2$ number of adders before the N-point FFT, which may cause the rise of connectivity complexity and word length effect when it processes through FFT processor. Otherwise, the proposed model is superior than the conventional model.

3.4 Summary

The UFMC was one of the candidate waveforms for 5G, but the computational and hardware complexity of the UFMC transceiver system has more than the CP-OFDM system due to filtering operation at the transmitter and 2N-point FFT processing at the receiver. In this point of view, here we proposed the simplified UFMC transmitter and receiver model. On the transmitter side, to cut down the complexity, the final UFMC symbol was obtained by implementing the sub-band filtering in frequency domain before processing through IFFT block. Therefore, the computational complexity was reduced approximately by 8.5 times for N = 512 and 14.2 times for N = 1024 with some greater OBE. At the receiver, the exact frequency domain UFMC received symbol after FFT processor and decimator derived and simplified to implement with a single N-point FFT and that reduced the computational complexity more than two times (i.e., 50%) compared to the traditional receiver model without degrading

66

the system performance. By this approach, at the receiver the zero-padding for processing 2N-point FFT and decimation part was simply replaced by a single N-point FFT, which reduced the number of hardware components at base band signal processing and the storage requirement for read/ write operation to process the data. This model reduced the hardware requirement and hence the power consumption. The real-time hardware implementation of this model is the future scope of this work.

Chapter 4

Optimal Filter Length Selection for the UFMC Systems

In previous chapters we had discussed that the UFMC waveform is a combined form of FBMC and F-OFDM, in which, a group of subcarriers (SCs) is filtered individually. The filtering operation in UFMC makes it more robust in relaxed synchronization conditions compared to OFDM, reduces the OBE, and is highly suitable for short packet transmission. The subband filtering can be physical resource block (PRB) based, service-based, and user-based [88, 89]. The UFMC is suitable for PRB-based subband filtering and massive machine-type communications and the F-OFDM may favor user- or service-based sub-band filtering for enhanced mobile broadband. The main drawback of the F-OFDM waveform uses a longer filter length than the UFMC waveform which is half of the OFDM symbol and which increases the latency. The multi-service or multi-user approach may save the signaling overhead but the subband filtering disrupts the orthogonality between the subcarriers and introduces ICI and inter-sub band/service interference (ISBI). In addition, the baseband complexity and computation complexity of the UFMC system are higher than the conventional OFDM due to the number of IFFT blocks and sub-band filters.

Recently, there are several filter optimization and baseband signal processing approaches have been proposed to mitigate the interference in the UFMC system [90–92]. In [90], introduces a new technique for pulse shaping in UFMC, which aims to mitigate the spectral leakage that occurs in adjacent subbands. This approach involves the utilization of Bohman filter-based pulse shaping in conjunction with antipodal symbol-pairs on the edge-subcarriers of

the subbands, resulting in a reduction of out-of-band radiation. The sub-band FIR filter is optimized based on the knowledge of expected timing offset and frequency offset [93] to reduce the out-band radiation and hence reduced the interference between the adjacent sub-bands. The active interference cancellation approach suggested in [91] uses a separate subcarrier inserted on both sides of the sub-band for interference cancellation and optimizes the weights of these subcarriers to maximize the overall signal-to-interference noise ratio (SINR) under the power constraints. With this approach, the spectral efficiency degraded due to the use of separate subcarriers for interference cancellation. An adaptive modulation and filter configuration was proposed in [94], in which the sub-band filter impulse response parameters were determined adaptively to reduce the interference caused by CFO. This method used some guard band between adjacent sub-bands that causes reduction in spectral usage with better BER performance compared to the conventional method. From the above literature, all the methods optimized the filter configuration to reduce the interference due to out of band emission, CFO and timing offset using an extra subcarrier or a guard interval, because of this the symbol utilization degraded. For the UFMC system, the sub-band filter operation protects from multipath fading effect and ISI like the CP in the OFDM system. However, the ramp (filter tail) of the sub-band filter on both sides of the symbol causes interference on the neighbor sub-bands, which relies upon the filter length. In practice, the sub-band filter length is preferred longer or equal to the wireless channel length to avoid the multipath fading effect. In some scenarios, the short filter length can be sufficient to get marginal system performance, which means further the system overhead can be reduced reasonably. In this chapter, we derived the closed form for the interference in the UFMC symbol due to filtering operation and then optimize the filter length with respect to sub-band size. Here the sub-carrier (sub-band size) allocation to each user depends on the user or service request such as data, video streaming, or online interactive game services. So, the length of each sub-band is different from the other. Which makes fewer computations at the sub-band filter and improves the symbol utilization ratio.

69

4.1 The Interference Analysis in UFMC Symbol

As we know that the FIR filtering operations provide less OBE and robustness in a relaxed synchronized system. But the filtering operation disrupts the orthogonality between the sub-carriers and causes interference. In general, the PRB based sub-band filtering is most preferable to implemented in the UFMC waveform [88]. In the case of multi-user and multi-services, there is design flexibility in the UFMC waveform to allocate multiple PRBs such that each service support multiple users, and one or more consecutive PRBs can be allocated to each user as shown in Figure 4.1. The inter-symbol interference (ISI) can be minimized by sub-band filtering operation in the UFMC system, but it might be causing some significant ISBI in the case of multi-service or multi-user systems as shown in figure 4.1. On the other hand the non-adjacent sub-bands/service bands/user bands, the ISBI is insignificant and does not affect the system performance.
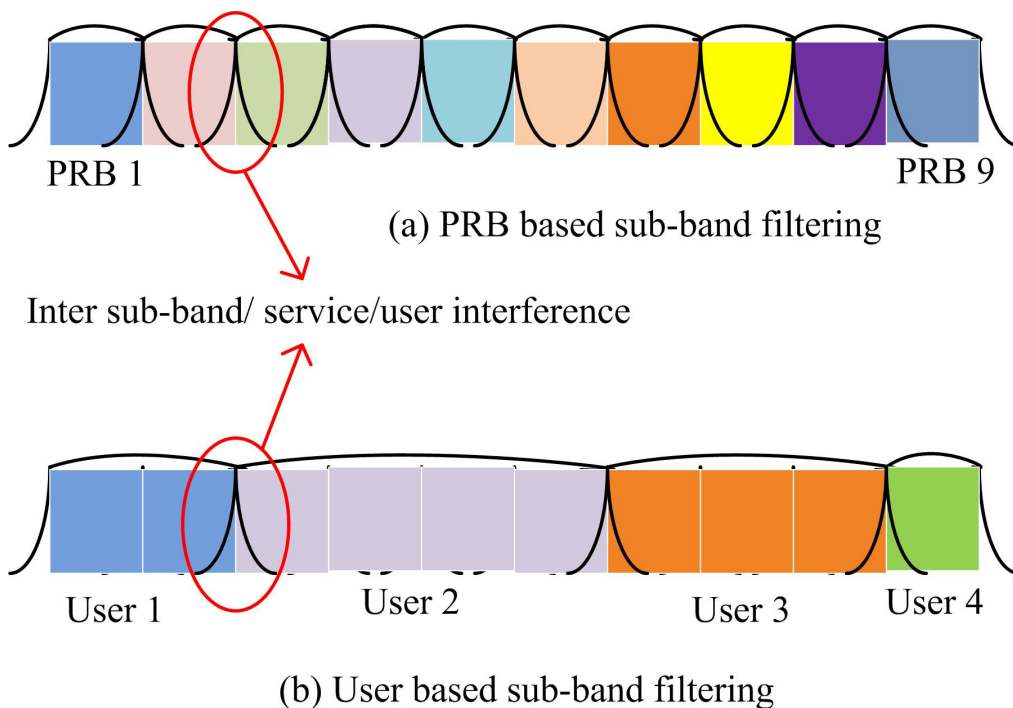
Figure 4.1: Types of sub-band filtering

4.1.1 Closed-form for Interference in the UFMC Symbol

As stated earlier, the non-orthogonality due to filtering operation may introduce interference between the adjacent subcarriers and sub-bands. To analyze the interference, let us define the ISBI and ICI in terms of desired data symbols and sub-band filter metrics. Consider the following assumptions for formulation and simplification:

- Assumption 1. The modulated data symbols mapping on subcarriers are uncorrelated with each other, have zero mean ($E[D_p(k)] = 0$) and variance $E\left[|\,D_p(k)\,|^2\right] = \sigma_{dp}^2$

- Assumption 2. The sub-band filter coefficients are normalized to have $\sum_{l=0}^{L_f-1}|\,f_p(l)\,|^2 = 1$

The average energy of any complex signal is defined by it's auto-correlation function, which is expressed as $E[x(n)\,x^*(x)]$. For UFMC signal, the mean energy is defined as

$$E_{UFMC} = \sum_{n=0}^{N+L_f-2}|\,x(n)\,|^2 = \sum_{n=0}^{N+L_f-2} x(n)\,x^*(n) \qquad (4.1)$$

By substituting equation 1.1 in above equation the energy of the UFMC symbol can be expressed as

$$E_{UFMC} = \sum_{n=0}^{N+L_f-2}\left(\sum_{p=0}^{B-1} x_p(n)\right)\left(\sum_{p=0}^{B-1} x_q^*(n)\right) \qquad (4.2)$$

Where $x^*(n)$ represents the complex conjugative of $x(n)$. The UFMC symbol energy can be composed of two components, one is the total sub-band energy E_{SB} for $p = q$ and another one is the ISBI component E_{ISBI} for $p \neq q$.

$$E_{UFMC} = \sum_{n=0}^{N+L_f-2}\sum_{p=q=0}^{B-1}|\,x_p(n)\,|^2 + \sum_{n=0}^{N+L_f-2}\sum_{p=0}^{B-1}\sum_{q=0,q\neq p}^{B-1} x_p(n)\,x_q^*(n) \quad (4.3)$$

71

After substituting 1.2 in above equation, the first component (sub-band energy) can be expressed as

$$E_{SB} = \sum_{n=0}^{N+L_f-2} \sum_{p=0}^{B-1} \sum_{l=0}^{L_f-1} \mid f_p\left(l\right)\mid^2 R_{d_p,d_p} \tag{4.4}$$

The second component in the above equation is

$$E_{ISBI} = \sum_{n=0}^{N+L_f-2} \sum_{p=0}^{B-1} \sum_{q=0,q\neq p}^{B-1} \sum_{l=0}^{L_f-1} f_p\left(l\right) f_q^*\left(l\right) R_{d_p,d_q} \tag{4.5}$$

Where R_{d_p,d_q} is the correlation sequence of the two different time-domain sub-band data sequence $d_p\left(n\right)$ and $d_q\left(n\right)$, which can be defined as $R_{d_p,d_q} = d_p\left(n-l\right) d_q^*\left(n-l\right)$. By substituting 3.4 here, we get

$$\begin{aligned} R_{d_p,d_q} &= \frac{1}{N^2} \sum_{k=m=0}^{\min Q_p-1,Q_q-1} D_p\left(k\right) D_q^*\left(k\right) e^{\frac{j2\pi}{N}\left(K_p-K_q\right)\left(n-l\right)} \\ &+ \frac{1}{N^2} \sum_{k=0}^{Q_p-1} \sum_{m=0,m\neq k}^{Q_q-1} D_p\left(k\right) D_q^*\left(m\right) e^{\frac{j2\pi}{N}\left(K_p-K_q+k-m\right)\left(n-l\right)} \end{aligned} \tag{4.6}$$

Since the modulated data sequences (frequency-domain data sequences) are uncorrelated or low correlated for $p \neq q$ and $k \neq m$. Therefore, neglecting the second term in 4.6 we have

$$R_{d_p,d_q} = \frac{1}{N^2} e^{\frac{j2\pi}{N}\left(K_p-K_q\right)\left(n-l\right)} \sum_{k=0}^{\min Q_p-1,Q_q-1} D_p\left(k\right) D_q^*\left(k\right) \tag{4.7}$$

For p = q the equation 4.6 can be written as

$$R_{d_p,d_p} = \frac{1}{N^2} \left(\sum_{k=0}^{\min Q_p-1,Q_q-1} \mid S_p\left(k\right)\mid^2 + \sum_{k=0}^{Q_p-1} \sum_{m=0,m\neq k}^{Q_q-1} D_p\left(k\right) D_p^*\left(m\right) e^{\frac{j2\pi}{N}\left(k-m\right)\left(n-l\right)} \right) \tag{4.8}$$

From equation 1.3, we have

$$f_p\left(l\right) f_q^*\left(l\right) = \mid f\left(l\right)\mid^2 e^{\frac{j2\pi}{N}\left(K_p-K_q+\frac{Q_p-Q_q}{2}\right)l} \tag{4.9}$$

Substitute 4.8 in 4.4, the total sub-band energy E_{SB} can be divided into two components: the sub-carrier energy (E_{SC}) component for $k = m$ and the ICI component (E_{ICI}) for $k \neq m$. Therefore, the total UFMC symbol energy becomes

$$E_{SB} = E_{SC} + E_{ICI} + E_{ISBI} \qquad (4.10)$$

where

$$E_{SC} = \frac{1}{N^2} \sum_{n=0}^{N+L_f-2} \sum_{p=0}^{B-1} \sum_{l=0}^{L_f-1} \mid f_p(l) \mid^2 \sum_{k=0}^{Q_p-1} \mid D_p(k) \mid^2 \qquad (4.11)$$

according to the assumption 2, the subcarrier energy can be written as

$$E_{SC} = \frac{N + L_f - 1}{N^2} \sum_{p=0}^{B-1} \sum_{k=0}^{Q_p-1} \mid D_p(k) \mid^2 \qquad (4.12)$$

and the ICI component is

$$E_{ICI} = \frac{1}{N^2} \sum_{p=0}^{B-1} \sum_{k=0}^{Q_p-1} \sum_{m=0,m\neq k}^{Q_q-1} D_p(k) D_p^*(m) \sum_{n=0}^{N+L_f-2} e^{\frac{j2\pi}{N}(k-m)n} E_{fp}(k,m,l) \qquad (4.13)$$

where

$$E_{fp}(k,m,l) = \sum_{l=0}^{L_f-1} \mid f_p(l) \mid^2 e^{\frac{-j2\pi}{N}(k-m)l} \qquad (4.14)$$

by substituting 4.7 and 4.9 in 4.5, the inter sub-band interference energy can be written as

$$E_{ISBI} = \frac{1}{N^2} \sum_{p=0}^{B-1} \sum_{q=0,q\neq p}^{B-1} \sum_{l=0}^{L_f-1} \mid f(l) \mid^2 e^{\frac{j2\pi}{N}(\frac{Q_p-Q_q}{2})l} \sum_{n=0}^{N+L_f-2} e^{\frac{j2\pi}{N}(K_p-K_q)n}$$
$$\sum_{k=0}^{\min Q_p-1,Q_q-1} D_p(k) D_q^*(k) \qquad (4.15)$$

For simplicity, let us consider the uniform subcarrier distribution among all subbands, that is $Q_p = Q_q = Q$ and $K_p = pQ$. Now the expression 4.15

becomes

$$E_{ISBI} = \frac{1}{N^2} \sum_{p=0}^{B-1} \sum_{q=0,q\neq p}^{B-1} \sum_{l=0}^{L_f-1} |f(l)|^2 \sum_{n=0}^{N+L_f-2} e^{\frac{j2\pi}{N}(p-q)Qn}$$

$$\sum_{k=0}^{Q-1} D_p(k) D_q^*(k) \quad (4.16)$$

4.1.2 ISBI and ICI Analysis in the UFMC Symbol

According to 4.13 and 4.16, both ICI and ISBI depend on the sub-band filter ramps on both sides of the sub-band and the size of sub-band. The filter ramps depend on the filter length, which is usually recommended to choose more than the channel length (CP length) to mitigate the multipath channel dispersion. Therefore, the filter length impacts the performance in different ways based on the sub-band size and the maximum-to-minimum filter gain ratio (MMFGR) among the subcarriers within a particular sub-band. The longer filter length leads to lower OBE in the adjacent sub-band (only some edge subcarriers may suffer from OBE), but the out of band radiation extends to a greater number of sub-bands with insignificant value within a sub-band. However, the cumulative ISBI increases with the number of sub-bands, and the ICI may increase with filter length due to a higher level of non-orthogonality. On other hand, the short filter length reduces overhead, lesser frequency localization, spreads higher OBE into more than one adjacent sub-bands but is limited to some sub-bands within the symbol resulting in more ISBI on the immediate adjacent sub-band as shown in Figure 4.2.

In addition, shorter filter length or narrow sub-band width leads to bad frequency localization, low MMFGR (i.e., the power allocation among the subcarriers in a sub-band is uniform) as shown in Figure 4.3. and thus, smaller performance loss. The UFMC system with a longer filter length results in a larger MMFGR (i.e., non-uniform power allocation among the subcarrier within a sub-band and higher at the middle of the sub-band) and higher frequency selectivity, but it leads to high possibility of error at the edges of the sub-band and causes a greater

74

(a) filter length = 73   (b) filter length = 23
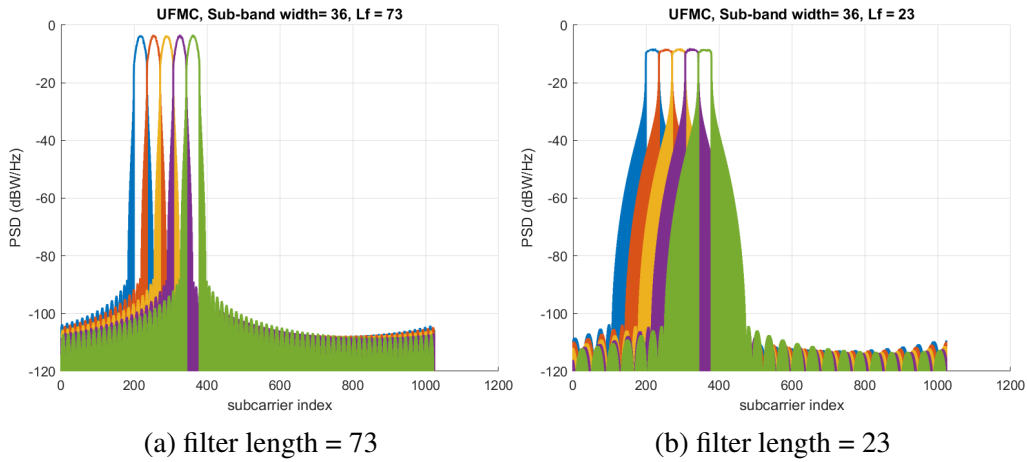
Figure 4.2: Power spectral density spread within the UFMC symbol

overall performance loss. This is further will be discuss in simulation results section.
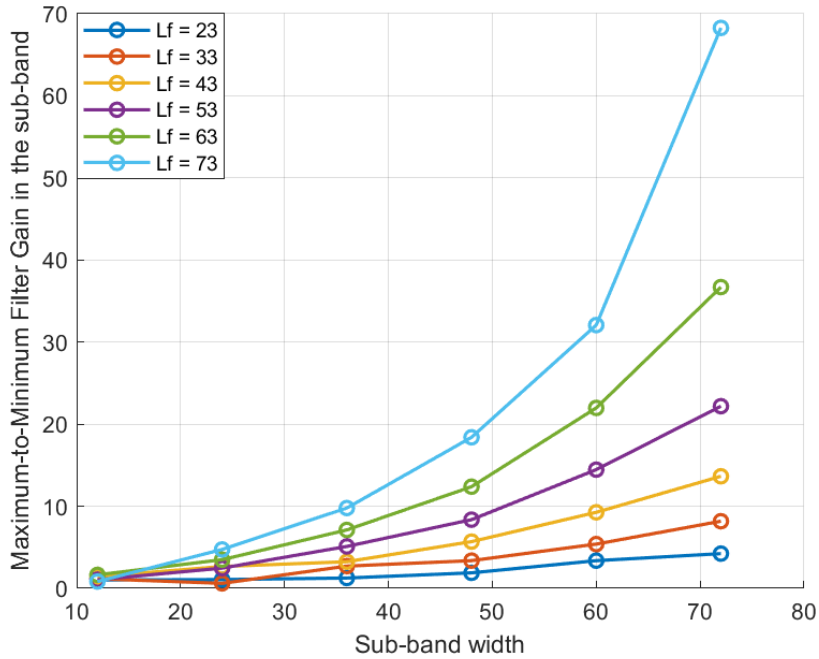
Figure 4.3: MMFGR variation according to the filter length and sub-band width

4.2 Optimal Filter Length Configuration for Subband Filter

The UFMC technology offers a higher spectral efficiency when compared to OFDM, owing to its ability to forego the transmission of a CP in the time domain. This CP, which constitutes approximately 7% of the OFDM symbol duration, can be omitted in UFMC, resulting in a 7% increase in data

transmission speed. However, the use of additional filtration in UFMC leads to longer symbol duration, which in turn reduces the data transmission rate as compared to OFDM. The sub-band filter design flexibility is one of the most significant advantages of the UFMC waveform compared to others, which enables to adjustment of the sub-band filtering configuration according to the requirement of service, user, and channel conditions. The optimization of the filter length in the process of development of sub-band filters for UFMC can lead to an increase in spectral efficiency. Therefore, this section includes the adaptation of the filter configuration based on the requirement.

According to Gibb's phenomenon, the magnitude response of the filter gives almost the same oscillatory behavior (i.e., ripples) after a finite value of its order. From this perspective point of view, we proposed a method that adopted the FIR filter order with respective sub-band sizes for flexible symbol duration and hence latency by maintaining a minimum level of OBE. In general, the filter design algorithms have been developed by a tolerance scheme, for an approximation to the ideal filter frequency response. The FIR filter design depends on the following parameters: pass band (f_p) and stop band edge frequencies (f_s), maximum absolute errors (δ_p and δ_s) known as ripples in the pass band, stop band, and filter length (L).

The sub-band filter length (L) is defined approximately as

$$L = \frac{-10 \log_1 0 \delta_p \delta_s - 13}{14.36 \Delta f} \text{ [95]} \tag{4.17}$$

Where Δf represents the normalized transition width with sampling frequency F_s, which is defined as i.e.,$\Delta f = ((f_s - f_p))/F_s$. The pass band and stop band edge frequencies can be defined based on the bandwidth requirements of the sub-band/ service. The bandwidth (BW) of the filter is defined from the number of subcarriers allocated to the sub-band as $BW = Q_p f_s c$, where f_{sc} is the subcarrier spacing, typically an integer multiple of 15 kHz for NR numerology. The lower (f_l) and upper (f_h) passband edge frequencies of the

sub-band are defined as

$$f_l = K_0 f_{sc} \text{and } f_h = (K_0 + Q_p) f_{sc} \tag{4.18}$$

Here the stop band frequency is determined from the general filter assumption, i.e., half of the sampling frequency $F_s/2$ or the guard band between the sub-band or service bands i.e., $f_s = N/2 f_{sc}$ and $\Delta f = 0.5 - \frac{K_0 + Q_p}{N}$. Substitute Δf in 4.17, we get

$$L = N \frac{-10 \log_1 0 \delta_p \delta_s - 13}{7.18N - K_0 - Q_p} \tag{4.19}$$

The sub-band filter length decides the level of non-orthogonality factor between subcarriers, the OBE, and hence the interference (ISBI and ICI). In this paper, the sub-band FIR filter length is adapted with respect to the sub-band size as mentioned in 4.19 to maintain a minimum level of interference. That is the filter length or tail in the symbol duration due to filtering operation can be flexible based on the sub-band width.

4.3 Simulation Results Analysis

In this section, the performance of the proposed method is evaluated through MATLAB simulation under various scenarios. To demonstrate the results clearly without sacrificing their generality, we adopted the 3GPP bandwidth configuration/ radio frame structure, i.e., the channel bandwidth of 10 MHz, 15 kHz subcarrier spacing, 624 data subcarriers, and the IFFT length N = 1024 for all simulation results. Let consider two different cases with different sub-band sizes (Q= 12 SCs and 36 SCs with 5 sub-bands) as shown in Figure 4.4. The first case depicted in Figure 4.4a, here the sub-band ramps (i.e., OBE) due to filtering operation extended to more than one sub-band for smaller sub-band size (Q), and the power distribution among the subcarriers in a sub-band is approximately equal. This results in less frequency selectivity and there is a high likelihood of accurate data detection in the sub-band with a higher signal-to-interference ratio (SIR). In the second case (i.e., for larger sub-band sizes) shown in Figure 4.4b, the ramp spread is less than one adjacent sub-band with a fixed filter length and

ineffective power distribution along the subcarriers in a sub-band. Which leads to greater frequency selectivity and reduced performance.

(a) 5 SB, 12 SCs each

(b) 5 SB, 36 SCs each
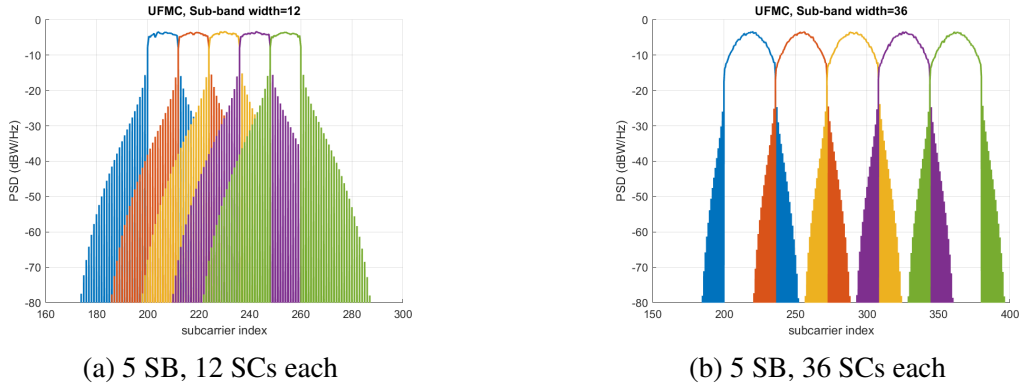
Figure 4.4: Power spectral density of the UFMC signal with the following specifications: filter length $L_f = 73$ and N = 1024

It is clear from the Figure 4.3, for a fixed sub-band size, the MMFGR increases with filter length and for a fixed filter length, the MMFGR increase with sub-band width. The UFMC system with a longer filter length results in a larger MMFGR (i.e., non-uniform power allocation among the subcarriers within a sub-band and higher at the middle of the sub-band) and higher frequency selectivity, but it leads to a high possibility of error at the edges of the sub-band and causes a greater overall performance loss in terms of SNR. The higher value of MMFGR may also be impact on the best pilot pattern design to estimate channel impulse response and frequency offset error. Pilots should be assigned to the subcarriers with the highest filter gain (i.e., in the middle of one sub-band). This may increase the complexity of estimation algorithms at the receiver. For instance, to obtain a specific MMFGR for a particular total number of subcarriers and filter length, we can choose the suitable sub-band bandwidth. Similarly, it is simple to calculate the corresponding MMFGR for a particular filter length and sub-band bandwidth, which can be used to assess the performance loss. To maintain a minimum level of MMFGR, here the filter length is adapted according to the allocated bandwidth of sub-bands and analyzed the variation of the interference with respect to filter length and sub-band width.

Table 4.1: Simulation parameters

Parameter	Value
IFFT size	1024
Modulation type	16-QAM
Sub-band size	Integer multiple of 12SC
Stopband attenuation (As)	40
Filter length	73 for conventional and variable for proposed
Channel type	AWGN/ Rayleigh fading

(a) sub-band size = 24 SC   (b) sub-band size = 48 SC
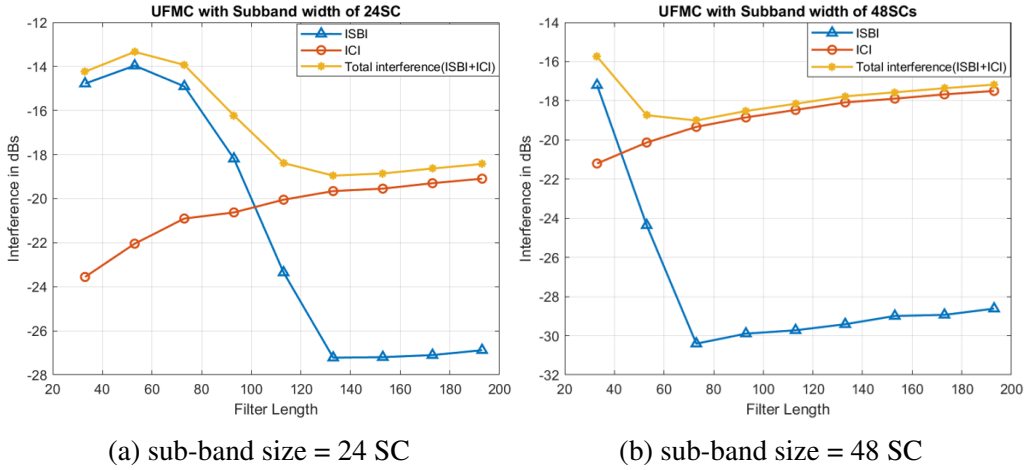
Figure 4.5: Interference variation in the UFMC symbol for uniform sub-band allocation

Figure 4.5 shows the variation of ISBI and ICI for simulation parameters (adopt from the 3GPP band configuration of 10 MHz bandwidth with 15 kHz subcarrier spacing) shown in Table 4.1. The simulation results from Figure 4.5 states that the cumulative ISBI decreases with the filter length due to lower OBE, and the ICI increases with filter length due to a higher level of non-orthogonality. In case of both uniform and non-uniform subcarrier allocation, the ISBI decreases, and ICI increases with the filter length. There is a tradeoff between the interference and the filter length (i.e., the ISBI dominates for a smaller filter length and the ICI dominates for a longer filter length. To reduce this effect the sub-band filter length can be dynamically modified with sub-band size to minimize the overall interference in the UFMC symbol. The simulation results as shown in Figure 4.6a, demonstrate the variation of average ISBI and ICI per sub-band for bandwidth of 10 MHz, sub-carrier spacing of 15 kHz with sub-band sizes 12, 36, 48, 72, and 96. From this, we concluded that the proposed model

| (a) ICI and ISBI comparison | (b) Signal to interference ratio (SIR) |
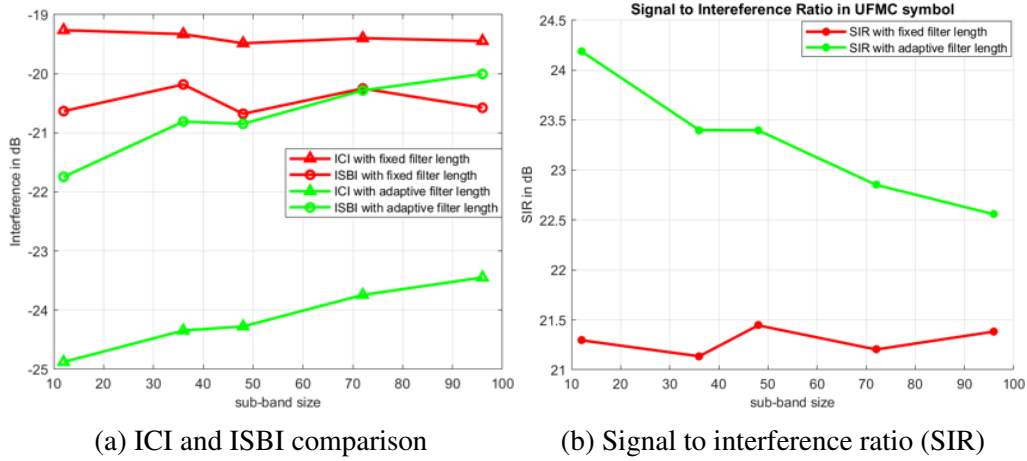
Figure 4.6: Interference and SIR with sub-band size

is superior in terms of ISBI compared to the conventional UFMC system and the ICI component increases with sub-band size and which is more for lower sub-band sizes.

With the proposed design of the adaptive filter approach, the total interference (ICI+ISBI) is reduced by around 1.5 to 3.2 dBs as shown in Figure 4.6 and hence improves the SIR. The inclusion of the filter and the unequal power distribution to various subcarriers lead the average BER performance of the UFMC system in one sub-band to be worse than that of the OFDM system. This is because a frequency-selective filter responds more favorably in the middle of the sub-band than at the subcarriers on its edges as shown in Figure 4.4. As a result, there is a high likelihood of inaccurate detection at the edges, and the response at intermediate subcarriers may occasionally be excessively high.

Table 4.2: Filter length selection for different Bandwidth (BW) configuration

	BW(MHz)/ SCS(kHz)	Data SCs/ IFFT size	$L_{f,conventional}$			$L_{f,proposed}$		
Subband size			12	36	60	12	36	60
	10/15	624/1024	73			11	13	15
	100/60	1200/2048	145			9	11	11

With the proposed method the filter length selection is based on the sub-band width, and the filter length values are 11, 13 and 15 for the sub-band widths

of 12 ,36 and 60 SCs respectively. These values are shorter than the fixed filter length (i.e., 73) approach hence the symbol utilization improved with the proposed method as shown in Table 4.2. By proposed method, the total interference contributed from ISBI and ICI is less than the conventional fixed filter length method results in improved SIR and hence improved the average BER performance of the system shown in Figure 4.7. Here, we can observe that the system attained the acceptable BER of 10^{-3} at around 21 dB and 23 dB with proposed and conventional methods respectively. Finally, the overall simulation results indicate that the proposed adaptive filter is appropriate for the UFMC system with multi-services. In addition, it reduces the symbol overhead due to the filter tail that leads to the smaller frequency selectivity of the sub-band. Thus, the proposed approach is most suitable for enhanced the symbol utilization.
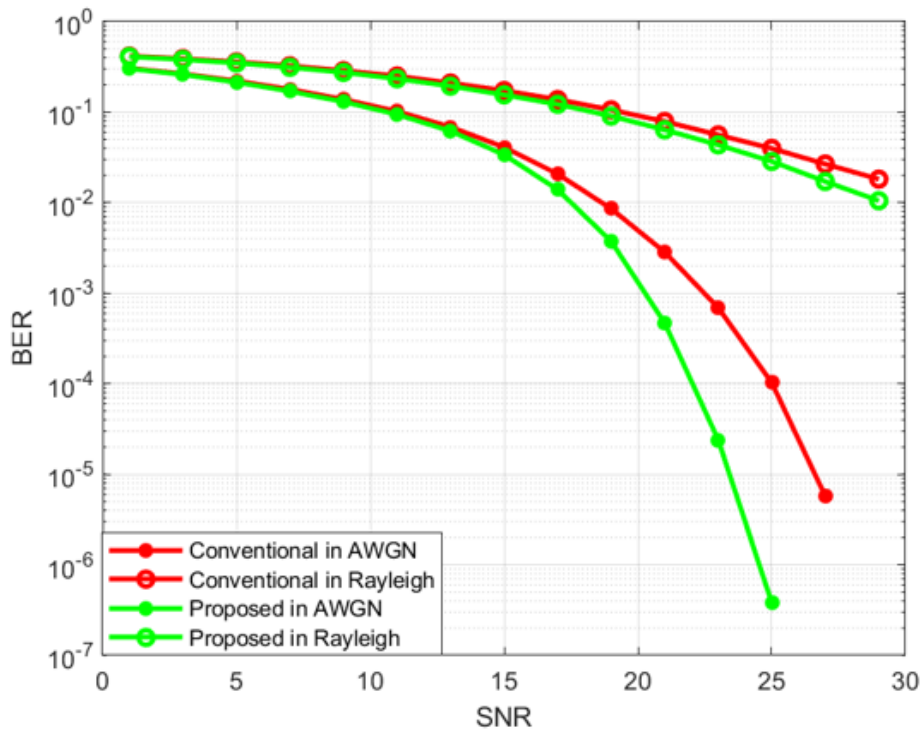
Figure 4.7: The BER performance comparison

81

4.4 Summary

The sub-band filtering process may affect the system performance in different ways directly in the UFMC based system. It's necessary to consider every subcarrier within the sub-band when selecting a filter to achieve a particular performance. Here is an idea for simplifying the filter length choice process in terms of filter response metrics. The filter length was dynamically modified to minimize interference with sub-band width. The resultant filter length obtained from the proposed method is shorter than the conventional fixed length approach. As a result, the SIR improved by 1 to 3 dBs thus improving the BER performance of the UFMC system. The computational complexity due to the filtering operation can be further reduced by applying the machine learning algorithms, this is the future scope of this work in progress.

Chapter 5

Proposed CFO Estimation and Compensation in the UFMC System

5.1 Introduction

The CFO is a significant phenomenon in wireless communications that arises due to the discrepancy between the carrier frequencies used by the sending and receiving ends. It simply defined as the disparity in the actual received signal carrier frequency compared to the nominal carrier frequency that the receiver is tuned to. Several factors contribute to CFO. These include imperfections in the design of oscillators at the transmitter and receiver, impact of multi-path fading channel and Doppler shift. It can cause ISI, where the symbols transmitted in one symbol interval interfere with the symbols transmitted in adjacent symbol intervals. This interference can result in errors in symbol detection and degrade the overall system performance. Moreover, CFO can cause a non-orthogonality among the subcarriers in the multicarrier modulation based wireless systems and that can cause massive ICI as shown in Figure 5.1, which seriously degrade the system performance.

The CFO in wireless systems can be expressed as

$$f_{os} = f_{c,t} - f_{c,r} + f_D \tag{5.1}$$

Where $f_{c,t}$ and $f_{c,r}$ local oscillator frequency at the transmitter and the receiver respectively; f_D represents the maximum Doppler spread. As a result of the extensive spectrum of novel frequencies that are introduced in 5G NR, time-frequency synchronization poses the biggest challenge. As a consequence
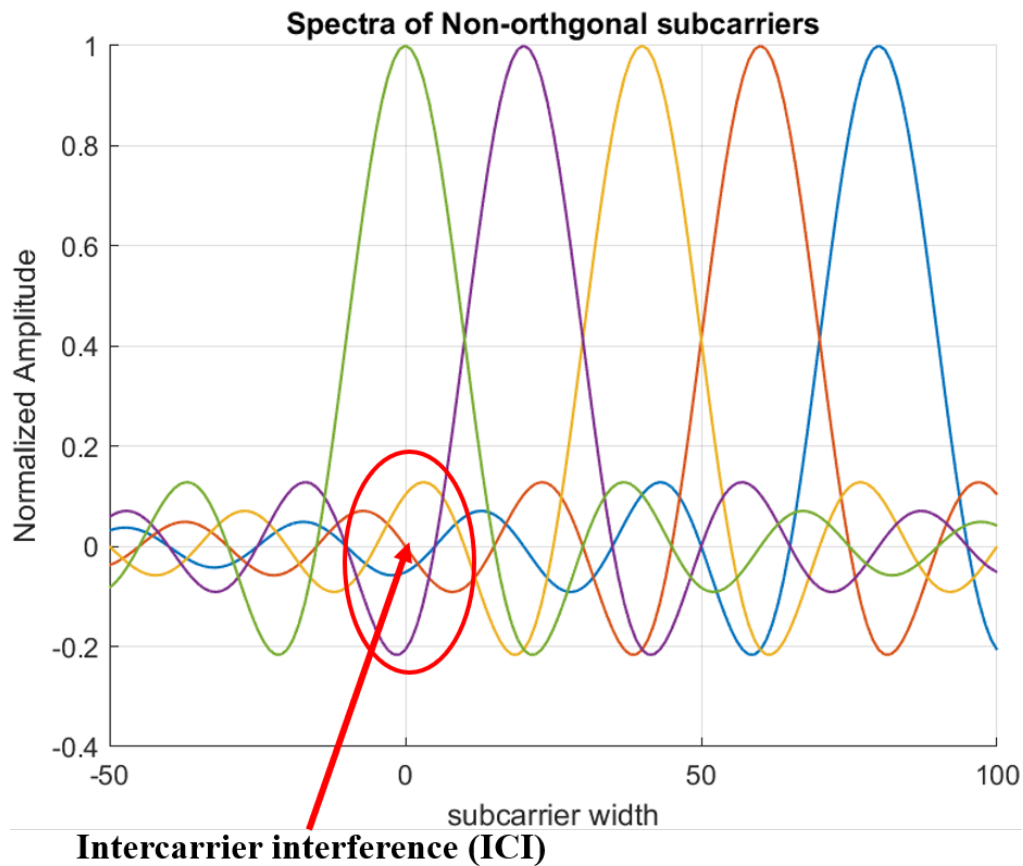
Figure 5.1: Non-orthogonality between the subcarriers

of these new frequency bands, systems are becoming more imperfect, leading to serious interference problems [51, 96]. In order to resolve this issue, a new and effective synchronization technique is needed, as well as a more accurate and expensive oscillator. In general, the CFO can be a function of the oscillator accuracy, and the environment factors (mostly temperature) that can affect the carrier frequency. The oscillator accuracy can be quantified in units of parts per million (ppm) which denotes the degree to which its frequency differs from the expected value. Let us examine a wireless system that operates at frequencies of 3, 6, and 27 GHz, with crystals of ±1 ppm a commonly accepted standard rating. In the worst-case scenario, the carrier frequency at either the transmitter or receiver may exhibit a maximum deviation of ±3, ±6, and ±27 kHz respectively for the above wireless system. The received signal experiences a continuous drift in frequency due to this frequency deviation. Therefore, it is imperative for the recipient to synchronize its carrier frequency according to the sender to

accurately retrieve the original data from received signal. However, in practice, attaining precise frequency synchronization can be a difficult task due to various factors.

5.2 Impact of CFO in the UFMC Based Systems

From earlier discussion, the CFO is a common phenomenon in wireless communication systems that mainly arises due to mismatches between transmitter and receiver carrier frequencies; Doppler shift, and doubly selective fading channel. It can degrade system performance by causing ISI and ICI. Consider a typical UFMC system discussed in chapter 3, the ith time-domain UFMC symbol:

$$x_i\left(n\right) = \sum_{p=0}^{B-1} f_p\left(n\right) * d_{i,p}\left(n\right) \tag{5.2}$$

where $d_{i,p}\left(n\right)$ represents the IFFT of pth subband data of the ith UFMC symbol represented by 1.4

After propagation through the wireless channel, the corresponding i^{th} UFMC base band received signal with carrier offset can be defined as

$$r_i\left(n\right) = e^{j\frac{2\pi}{N}\beta\left(iN_T+n\right)}y_i\left(n\right) + z_i\left(n\right) \tag{5.3}$$

The given expression pertains to the normalized CFO value with subcarrier spacing denoted by β. Additionally, the expression involves the UFMC symbol's total length, represented as $N_T = N + L - 2$, where $L = L_f + L_h$. Moreover, the expression involves the convolution sequnce $y_i\left(n\right)$ of transmitted UFMC signal denoted by $x_i\left(n\right); n \in [0, N + L_f - 1]$, the wireless channel coefficients vector is represented by $h\left(l\right); l \in [0, L_h - 1]$. and $z_i\left(n\right)$ denotes the complex- valued AWGN with $E\left[z_i\left(n\right)\right] = 0$ and $E\left[z_i\left(n\right)z_i^*\left(n\right)\right] = \sigma_z^2$.

The received signal undergoes zero-padding and is subjected to a 2N-point FFT at the UFMC receiver end. Subsequently, down-sampled this signal by a factor of 2 to enable individual estimation of the received data symbols.

Mathematically, the received UFMC signal's 2N-point DFT represented as

$$R_{i,2N}(m) = \sum_{n=0}^{2N-1} r_i(n) e^{-j\frac{2\pi}{2N}mn}; m = 0, 1, ..., 2N - 1 \qquad (5.4)$$

The retrieval of data symbols can be achieved directly through even-numbered samples. For even-numbered samples, m = 0, 2, ..., 2N-2 and $k' = m/2$

$$R_{i,even}(k') = \sum_{n=0}^{2N-1} r_i(n) e^{-j\frac{2\pi}{N}k'n} \qquad (5.5)$$

By substituting 5.3 in 5.5 and after simplification we will get

$$R_{i,even}(k') = e^{j\frac{2\pi}{N}\beta i N_T} \sum_{p=0}^{P-1} \frac{1}{N} \sum_{k=0}^{N-1} D_{i,p}(k) F_{i,p}(k) H_i(k) \sum_{n=0}^{2N-1} e^{j\frac{2\pi}{N}(\beta+k-k')n}$$
$$+ Z_{i,N}(k') \qquad (5.6)$$

where $F_{i,p}$ and H_i are the N-point DFT of the pth subband filter coefficient vector and the CIR respectively. The even numbered sample can be re-written as

$$R_{i,even}(k') = e^{j\frac{2\pi}{N}\beta i N_T} \frac{1}{N} \sum_{p=0}^{P-1} \Bigg(D_{i,p}(k') F_{i,p}(k') H_i(k') \sum_{n=0}^{2N-1} e^{j\frac{2\pi}{N}\beta n}$$
$$+ \sum_{k=0,k\neq k'}^{N-1} D_{i,p}(k) F_{i,p}(k) H_i(k) \sum_{n=0}^{2N-1} e^{j\frac{2\pi}{N}(\beta+k-k')n} \Bigg)$$
$$+ Z_{i,N}(k') \qquad (5.7)$$

The 1st term in equation 5.7 pertains to the symbol that is necessary for data detection, and the 2nd term pertains to the ICI that arises from the adjacent subcarriers due to the CFO. The 3rd term, on the other hand, represents the AWGN.

For i = 0, the zeroth UFMC received symbol is

$$R_{0,even}(k') = \frac{1}{N} \sum_{p=0}^{P-1} \left(D_{0,p}(k') F_{0,p}(k') H_0(k') \sum_{n=0}^{2N-1} e^{j\frac{2\pi}{N}\beta n} \right.$$
$$\left. + \sum_{k=0,k\neq k'}^{N-1} D_{0,p}(k) F_{0,p}(k) H_0(k) \sum_{n=0}^{2N-1} e^{j\frac{2\pi}{N}(\beta+k-k')n} \right)$$
$$+ Z_{0,N}(k') \tag{5.8}$$

After simplification of 5.8, the final expression can be in the form of

$$R_{0,e} = \alpha_0 X_{0,data}(k') + ICI_{k',k} + Z_{0,N}(k') \tag{5.9}$$

where

$$\alpha_0 = \frac{1}{N} e^{j\pi\beta\left(2-\frac{1}{N}\right)} \frac{\sin 2\pi\beta}{\sin \frac{\pi\beta}{N}} \tag{5.10}$$

$$X_{0,data}(k') = \sum_{p=0}^{B-1} D_{0,p}(k') F_{0,p}(k') H_0(k') \tag{5.11}$$

$$ICI_{k',k} = \frac{1}{N} \sum_{p=0}^{B-1} \sum_{k=0,k\neq k'}^{N-1} D_{0,p}(k) F_p(k) H_0(k) ICI_{coeff} \tag{5.12}$$

The ICI coefficients are contingent upon the CFO and are expressed as follows:

$$ICI_{coeff} = e^{j\Phi\left(2-\frac{1}{N}\right)} \frac{\sin 2\Phi}{\sin \frac{\Phi}{N}} \tag{5.13}$$

where $\Phi = \pi(\beta + k - k')$. The term in equation 5.9 represents the modified UFMC data symbol by channel and sub-band filter given by 5.11 that experiences by some attenuation and phase shift factor due to presence of CFO given by 5.10, second term represents the ICI on k'^{th} subcarrier due to k^{th} subcarrier in the presence of CFO expressed in the equation 5.12.

The UFMC system's bit error probability with CFO is mathematically formulated in [97] under AWGN channel conditions. Figure 5.2a depicts the influence of the frequency offset value on BER and 5.2b illustrates the variation MSE of the CFO estimation with MLE method using two identical

(a) The BER performance   (b) The MSE Performance
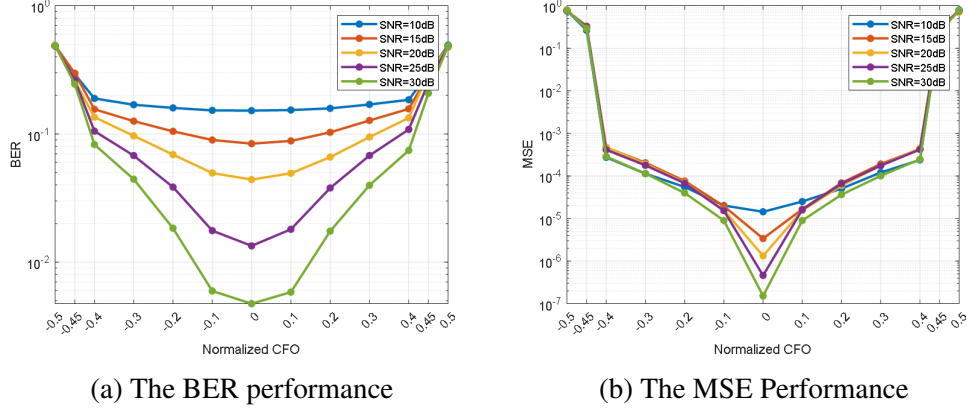
Figure 5.2: The UFMC system performance for 16-QAM with CFO range - 0.5 to + 0.5

training sequences. This simulation performed in the CFO range of ± 0.5 for various SNR values for studying the system performance. The UFMC system's performance in terms of BER degraded with increased CFO values as shown in Figure 5.2. Also, it can be observed SNR is reduced for larger CFO compared to smaller CFO.

From above equations, the SINR can be given by

$$SINR = \frac{E\left[|\alpha_0 X_{0,data}(k)|^2\right]}{E\left[|ICI_{k,m}|^2\right] + E\left[|Z_{0,N}|^2\right]} \tag{5.14}$$

From above discussion it is clear that the CFO is a crucial factor to consider in wireless systems as it significantly impacts the sensitivity of the system to any discrepancies between the transmitter and receiver. Inadequate compensation of subcarrier orthogonality and ignoring the CFO may produce non-orthogonality and consequent ICI. Hence, the performance of the wireless network as a whole may suffer. To mitigate the impact of CFO, wireless communication systems employ various techniques to estimate the CFO before channel estimation. These techniques include pilot symbols or reference signals that are periodically inserted into the transmitted signal to compute the CFO that will be experienced at the receiver. Advanced algorithms and signal processing methodologies are employed to find the CFO and correct it to recover the original transmitted signal accurately. The blind estimation technique typically entails considerable

computational expenses and necessitates a minimum of ten symbols to achieve precise estimation, rendering it unsuitable for channels that undergo temporal variations. The utilization of data-aided scheme necessitates additional bandwidth resources to facilitate the transmission of training sequences or pilots. The literature has covered a wide range of CFO estimation techniques, including both blind and data-aided methods.

5.3 Proposed CFO Estimation Method Using SIT Sequence

When addressing channel estimation in wireless systems, it is common for researchers to make the consideration that there is no frequency offset. In practical terms, the offset is sufficiently minute such that the demodulated signal experiences insignificant phase rotations within the duration of the preamble. The utilization of stable oscillators is not a feasible approach to fulfill such conditions, as a rule, due to excessively strict stability criteria. In addition, it should be noted that even under ideal circumstances, oscillators would prove insufficient in a mobile communication setting that is subject to considerable Doppler shifts. The sole resolution is to precisely quantify the frequency deviation.

Recent times, there has drawn significant attention on the SIT based channel estimation method for wireless communications [83, 98–100]. This method involves superimposing a pilot symbol sequence on top of a data symbol sequence and then transmitting both of them together. Therefore, the data transfer rate remains constant. The correlation operation is performed between the known SIT and received symbols by the receiver in order to estimate the CIR. But, this correlation has a negative impact on this estimation accuracy.

The present work explores the simultaneous estimation for both the CFO and CIR using a periodic SIT sequence. The solution comprises of two distinct stages, namely a frequency-offset estimator and a channel estimator after compensation of the frequency discrepancy within the received signal.

The concept of SIT method involves the inclusion of adding a repetitive
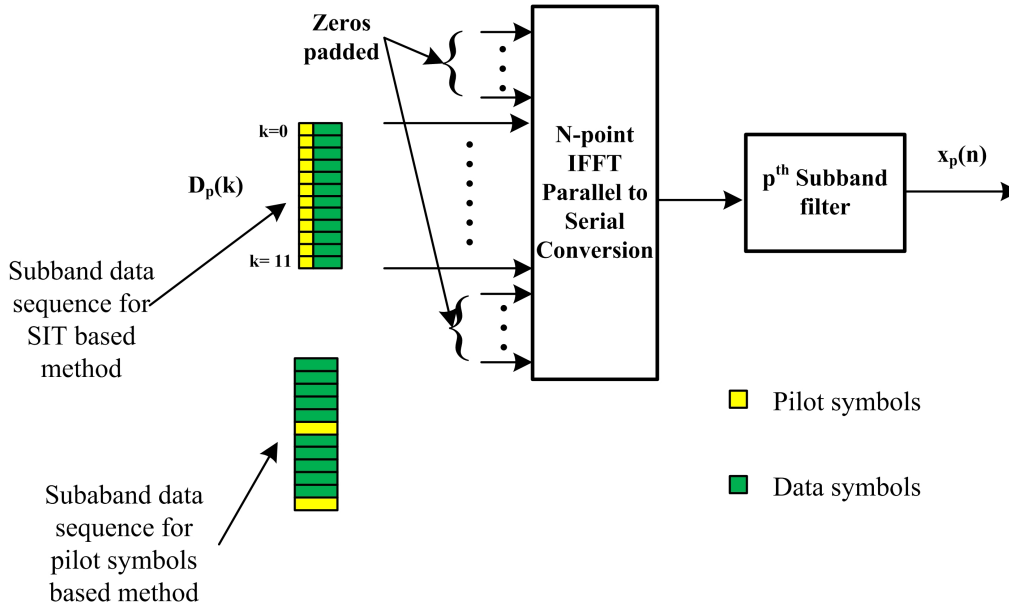
Figure 5.3: The UFMC subband signal generation for SIT and pilot based method (frequency domain)

training symbols in the time/frequency domain to the data symbols prior to their transmission as depicted in Figure 5.3. This technique results in an increased transmission efficiency. Within this framework, the data symbols are regarded as sources of additive interference in the estimation process. On other hand, the SIT sequence is commonly perceived as an additive interference that affects data detection.

5.3.1 Novelty of the proposed method

The CFO (Carrier Frequency Offset) estimation is a crucial task in wireless communication systems, especially in OFDM (Orthogonal Frequency Division Multiplexing) and other similar modulation schemes like UFMC. The SIT based methods are a technique used to improve estimation accuracy with efficient band utilization. Here's how they introduce novelty to CFO estimation:

Improved Accuracy: The SIT sequence based method involve embedding known pilot symbols within the data symbols. This addition of known symbols helps in accurately estimating the CFO. The CFO can be estimated by comparing the received signal with the expected values of the SIT sequence, improving accuracy.

90

Robustness: The CFO estimation is susceptible to various impairments, including channel fading, noise, and interference. The proposed method make CFO estimation more robust by providing a reference that can withstand such adverse conditions, leading to more reliable CFO estimates.

Reduced Overhead or Improved spectral efficiency: Traditional CFO estimation methods may require dedicated pilots or training symbols, which consume valuable bandwidth and reduce data throughput. The proposed SIT based method use the same symbols for data and reference, minimizing the overhead and maximizing spectral efficiency. That means, it allows for a more efficient utilization of the available bandwidth, as training and data symbols are combined, ensuring that no spectrum goes to waste. This can be particularly important in scenarios with limited bandwidth.

Adaptability: The SIT sequences can adapt to changing channel conditions. By including training symbols in the data stream, they provide a continuous source of reference for CFO estimation, even when the channel conditions change over time (i.e., under dynamic channel conditions).

Diversity and MIMO Systems: In multiple antenna systems like MIMO, the SIT sequences can be extended to provide diversity, helping estimate CFO for different antennas more effectively. This is essential for high-throughput, multi-antenna systems.

Compatibility with Modern Modulation Schemes: This approach is compatible with advanced modulation schemes, including those used in 5G and beyond, where higher order modulations are commonly employed. It enables accurate CFO estimation in high data rate and bandwidth-efficient systems.

Machine Learning Integration: The SIT sequences can be used in conjunction with machine learning techniques to further improve CFO estimation accuracy and its computational complexity. This combination can lead to highly adaptive and efficient estimation methods.

In summary, the novelty of CFO estimation using SIT sequence lies in their

ability to improve accuracy, robustness, adaptability, and efficiency while reducing overhead. This approach is well-suited to modern and future communication systems, particularly in scenarios where spectral efficiency and robust synchronization are essential.

The system model for this method is thoroughly explained in the subsequent subsections.

5.3.2 System Modeling

The training sequence is incorporated into the transmitted UFMC signal at the transmitter by means of arithmetic addition in time-domain, with a specified power allocation ratio, prior to propagation through the channel. Through this approach, it becomes possible to transmit data symbols across all time-frequency slots, resulting in a reduction of bandwidth usage in comparison to traditional estimation techniques. The estimation of CFO and CIR is performed collaboratively at the receiver through the use of the same training sequence that was superimposed at the transmitter.

Transmitter Model

The basic steps involved in the SIT-based UFMC transmitter are as follows:

- Selection of SIT sequence: Choose a known pilot or training sequence that will be superimposed on the transmitted signal. This sequence should have good auto-correlation properties and known properties at the receiver.

- Superimpose the sequence: To the transmitted signal, the selected SIT sequence is algebraically added at stage. This can be done by overlaying the SIT sequence on the data symbols.

The Figure 5.4 represents the model of UFMC's transmitter for the SIT sequence based method. Here, the input data are grouped into subbands and each subband data symbols processed through N-point IFFT then FIR filter to generated the time-domain UFMC signal. The SIT sequence is algebraically added to the final

UFMC signal (sum of subband filters output) in time-domain at a predetermined data to training/pilot power ratio. That means, both the SIT and data sequences are transmitting at the same instant time. Let $x_i(n)$ denotes the ith time-domain UFMC symbol and $c(n)$ denotes the SIT sequence that is a nonrandom periodic sequence with period of transmitted UFMC symbol duration. The resulting symbols after superimposing (known as data-training symbols) is

$$s_i(n) = a_d x_i(n) + a_c c(n) \qquad (5.15)$$

where a_d and a_c are the arbitrary amplitude coefficients of the data training sequence respectively that are depends on power constraint of the transmitted signal that how it distributed among data and training symbols. The power distribution factor (power allocation ratio) defined as $\alpha = \frac{\sigma_c^2}{\sigma_x^2 + \sigma_c^2}$. Where $\sigma_x^2 = E[x(n)x^*(n)]$ and $\sigma_c^2 = E[c(n)c^*(n)]$. Now the amplitude coefficients are defined related to the power allocation factor as $a_d = \sqrt{(1-\alpha)/\sigma_s^2}$ and $a_c = \sqrt{\alpha/\sigma_c^2}$. The time-domain UFMC symbol $x_i(n)$ is defined from 5.2 as

$$x_i(n) = \sum_{p=0}^{B-1} \sum_{l=0}^{L_f-1} f_p(l) d_{i,p}(n-l) \qquad (5.16)$$

$$d_{i,p}(n) = \frac{1}{N} \sum_{k=0}^{Q-1} D_{i,p}(k) e^{\frac{j2\pi}{N}(K_0 + (p-1)Q + k)n} \qquad (5.17)$$
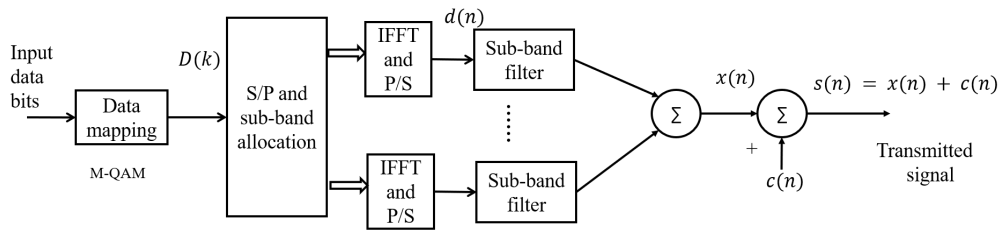

Figure 5.4: The UFMC transmitter model for proposed CFO estimation method

The matrix form represent ion of the time-domain UFMC symbol 5.2:

$$X_i = \sum_{p=0}^{B-1} \mathcal{F}_p \mathcal{W}_p \mathcal{D}_{i,p} \qquad (5.18)$$

93

where $\mathcal{F}_p$ is a Toeplitz matrix of pth sub-band filter coefficients with dimensions $N + L_f - 1 \times N$ having the first column elements of $[f_p(0), f_p(1), \ldots, f_p(L_f - 1), [0]_{(1 \times N-1)}]^T$ and first row $[f_p(0), [0]_{(1 \times N-1)}]$, $\mathcal{W}_p$ is the IFFT matrix that relevant to p^{th} sub-band carriers with dimensions $N \times Q$ and $\mathcal{D}_{i,p}$ is the column matrix of the pth sub-and data sequence.

5.3.3 SIT Sequence

The initial stage of developing a communication connection to address timing and frequency uncertainties between transceivers involves synchronization, which is commonly accomplished through the utilization of a designated reference or pilot sequence. To fulfill such a goal, the employ sequences in wireless communication systems that have a good auto-correlation properties and a zero cross-correlation function for many practical applications. Zadoff-Chu (ZC) sequences have gained popularity in contemporary wireless communication systems as a synchronization tool, supplanting traditional pseudo-random noise sequences, owing to their impeccable auto-correlation characteristics. The training sequence comprises the digitized samples of a linear frequency modulated signal. The time domain magnitude of the sequence remains constant, rendering it optimal with respect to PAPR [101, 102]. The training sequence is defined as

$$c(n) = \begin{cases} e^{j\frac{2\pi}{N}n^2} & \text{N is even} \\ e^{j\frac{2\pi}{N}n(n+1)} & \text{N is odd} \end{cases} \tag{5.19}$$

The training sequence have the following advatages

1. The distribution of energy across the sequences is uniform across all subcarriers in the data set. Additionally, these sequences are mutually orthogonal, thereby fulfilling the prescribed selection criterion.

2. The magnitude of the sequence remains constant in the temporal domain. These sequences are recognized as being optimal with regards to the PAPR of the combined data and training signals. as discussed in [103].

Wireless Channel Model

Modern wireless systems have been developed to provide better data rates while supporting high velocities of the terminal. In wireless communication systems, signals propagate through various channels that can introduce distortions, such as multipath fading, due to reflections, diffractions, and scattering. The phenomenon of ISI is caused by multi-path fading, which is a result of high-data rates. A channel that exhibits the property of selectively passing certain frequencies over others is referred to as a frequency-selective type. However, it is crucial to keep in mind that the received signal may experience frequency shifts, also known as Doppler shifts, and consequent time-variation, as a result of mobility and/or CFO. The phenomenon of Doppler effect, when combined with ISI, results in the emergence of a time-varying frequency selective (doubly-selective channel) [104]. This CIR is mathematical represented as

$$h(t, \tau) = \sum_{i=0}^{L_h-1} g_i(t)\delta(\tau - \tau_i) \tag{5.20}$$

The time-varying i^{th} path's amplitude is denoted as $g_i(t)$, while τ_i represents the ith propagation path delay. The channel taps/length is denoted by L_h. It is postulated that the amplitude of each path follows a Rayleigh process. The CIR is characterized by a probability distribution that corresponds to zero-mean complex Gaussian with uncorrelated paths. From the Jake's power spectrum, the attenuated coefficients of each path are determined independently. which is given by

$$P_J(f) = \frac{1.5}{\pi f_D \sqrt{1 - \frac{f-f_c}{f_D}^2}} \text{ [104]} \tag{5.21}$$

Channel Simulation

In practical implementations, the channel models often incorporate statistical models to capture the random nature of fading and time variations. These statistical models can be derived from measurements or based on theoretical assumptions about the propagation environment. The tapped delay line (TDL)

models are the commonly employed models to simulate of wireless mobile networks. The TDL model represents the channel as a series of taps, each corresponding to a multi-path component. These taps have different attenuation, delays, and phases, which are typically modeled as time-varying parameters. In accordance with this model, the channel can be produced by substituting the predetermined delay values of the taps in place of selecting arbitrary delay values. The selection of the number of sums associated with a single tap must be proportionate to the tap's relative amplitude. That is,

$$h(f,t) = \sum_{k=0}^{L-1} e^{j\phi_k} e^{j2\pi v_k t} e^{-j2\pi f \tau_k} \tag{5.22}$$

The variables ϕ_k, v_k, and τ_k are considered to be random variables that exhibit statistical independence and identical distribution across distinct values of k. In order to provide greater precision, it is posited that the stochastic variable ϕ_k is statistically independent of both v_k and τ_k, and that it conforms to a uniform distribution across the unit circle. The reference documents [105–107] and [108] provides a list of significant tapped delay line models utilized for 5G channel simulations

Receiver Model

In cases where synchronization is not achieved with complete accuracy, it is common to represent the TO as a delay and FO is typically represented as a phase shift in the time-domain representation of the received signal. Here, we assumed the system is perfectly time synchronized. The baseband received signal in presence of frequency offset is

$$r_{i,\beta}(n) = e^{j\frac{2\pi}{N}\beta(iN_T + n)} s_i(n) * h_i(n) + z(n) \tag{5.23}$$

The equivalent baseband received signal 5.23 can be expressed in matrix form as

$$R_{i,\beta} = \Psi_i \mathcal{S}_i h_i + Z_i \tag{5.24}$$

where $\mathcal{S}_i = \mathcal{X}_i + \mathcal{C}$, $\mathcal{X}_i$ and $\mathcal{X}_i$ are the Toeplitz matrices of the transmitted UFMC symbol and SIT sequence with dimension $(N + L_f - 1) \times L_h$ respectively, h_i denoted the channel coefficients vector with the order of $L_h \times 1$, Z_i AWGN vector of order $N \times 1$. The matrix Ψ_i, which is dependent on the frequency offset, is defined as follows:

$$\Psi_i = e^{j\frac{2\pi}{N}\beta i N_T} \text{diag}\left\{1, e^{j\frac{2\pi}{N}\beta}, ... e^{j\frac{2\pi}{N}\beta(N_T-1)}\right\} \tag{5.25}$$
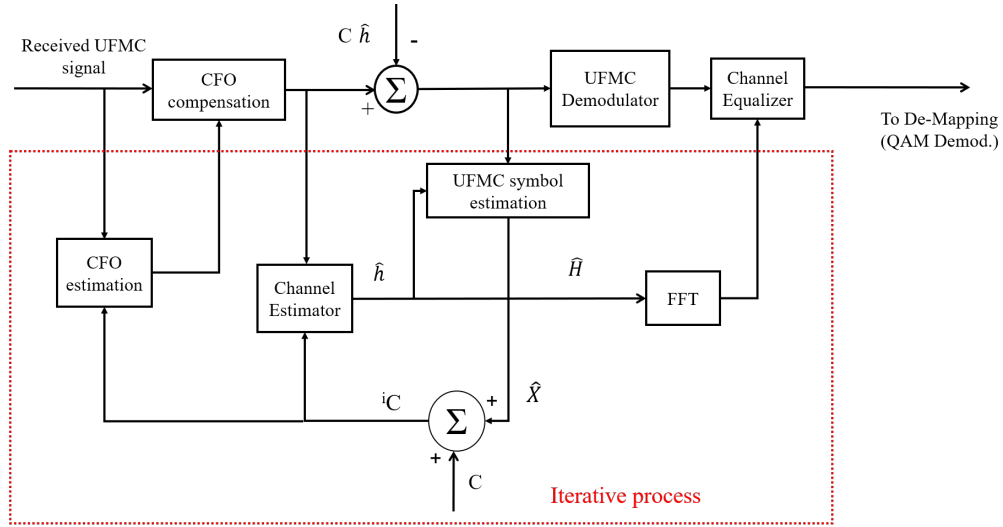
Figure 5.5: The UFMC receiver model for proposed CFO estimation method

Figure 5.5 demonstrates the proposed receiver model for the UFMC system. The processing steps in this model are typically include:

- In general, the incoming signal at receiver is typically down-converted to baseband and the being processed by a matched filter to enhance the correlation properties of the training sequence.

- Synchronization: Synchronize the receiver with the transmitted signal, including frame synchronization, symbol synchronization, and carrier synchronization. Here we assumed that the system perfectly frame and symbol synchronized.

- CFO estimation: Estimate the CFO by analyzing the phase or frequency deviation using the SIT sequence. This method is detailed in section 5.3.4 .

- CFO compensation: Once the CFO estimation is completed, it is possible to compensate by applying an appropriate correction to the received signal. The aforementioned rectification can be attained through the process of frequency shifting the signal that has been received.

- Data demodulation: After CFO compensation, perform the remaining receiver processing steps such as channel estimation, equalization, and demodulation. The demodulation process is based on the modulation technique implemented within the given system.

5.3.4 The CFO Estimation Using SIT Sequence

The present study adopts certain assumptions in order to derive a formulation for the estimation:

1. The underlying assumption is that the input data symbols are random variable with independence and identical distribution characteristics (commonly referred to as i.i.d) having zero mean/expected value and a covariance matrix of zero. i.e., $E\left[D_i\right] = 0$ and

$$E\left[D_i D_j^H\right] = \begin{cases} 0; & \text{for } i \neq j \\ \sigma_d^2 I; & \text{for } i \equiv j \end{cases} \tag{5.26}$$

2. The transmitted UFMC symbols exhibit no correlation with one another and possess a mean value of zero i.e., $E\left[\mathcal{X}_i\right] = 0$ and

$$E\left[\mathcal{X}_i \mathcal{X}_j^H\right] = \begin{cases} 0; & \text{for } i \neq j \\ \sigma_x^2 I; & \text{for } i \equiv j \end{cases} \tag{5.27}$$

3. The UFMC transmitted data symbols are uncorrelated with the superimposed training sequence, i.e., $E\left[\mathcal{X}_i \mathcal{C}^H\right] = E\left[\mathcal{X}_i^H \mathcal{C}\right] = 0$ and $E\left[\mathcal{C}^H \mathcal{C}\right] = \sigma_c^2$; where $()^H$ denotes the Hermitian matrix.

4.

$$E\left[\mathcal{S}_i\mathcal{S}_j^H\right] = \begin{cases} \sigma_c^2; & \text{for } i \neq j \\ \left(\sigma_x^2 + \sigma_c^2\right)I; & \text{for } i = j \end{cases} \tag{5.28}$$

At the receiver, the same SIT sequence is used to determine the CFO and channel coefficients by correlation property and least squares (LS) algorithm. The received UFMC signal at baseband level 5.24 can be represented as

$$R_i = \Psi_i\left(\mathcal{X}_i + \mathcal{C}\right)h_i + Z_i \tag{5.29}$$

The practical wireless communication systems exhibit a block fading channel, which enables us to make an assumption that a number of data symbols experienced by the same channel effect, subject to the coherence time of the channel. That is, $h_i = h_{i+1} = h$; for $i = 0, 1, \ldots, N_C$; where N_C denotes the number of data symbols underwent approximately equivalent fading coefficients of the channel.. Typically the N_C may 6 or 7 that defined in the 3GPP standards for a maximum Doppler shift of 555 Hz and at 120 kmphr speed of mobile. The correlation between received baseband UFMC symbols is defined as

$$\begin{aligned} Corr_{R_i,R_{i+1}} = R_{i,\beta}^H R_{i+1,\beta} &= \left(h^H\left(\mathcal{X}_i^H + \mathcal{C}^H\right)\Psi_i^H + Z_i^H\right)\left(\Psi_{i+1}\left(\mathcal{X}_{i+1} + \mathcal{C}\right)h + Z_{i+1}\right) \\ &= e^{j\frac{2\pi N_T}{N}\beta}\left(\sigma_c^2 I + \mathcal{X}_i^H\mathcal{C} + \mathcal{C}^H\mathcal{X}_{i+1} + \mathcal{X}_i^H\mathcal{X}_{i+1}\right)\sigma_h^2 \end{aligned} \tag{5.30}$$

where

$$\Psi_i^H\Psi_{i+1} = e^{j\frac{2\pi N_T}{N}\beta}I; \sigma_h^2 = h^H h; \tag{5.31}$$

According to the assumption described in above section, the correlation function $Corr_{R_i,Ri+1}$ can be simplified as

$$Corr_{R_iR_{i+1}} = e^{j\frac{2\pi N_T}{N}\beta}\sigma_c^2\sigma_h^2 I + \sigma_z^2 I \tag{5.32}$$

From equation 5.32, the estimated CFO is given by

$$\hat{\beta}_i = \frac{N}{2\pi N_T} \arg\left\{Corr_{R_i,R_{i+1}}\right\}; i = 0, 1, ..., N_C - 2 \qquad (5.33)$$

A more accurate estimation can be achieved by calculating the average of estimated CFO across the $N_C - 1$ number of UFMC symbols.

$$\hat{\beta} = \frac{1}{N_C - 1} \sum_{i=0}^{N_C-2} \hat{\beta}_i \qquad (5.34)$$

Now the CFO is compensated by the following expression

$$R_{i,comp} = R_{i,\beta} e^{-j\frac{2\pi}{N}\hat{\beta}iN_T} diag\left\{1, e^{-j\frac{2\pi\hat{\beta}}{N}}, \dots, e^{-j\frac{2\pi\hat{\beta}(N_T-1)}{N}}\right\} \qquad (5.35)$$

From this received base band signal (after CFO compensation), the channel coefficients are estimated using LS method using known SIT sequence, that is

$$\hat{h}_i = \left(\mathcal{C}^H \mathcal{C}\right)^{-1} \mathcal{C}^H R_{i,comp}; i = 0, 1, \dots, N_C - 1 \qquad (5.36)$$

We know that the channel is constant over the N_C UFMC data symbols (which is depends on the coherence time). Therefore, to get better estimation

$$\hat{h} = \frac{1}{N_C} \sum_{i=0}^{N_C-1} \hat{h}_i \qquad (5.37)$$

Data Detection

After the CFO compensation, the resulting signal $R_{i,comp}$ is used to obtain the estimated UFMC transmitted symbol with channel effect by removing the interference of SIT sequence. That is,

$$\hat{R}_i = R_{i,comp} - \mathcal{C}\hat{h} \qquad (5.38)$$

Now this estimated received UFMC symbols are processed through the UFMC de-modulator that performs FFT and frequency domain equalizer per subcarrier.

From this resulting received symbols, the data symbols are recovered by equalization.

Iterative Process

The transmitted UFMC data and SIT sequence may not exactly uncorrelated in practice. So, according to the equation 5.30, the unknown transmitted UFMC symbol may interfere on the estimation and reduce the estimate accuracy. This estimated accuracy can be improved with iterative process according to the Algorithm 1. To explain this, let consider the appropriated correlation between received baseband UFMC symbols from equation 5.30

$$Corr_{RR} = e^{j\frac{2\pi N_T}{N}\beta}\left(\sigma_c^2 + \mathcal{X}_i^H\mathcal{C} + \mathcal{C}^H\mathcal{X}_{i+1} + \mathcal{X}_i^H\mathcal{X}_{i+1}\right)\sigma_h^2 I \qquad (5.39)$$

For convenience, assume that the channel coefficients are normalized to have $\sigma_h^2 = h^H h = \sum_{l=0}^{L_h-1}\|h(l)\|^2 = 1$.

$$\begin{aligned} Corr_{RR} &= e^{j\frac{2\pi N_T}{N}\beta}\left((\mathcal{X}_i + \mathcal{C})^H(\mathcal{X}_{i+1} + \mathcal{C})\right) \\ &= e^{j\frac{2\pi N_T}{N}\beta}\mathcal{C}^H\mathcal{C} + e^{j\frac{2\pi N_T}{N}\beta}\left(\mathcal{X}_i^H\mathcal{C} + \mathcal{C}^H\mathcal{X}_{i+1} + \mathcal{X}_i^H\mathcal{X}_{i+1}\right) \end{aligned} \qquad (5.40)$$

In above equation 5.40, the first term utilized for the purpose of estimating CFO and the second one represents the error component arises from the mutual interference between the SIT and data sequences. To reduce this impact on the estimation, we are implementing the iterative process. In this process, the estimated received data symbols that are obtained from 5.38 fed back to estimate the UFMC data symbol $^j\hat{X}_i$ for the jth iteration. That is

$$^j\hat{X}_i = {}^{j-1}\mathcal{H}^{H\,j-1}\mathcal{H}\hat{R}_i \qquad (5.41)$$

Algorithm 1 Computation of CFO with iterative process

1: **Inputs:**

   $R_{i,\beta}; i = 0, \ldots, N_{symb} - 1 \leftarrow$ The received baseband
   UFMC symbol block with CFO
   $\mathcal{C}$ = Toeplitz matrix of SIT sequence
   I = number of iterations

2: **Initialize:**

   ${}^0\hat{X}_i \leftarrow 0; {}^0\hat{\Psi}_i \leftarrow 0; j = 1$

3: **for** $i = 0; i \leq N_C - 2; i + +$ **do**

4: $\quad \Phi_i = \tan^{-1}\left(\frac{Im\left\{R_{i,\beta}^H R_{i+1,\beta}\right\}}{Re\left\{R_{i,\beta}^H R_{i+1,\beta}\right\}}\right);$

5: $\quad \hat{\beta}_i = \frac{N}{2\pi N_T}\Phi_i;$

6: **end for**

7: $\hat{\beta} = \frac{1}{N_C}\sum_{i=0}^{N_C-1}\hat{\beta}_i$

8: $\hat{\Psi}_i = \exp\left\{j\frac{2\pi}{N}\hat{\beta}iN_T\right\}diag\left\{1, e^{j\frac{2\pi\hat{\beta}}{N}}, \ldots, e^{j\frac{2\pi\hat{\beta}(N_T-1)}{N}}\right\}$

9: $R_{i,comp} = conj\left\{\hat{\Psi}_i\right\}R_{i,\beta}; i = 0, \ldots, N_C - 1$

10: $\hat{h} = \frac{1}{N_C}\sum_{i=0}^{N_C-1}\left(\mathcal{C}^H\mathcal{C}\right)^{-1}\mathcal{C}^H R_{i,comp}$

11: $\hat{R}_i = R_{i,comp} - \mathcal{C}\hat{h}$

12: $\hat{\mathcal{H}} = Toeplitz\left(\hat{h}\right)$

13: $\hat{X}_i = \left(\hat{\mathcal{H}}^H\hat{\mathcal{H}}\right)^{-1}\hat{\mathcal{H}}^H\hat{R}_i$

14: For iterative process: ${}^0\hat{\mathcal{X}}_i \leftarrow Toeplitz\left(\hat{X}_i\right); {}^0\hat{h} \leftarrow \hat{h}$

15: **while** $j \leq I$ **do**

16: $\quad$ **for** $i = 0; i \leq N_C - 2; i + +$ **do**

17: $\quad\quad$ Determine ${}^jCorr_{RR}$ according to 5.42

18: $\quad\quad$ Estimate ${}^j\hat{\beta}_i$ according to 5.43

19: $\quad$ **end for**

20: $\quad$ Repeat steps from 7 to 9 to compute ${}^j\hat{\beta}$ and ${}^jR_{i,comp}$

21: $\quad {}^j\hat{S}_i \Leftarrow \mathcal{C} + {}^0\hat{\mathcal{X}}_i$

22: $\quad$ Estimate ${}^j\hat{h}$ according to 5.44

23: $\quad {}^j\hat{R}_i = {}^jR_{i,comp} - \mathcal{C}\hat{h^j}$

24: $\quad \hat{\mathcal{H}} = Toeplitz\left(\hat{h^j}\right)$

25: $\quad$ Go to step 13 to compute ${}^j\hat{X}_i$

26: $\quad$ Process for data detection ${}^j\hat{D}_i$

27: $\quad$ Update: $j \leftarrow j + 1$

28: **end while**

---

where $^{j-1}\hat{\mathcal{H}}$ represents the Toeplitz matrix of $^{j-1}\hat{h}$. For j^{th} iteration, the correlation matrix between the two consecutive received symbols is given by

$$^{j}Corr_{RR} = {}^{j-1}Corr_{RR} - e^{j\frac{2\pi N_T}{N}{}^{j-1}\hat{\beta}} \left({}^{j-1}\hat{\mathcal{X}}_i^H \mathcal{C} + \mathcal{C}^{H\,j-1}\hat{\mathcal{X}}_{i+1} + {}^{j-1}\hat{\mathcal{X}}_i^{Hj}\hat{\mathcal{X}}_{i+1} \right)$$
(5.42)

Now, the estimated CFO for the jth iteration is given by

$$^{j}\hat{\beta} = \frac{N}{2\pi N_T} \arg \left\{ {}^{j}Corr_{RR} \right\}$$
(5.43)

Furthermore, in order to enhance the precision of channel estimation in an iterative manner, it is possible to utilize the estimated symbol $^{j}\hat{X}_i$. The channel coefficients for j^{th} iteration can be estimated by

$$^{j}\hat{h} = \frac{1}{N_C} \sum_{i=0}^{N_C-1} \left({}^{j}\mathcal{S}_i^{Hj} \mathcal{S}_i \right)^{-1} {}^{j}\mathcal{S}_i^{Hj} R_{i,comp}$$
(5.44)

where $^{j}\mathcal{S}_i = {}^{j}\hat{\mathcal{X}}_i + \mathcal{C}$. Similarly to further improve the estimation accuracy, the steps from 5.41 to 5.44 can repeat again and again.

The SIT-based approach enforces a predetermined transmission power budget, which restricts the summation of powers for both training and data symbols. Achieving accurate data detection necessitates precise estimation, which can be facilitated by allocating greater transmit power to training symbols. However, this approach may lead to a reduction in the amount of power available for data transmission, thereby resulting in a deterioration in the overall functioning of the system. Hence, it is imperative to contemplate a power allocation trade-off between training and data symbols. That is, the performance of the system is reliant on the interdependent power interruption of data and training symbols. In this point of view, the power allocation ratio should be optimize for better system's performance.

5.4 Simulation Results

The evaluation of the suggested technique and the estimation algorithms are examined through simulation. In this simulation, we considered the UFMC system that uses 1024 or 2048 FFT size according to the NR bandwidth configuration defined by 3GPP [15], at carrier frequency of range FR1 or FR2. The present investigation incorporates two distinct cases, namely under AWGN channel and multi-path channel simulated through Rayleigh process. Table 5.1 outlines the simulation parameters employed in this methodology. The

Table 5.1: Simulation Parameters

Name of the Parameter	Value
Operating carrier frequency	6 GHz
Channel bandwidth	10/20 MHz
Subcarrier Spacing	15/30 kHz
IFFT size	1024/2048
Modulation scheme	QPSK/16-QAM
Sub-band size	12SC
Stop band attenuation	40 dB
Filter length	73/145
Wireless channel	Rayleigh

CFO/channel estimation accuracy of the proposed SIT based method for UFMC system depends on the power allocated for the training sequence. Figure 5.6 and 5.7 depicts the combined effect of power allocation factor/ratio α and estimation errors on QPSK/16-QAM modulation performance for various channel models. For a fixed power budget, the higher value of α implies results in a reduction of power in the data sequence and an increase in estimation accuracy, leading to a low effective SNR. The smaller value of α increased power in the data symbol and decrease estimation accuracy. It can be observed in the Figure 5.6 that the MSE decrease with the power allocation ratio. At higher power allocation ratio, the MSE minimum but the data detection process produces more number of bit error due the interference of SIT sequence on the data symbols and which result in higher BER. There is trad-off between the system BER performance and the estimation accuracy. To optimize the power allocation ratio to minimize the interference and getting better BER performance, the simulations are performed

for the various channel models and the modulation techniques with a different orders. For ITU VehA or SUI-3 channel model, the MSE variation with respect to the power allocation factor is almost same but the BER variation is different as shown in Figure 5.6. This mainly due to the channel variation that changes with the channel delay spread. For the case of rapid channel fluctuation, the data symbols may be impacted in amplitude. To overcome from this, it required more power to allocate data. Therefore, the optimal power allocation ratio is less (between 0.2 to 0.3) for ITU VehA channel and more (approximately 0.5) for SUI channels.

(a) For ITU VehA channel   (b) For SUI channel
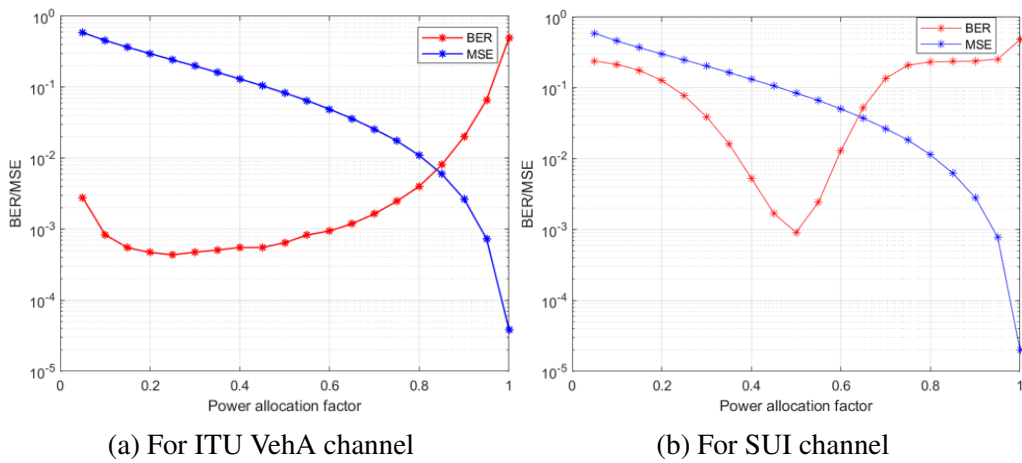
Figure 5.6: BER and MSE variation with Power allocation ratio/factor

The graph 5.7 shows that the optimal power allocation ratio varies with type of channel and modulation order. For higher order modulation techniques, the power required is more than the lower order for better data detection. It can be observed that the optimal power allocation ratio is less (more power is allocated to data) for 16-QAM and more (between 0.5 to 0.6) for QPSK modulation. At these ratios the proposed method obtained better performance.

5.4.1   BER Performance

In this study, we conduct a comparison of the BER of the UFMC system under the influence of frequency offset errors with SIT based and pilot based methods shown in figure 5.8. The evaluation of BER performance is conducted for the system parameters N = 1024, 16-QAM, and the optimal power ratio $\alpha = 0.3$ for

(a) For QPSK   (b) For 16-QAM
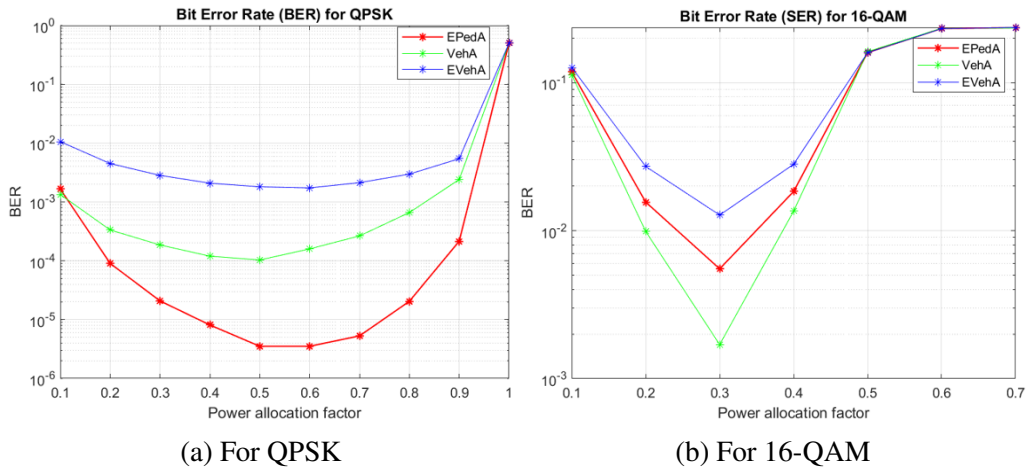
Figure 5.7: BER variation with power allocation ratio/factor in different scenarios
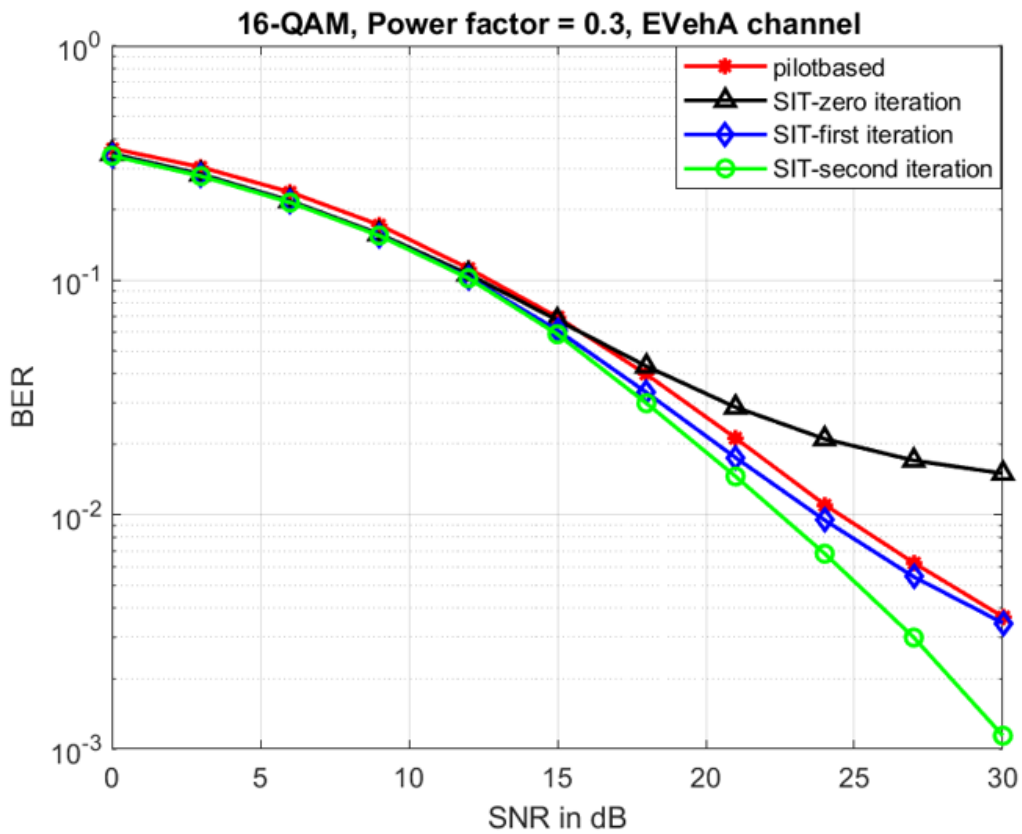
Figure 5.8: BER performance comparison for ITU EVehA channel

EVeh-A channel model. Also, here we are assuming the both CFO and CIR are unknown. These two are jointly computed with SIT and pilot based methods. Based on the simulation outcomes, it is evident that the conventional approach, which relies on pilot-based techniques, outperforms the proposed method that involves zero iterations. However, for the first and second iteration, the SIT

method performs superior than the conventional pilot-based estimator at the cost of higher computational complexity. In addition, with proposed method we can save 1 to 2 dB power to attain the threshold BER value of about 10^{-2} (that is if we assume this is the minimum acceptable BER of the system).

5.4.2 Spectral Efficiency Comparison

The primary benefit of the proposed scheme is the bandwidth efficiency. Let consider a single PRB which consists of 72 or 84 subcarriers (i.e., 12 subcarriers with 6 or 7 UFMC symbols) as illustrated in Figure 5.9. This figure demonstrates, how many subcarriers used to transmit data symbols and how many are used for the training/pilot symbols to estimate the CFO and CIR. It is clearly states that the training based method used two successive symbols for transmitting the known training sequence to estimate the CFO that means 24 subcarriers are used or dedicated for the TS transmission in one PRB. This training-based method utilized only 48 or 60 subcarriers for data symbol transmission out of 72 or 84 respectively, that is around 33 to 28% bandwidth wasted for the PS or TS. The another alternative estimation method is pilot based approach that uses a different pilot pattern as shown in Figure 5.9 (b) and (c) to estimate CIR and CFO. The 2-D pilot based method uses four number subcarriers for pilots and hence it gives better spectral efficiency. But, with the SIT based method all subcarriers are used for both data and training sequence. That is the subcarriers are not dedicated completely to the TS transmission. Therefore, the proposed method improves the spectral efficiency of 4.76 to 5.55 compared to the conventional method.

5.5 Summary

In summary, the performance of the UFMC systems may degrade if the CFO exceeds a certain value. Here, we have presented a SIT based CFO estimation algorithm. The SIT-based CFO estimation in UFMC systems is a method that leverages strategically embedded known training sequences to accurately estimate and compensate for frequency offsets. That means, the
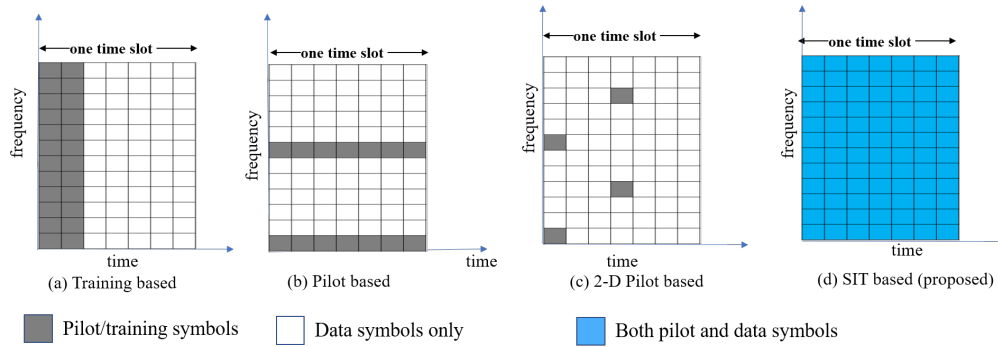
Figure 5.9: Spectral efficiency analysis

training/pilot sequence is superimposed on the data and there are no dedicated subcarriers for pilot sequence. This approach enhances the robustness of UFMC systems in challenging communication environments and contributes to overall performance improvements. The spectral utilization improves about 4.76% compared to conventional (pilot based) method. The iterative process is used to improve the accuracy of estimation. For second iteration, the proposed method improved the BER performance and the required SNR reduced by 1 to 2 dB for the acceptable BER of 10^{-2}. Due to this iterative process, the computational complexity increases greatly to get better performance, this is main disadvantage of this method.

Chapter 6

Conclusion and Future Scope

This chapter provides a synopsis of the primary findings of the thesis and outlines potential avenues for future research.

6.1 Conclusions

The UFMC is one of the emerging waveform technologies for NGWN because of its abilities. However, the computational and hardware complexity of the UFMC transceiver system has more than the conventional 4G waveform like CP-OFDM due to filtering operation at the transmitter and 2N-point FFT processing at the receiver. In addition, the filtering operation in the UFMC system destroyed the orthogonality between subcarriers and hence generates interference. Overall, the UFMC system is characterized by its complexity in filtering, synchronization, equalization, digital signal processing, and RF front-end implementation. These complexities are necessary to attain the desired performance, robustness against interference, and ability to support high data rates. As technology advances, efforts are being made to improve the efficiency of the UFMC system at low complexity through advancements in algorithms, hardware, and integrated circuit design. In this point of view, here we proposed the simplified UFMC transceiver model along with the efficient CFO estimation method. The following are the major conclusions of this work:

- A simplified UFMC transmitter model is proposed by simplifying the appropriated transmitted time-domain UFMC symbol and the filtering effect is implemented in frequency domain before processing through IFFT block. This model is implemented like OFDM without filtering

operations by introducing more OBE than the traditional transmitter. This model reduced the computational complexity approximately 8 to 13 times based on the FFT's size.

- The UFMC receiver is developed with less computations, where the exact frequency domain UFMC received symbol after FFT processor and decimator is derived and simplified to implement with a single N-point FFT and that reduced the computational complexity more than two times (i.e., 50%) compared to the traditional receiver model without degrading the system performance. The zero-padding for processing 2N-point FFT and decimation part is simply replaced by single N-point FFT at the receiver, which reduced the number of hardware components at baseband signal processing and the storage requirement for read/ write operation to process the data and the number of computations or operations. This model reduced the hardware requirement and hence the power consumption.

- Furthermore, the interference was analyzed due to filtering operation in the UFMC symbol by deriving the closed form of the interference energy related to the subband filter length. According to this analysis, the filter length was dynamically modified to minimize interference. This approach reduces the interference by approximately 1.5 to 3.2 dBs thus improving the system performance.

- Finally we have presented a SIT based CFO estimation algorithm. In this method, the training/pilot sequence is superimposed on the data and there are no dedicated subcarriers for pilot sequence. Hence it can improve the spectral utilization about 4.76% compared to conventional (pilot based) method. The iterative process is used to improve the accuracy of the estimation. For second iteration, the proposed method improved the BER performance and the required SNR reduced to 1-2 dB for the acceptable BER of 10^{-2}. Due to this iterative process, the computational complexity increases greatly to get better performance, this is main disadvantage of

this method.

6.2 Future Directions

The UFMC is considered as one of the candidate waveforms for future wireless communication systems, including 5G and beyond. Its ability to accommodate various deployment scenarios, support massive connectivity, and provide high data rates makes it an attractive option for future wireless networks. The main opportunities for further research are as follows:

- UFMC's filtering capabilities allow better spectral shaping and improved spectral efficiency compared to OFDM. Future research and development can focus on optimizing the filter design and system parameters to further enhance spectral efficiency. That is the application AI/ML/deep learning algorithms to reduce the computational complexity to generate and process the UFMC signal.

- The UFMC's inherent flexibility in frequency and time domain allocation makes it well-suited for cognitive radio systems. These systems can dynamically adapt to changing radio frequency environments by intelligently selecting the most appropriate subcarriers and adjusting their power levels (intelligent resource allocation algorithms).

- As energy efficiency becomes a crucial aspect of wireless communication systems, UFMC can be optimized to reduce power consumption. Future research can explore low-power implementations, and adaptive modulation techniques to enhance power efficiency while maintaining higher data rates.

- The real-time hardware implementation of the efficient UFMC transceiver model.

Bibliography

[1] M. Alsabah, M. A. Naser, B. M. Mahmmod, S. H. Abdulhussain, M. R. Eissa, A. Al-Baidhani, N. K. Noordin, S. M. Sait, K. A. Al-Utaibi, and F. Hashim, "6G Wireless Communications Networks: A Comprehensive Survey," *IEEE Access*, vol. 9, pp. 148191–148243, 2021.

[2] M. Morelli, C.-C. J. Kuo, and M.-O. Pun, "Synchronization techniques for orthogonal frequency division multiple access (ofdma): A tutorial review," *Proceedings of the IEEE*, vol. 95, no. 7, pp. 1394–1427, 2007.

[3] F. Schaich, T. Wild, and Y. Chen, "Waveform Contenders for 5G - Suitability for Short Packet and Low Latency Transmissions," in *2014 IEEE 79th Vehicular Technology Conference (VTC Spring)*, pp. 1–5, 2014.

[4] 3GPP TS 38.101:, "NR: User Equipment (UE) radio transmission and reception part1," tech. rep.

[5] E. Dahlman, S. Parkvall, and J. Skold, *4G, LTE-advanced Pro and the Road to 5G*. Academic Press, 2016.

[6] J. S. Erik Dahlman, Stefan Parkvall and P. Beming, *3G EVOLUTION : HSPA AND LTE FOR MOBILE BROADBAND*. Burlington: Academic Press is an imprint of Elsevier, second ed., 2008.

[7] 3GPP TR 25.892v6.0.0, "Feasibility Study for Orthogonal Frequency Division Multiplexing (OFDM) for UTRAN enhancement (Release 6)," tech. rep., 2004.

[8] 3GPP TS 36.211 V8.2.0, "LTE; Evolved Universal Terrestrial Radio Access (E-UTRA); Physical channels and modulation," tech. rep., March 2008.

[9] ETSI TS 136 300 V8.12.0:, " LTE; Evolved Universal Terrestrial Radio Access (E-UTRA) and Evolved Universal Terrestrial Radio Access Network (E-UTRAN); Overall description," tech. rep., 2010.

[10] C.-X. Wang, F. Haider, X. Gao, X.-H. You, Y. Yang, D. Yuan, H. M. Aggoune, H. Haas, S. Fletcher, and E. Hepsaydir, "Cellular architecture and key technologies for 5G wireless communication networks," *IEEE Communications Magazine*, vol. 52, no. 2, pp. 122–130, 2014.

[11] L. Chettri and R. Bera, "A Comprehensive Survey on Internet of Things (IoT) Toward 5G Wireless Systems," *IEEE Internet of Things Journal*, vol. 7, no. 1, pp. 16–32, 2020.

[12] X. Lin, J. Li, R. Baldemair, J.-F. T. Cheng, S. Parkvall, D. C. Larsson, H. Koorapaty, M. Frenne, S. Falahati, A. Grovlen, and K. Werner, "5G New Radio: Unveiling the Essentials of the Next Generation Wireless Access Technology," *IEEE Communications Standards Magazine*, vol. 3, no. 3, pp. 30–37, 2019.

[13] 3GPP TR 36.913 v9.0.0, " Requirements for further advancements for Evolved Universal Terrestrial Radio Access (E-UTRA) (LTE-Advanced) (Release 9)," tech. rep., 2010.

[14] M. Benisha, R. Prabu, and V. Bai, "Requirements and challenges of 5g cellular systems," in *2016 2nd International Conference on Advances in Electrical, Electronics, Information, Communication and Bio-Informatics (AEEICB)*, pp. 251–254, 2016.

[15] 3GPP TS 38.211:, "5G NR; Physical Channels and Modulation Release 15," tech. rep.

[16] A. Ghosh, A. Maeder, M. Baker, and D. Chandramouli, "5G Evolution: A View on 5G Cellular Technology Beyond 3GPP Release 15," *IEEE Access*, vol. 7, pp. 127639–127651, 2019.

[17] X. Lin, "An Overview of 5G Advanced Evolution in 3GPP Release 18," *IEEE Communications Standards Magazine*, vol. 6, no. 3, pp. 77–83,

2022.

[18] 3GPP TR 21.917:, "Technical Specification Group Services and System Aspects; Release 17 Description; Summary of Rel-17 Work Items (Release 17) ," tech. rep.

[19] L. U. Khan, I. Yaqoob, M. Imran, Z. Han, and C. S. Hong, "6G Wireless Systems: A Vision, Architectural Elements, and Future Directions," *IEEE Access*, vol. 8, pp. 147029–147044, 2020.

[20] X. You, C.-X. Wang, J. Huang, X. Gao, Z. Zhang, M. Wang, Y. Huang, C. Zhang, Y. Jiang, J. Wang, *et al.*, "Towards 6G wireless communication networks: Vision, enabling technologies, and new paradigm shifts," *Science China Information Sciences*, vol. 64, no. 1, pp. 1–74, 2021.

[21] C. Zhang, Y.-L. Ueng, C. Studer, and A. Burg, "Artificial Intelligence for 5G and Beyond 5G: Implementations, Algorithms, and Optimizations," *IEEE Journal on Emerging and Selected Topics in Circuits and Systems*, vol. 10, no. 2, pp. 149–163, 2020.

[22] T. S. Rappaport, S. Sun, R. Mayzus, H. Zhao, Y. Azar, K. Wang, G. N. Wong, J. K. Schulz, M. Samimi, and F. Gutierrez, "Millimeter Wave Mobile Communications for 5G Cellular: It Will Work!," *IEEE Access*, vol. 1, pp. 335–349, 2013.

[23] T. S. Rappaport, Y. Xing, G. R. MacCartney, A. F. Molisch, E. Mellios, and J. Zhang, "Overview of Millimeter Wave Communications for Fifth-Generation (5G) Wireless Networks—With a Focus on Propagation Models," *IEEE Transactions on Antennas and Propagation*, vol. 65, no. 12, pp. 6213–6230, 2017.

[24] C. Dehos, J. L. González, A. De Domenico, D. Kténas, and L. Dussopt, "Millimeter-wave access and backhauling: the solution to the exponential data traffic increase in 5G mobile communications systems?," *IEEE Communications Magazine*, vol. 52, no. 9, pp. 88–95, 2014.

[25] T. S. Rappaport, J. N. Murdock, and F. Gutierrez, "State of the Art in 60-GHz Integrated Circuits and Systems for Wireless Communications," *Proceedings of the IEEE*, vol. 99, no. 8, pp. 1390–1436, 2011.

[26] D. Brake, "A US national strategy for 5G and future wireless innovation," tech. rep., Information Technology and Innovation Foundation, 2020.

[27] X. Zhang, L. Chen, J. Qiu, and J. Abdoli, "On the Waveform for 5G," *IEEE Communications Magazine*, vol. 54, no. 11, pp. 74–80, 2016.

[28] Y. Liu, X. Chen, Z. Zhong, B. Ai, D. Miao, Z. Zhao, J. Sun, Y. Teng, and H. Guan, "Waveform Design for 5G Networks: Analysis and Comparison," *IEEE Access*, vol. 5, pp. 19282–19292, 2017.

[29] M. Elkourdi, B. Peköz, E. Güvenkaya, and H. Arslan, "Waveform design principles for 5G and beyond," in *2016 IEEE 17th Annual Wireless and Microwave Technology Conference (WAMICON)*, pp. 1–6, 2016.

[30] S.-Y. Lien, S.-L. Shieh, Y. Huang, B. Su, Y.-L. Hsu, and H.-Y. Wei, "5G New Radio: Waveform, Frame Structure, Multiple Access, and Initial Access," *IEEE Communications Magazine*, vol. 55, no. 6, pp. 64–71, 2017.

[31] T. Hwang, C. Yang, G. Wu, S. Li, and G. Ye Li, "OFDM and Its Wireless Applications: A Survey," *IEEE Transactions on Vehicular Technology*, vol. 58, no. 4, pp. 1673–1694, 2009.

[32] G. P. Fettweis, M. Krondorf, and S. Bittner, "GFDM - Generalized Frequency Division Multiplexing," *VTC Spring 2009 - IEEE 69th Vehicular Technology Conference*, pp. 1–4, 2009.

[33] N. Michailow, M. Matthé, I. S. Gaspar, A. N. Caldevilla, L. L. Mendes, A. Festag, and G. Fettweis, "Generalized Frequency Division Multiplexing for 5th Generation Cellular Networks," *IEEE Transactions on Communications*, vol. 62, no. 9, pp. 3045–3061, 2014.

[34] G. Wunder, M. Kasparick, T. Wild, F. Schaich, Y. Chen, M. Dryjanski, M. Buczkowski, S. Pietrzyk, N. Michailow, M. Matthé, I. Gaspar, L. Mendes, A. Festag, G. Fettweis, J.-B. Doré, N. Cassiau, D. Kténas, V. Berg, B. Eged, and P. Vago, "5GNOW: Intermediate frame structure and transceiver concepts," in *2014 IEEE Globecom Workshops (GC Wkshps)*, pp. 565–570, 2014.

[35] B. Farhang-Boroujeny, "OFDM Versus Filter Bank Multicarrier," *IEEE Signal Processing Magazine*, vol. 28, no. 3, pp. 92–112, 2011.

[36] B. Farhang-Boroujeny, "Filter bank multicarrier modulation: A waveform candidate for 5G and beyond," *Advances in Electrical Engineering*, vol. 2014, 2014.

[37] R. Nissel, S. Schwarz, and M. Rupp, "Filter Bank Multicarrier Modulation Schemes for Future Mobile Communications," *IEEE Journal on Selected Areas in Communications*, vol. 35, no. 8, pp. 1768–1782, 2017.

[38] V. Vakilian, T. Wild, F. Schaich, S. ten Brink, and J.-F. Frigon, "Universal-filtered multi-carrier technique for wireless systems beyond LTE," in *2013 IEEE Globecom Workshops (GC Wkshps)*, pp. 223–228, 2013.

[39] F. Schaich and T. Wild, "Waveform contenders for 5G — OFDM vs. FBMC vs. UFMC," in *2014 6th International Symposium on Communications, Control and Signal Processing (ISCCSP)*, pp. 457–460, 2014.

[40] L. Zhang, A. Ijaz, P. Xiao, M. M. Molu, and R. Tafazolli, "Filtered OFDM Systems, Algorithms, and Performance Analysis for 5G and Beyond," *IEEE Transactions on Communications*, vol. 66, no. 3, pp. 1205–1218, 2018.

[41] T. Wild and F. Schaich, "A Reduced Complexity Transmitter for UF-OFDM," in *2015 IEEE 81st Vehicular Technology Conference (VTC*

Spring), pp. 1–6, 2015.

[42] M. Matthe, D. Zhang, F. Schaich, T. Wild, R. Ahmed, and G. Fettweis, "A Reduced Complexity Time-Domain Transmitter for UF-OFDM," in *2016 IEEE 83rd Vehicular Technology Conference (VTC Spring)*, pp. 1–5, 2016.

[43] A. R. Jafri, J. Majid, M. A. Shami, M. A. Imran, and M. Najam-Ul-Islam, "Hardware Complexity Reduction in Universal Filtered Multicarrier Transmitter Implementation," *IEEE Access*, vol. 5, pp. 13401–13408, 2017.

[44] K. Cain, V. Vakilian, and R. Abdolee, "Low-Complexity Universal-Filtered Multi-Carrier for Beyond 5G Wireless Systems," in *2018 International Conference on Computing, Networking and Communications (ICNC)*, pp. 254–258, 2018.

[45] M. Saad, A. Al-Ghouwayel, and H. Hijazi, "UFMC Transceiver Complexity Reduction," in *2018 25th International Conference on Telecommunications (ICT)*, pp. 295–301, 2018.

[46] Z. Guo, Q. Liu, W. Zhang, and S. Wang, "Low Complexity Implementation of Universal Filtered Multi-Carrier Transmitter," *IEEE Access*, vol. 8, pp. 24799–24807, 2020.

[47] V. Kumar, M. Mukherjee, and J. Lloret, "Reconfigurable Architecture of UFMC Transmitter for 5G and Its FPGA Prototype," *IEEE Systems Journal*, vol. 14, no. 1, pp. 28–38, 2020.

[48] M. Wu, J. Dang, Z. Zhang, and L. Wu, "An Advanced Receiver for Universal Filtered Multicarrier," *IEEE Transactions on Vehicular Technology*, vol. 67, no. 8, pp. 7779–7783, 2018.

[49] C.-H. Yih, "BER Analysis of OFDM Systems Impaired by DC Offset and Carrier Frequency Offset in Multipath Fading Channels," *IEEE Communications Letters*, vol. 11, no. 11, pp. 842–844, 2007.

117

[50] L. Weng, E. K. Au, P. W. C. Chan, R. D. Murch, R. S. Cheng, W. H. Mow, and V. K. Lau, "Effect of Carrier Frequency Offset on Channel Estimation for SISO/MIMO-OFDM Systems," *IEEE Transactions on Wireless Communications*, vol. 6, no. 5, pp. 1854–1863, 2007.

[51] A. Aminjavaheri, A. Farhang, A. RezazadehReyhani, and B. Farhang-Boroujeny, "Impact of timing and frequency offsets on multicarrier waveform candidates for 5G," in *2015 IEEE Signal Processing and Signal Processing Education Workshop (SP/SPE)*, pp. 178–183, 2015.

[52] X. Wang, T. Wild, and F. Schaich, "Filter Optimization for Carrier-Frequency- and Timing-Offset in Universal Filtered Multi-Carrier Systems," in *2015 IEEE 81st Vehicular Technology Conference (VTC Spring)*, pp. 1–6, 2015.

[53] P. Moose, "A technique for orthogonal frequency division multiplexing frequency offset correction," *IEEE Transactions on Communications*, vol. 42, no. 10, pp. 2908–2914, 1994.

[54] T. Schmidl and D. Cox, "Robust frequency and timing synchronization for OFDM," *IEEE Transactions on Communications*, vol. 45, no. 12, pp. 1613–1621, 1997.

[55] M. Morelli and U. Mengali, "An improved frequency offset estimator for OFDM applications," *IEEE Communications Letters*, vol. 3, no. 3, pp. 75–77, 1999.

[56] Z. Zhang, W. Jiang, H. Zhou, Y. Liu, and J. Gao, "High accuracy frequency offset correction with adjustable acquisition range in ofdm systems," *IEEE Transactions on Wireless Communications*, vol. 4, no. 1, pp. 228–237, 2005.

[57] C. Yan, S. Li, Y. Tang, X. Luo, and J. Fang, "A novel frequency offset estimation method for OFDM systems with large estimation range," *IEEE Transactions on Broadcasting*, vol. 52, no. 1, pp. 58–61, 2006.

[58] G. Ren, Y. Chang, H. Zhang, and H. Zhang, "An Efficient Frequency Offset Estimation Method With a Large Range for Wireless OFDM Systems," *IEEE Transactions on Vehicular Technology*, vol. 56, no. 4, pp. 1892–1895, 2007.

[59] J. Yu and Y. Su, "Pilot-assisted maximum-likelihood frequency-offset estimation for OFDM systems," *IEEE Transactions on Communications*, vol. 52, no. 11, pp. 1997–2008, 2004.

[60] P. Sun and L. Zhang, "Low complexity pilot aided frequency synchronization for OFDMA uplink transmission," *IEEE Transactions on Wireless Communications*, vol. 8, no. 7, pp. 3758–3769, 2009.

[61] P. Muneer and S. M. Sameer, "Iterative Joint Carrier Frequency Offset and Doubly Selective Channel Estimation in High-Mobility MIMO-OFDMA Uplink Using Oblique Projection," *IEEE Transactions on Vehicular Technology*, vol. 65, no. 9, pp. 7110–7121, 2016.

[62] D. Huang and K. Letaief, "Enhanced carrier frequency offset estimation for OFDM using channel side information," *IEEE Transactions on Wireless Communications*, vol. 5, no. 10, pp. 2784–2793, 2006.

[63] J. van de Beek, M. Sandell, and P. Borjesson, "ML estimation of time and frequency offset in OFDM systems," *IEEE Transactions on Signal Processing*, vol. 45, no. 7, pp. 1800–1805, 1997.

[64] T.-C. Lin and S.-M. Phoong, "A New Cyclic-Prefix Based Algorithm for Blind CFO Estimation in OFDM Systems," *IEEE Transactions on Wireless Communications*, vol. 15, no. 6, pp. 3995–4008, 2016.

[65] H. Liu and U. Tureli, "A high-efficiency carrier estimator for OFDM communications," *IEEE Communications Letters*, vol. 2, no. 4, pp. 104–106, 1998.

[66] U. Tureli, H. Liu, and M. Zoltowski, "OFDM blind carrier offset estimation: ESPRIT," *IEEE Transactions on Communications*, vol. 48, no. 9, pp. 1459–1461, 2000.

[67] R. Roy, A. Paulraj, and T. Kailath, "ESPRIT–A subspace rotation approach to estimation of parameters of cisoids in noise," *IEEE Transactions on Acoustics, Speech, and Signal Processing*, vol. 34, no. 5, pp. 1340–1342, 1986.

[68] T. Roman, S. Visuri, and V. Koivunen, "Blind Frequency Synchronization in OFDM via Diagonality Criterion], year=2006, volume=54, number=8, pages=3125-3135, doi=10.1109/TSP.2006.877636," *IEEE Transactions on Signal Processing*.

[69] H.-G. Jeon, K.-S. Kim, and E. Serpedin, "An Efficient Blind Deterministic Frequency Offset Estimator for OFDM Systems," *IEEE Transactions on Communications*, vol. 59, no. 4, pp. 1133–1141, 2011.

[70] Y. Yao and G. Giannakis, "Blind carrier frequency offset estimation in SISO, MIMO, and multiuser OFDM systems," *IEEE Transactions on Communications*, vol. 53, no. 1, pp. 173–183, 2005.

[71] W. Zhang, Q. Yin, and F. Gao, "Computationally Efficient Blind Estimation of Carrier Frequency Offset for MIMO-OFDM Systems," *IEEE Transactions on Wireless Communications*, vol. 15, no. 11, pp. 7644–7656, 2016.

[72] X. Ma, C. Tepedelenlioglu, G. Giannakis, and S. Barbarossa, "Non-data-aided carrier offset estimators for OFDM with null subcarriers: identifiability, algorithms, and performance," *IEEE Journal on Selected Areas in Communications*, vol. 19, no. 12, pp. 2504–2515, 2001.

[73] D. Huang and K. Letaief, "Carrier frequency offset estimation for OFDM systems using null subcarriers," *IEEE Transactions on Communications*, vol. 54, no. 5, pp. 813–823, 2006.

[74] X. Wang, T. Wild, F. Schaich, and S. ten Brink, "Pilot-aided channel estimation for universal filtered multi-carrier," in *2015 IEEE 82nd Vehicular Technology Conference (VTC2015-Fall)*, pp. 1–5, 2015.

[75] Y. Li, B. Tian, K. Yi, and Q. Yu, "A Novel Hybrid CFO Estimation Scheme for UFMC-Based Systems," *IEEE Communications Letters*, vol. 21, no. 6, pp. 1337–1340, 2017.

[76] Q. Liu and G. Kai, "An Effective Preamble-based CFO Synchronization for UFMC Systems," in *2018 10th International Conference on Communications, Circuits and Systems (ICCCAS)*, pp. 484–488, 2018.

[77] T. Chen and T. Lin, "Low-complexity carrier frequency offset estimation for UFMC systems," *Electronics Letters*, vol. 55, no. 14, pp. 819–821, 2019.

[78] T.-T. Lin and F.-H. Hwang, "Design of a Blind Estimation Technique of Carrier Frequency Offset for a Universal-Filtered Multi-Carrier System Over Rayleigh Fading," *IEEE Wireless Communications Letters*, vol. 11, no. 5, pp. 1027–1031, 2022.

[79] T.-T. Lin and F.-H. Hwang, "Blind CFO Estimation in a UFMC System Aided With Virtual Carriers," *IEEE Transactions on Vehicular Technology*, vol. 71, no. 4, pp. 4495–4499, 2022.

[80] P. Hoeher and F. Tufvesson, "Channel estimation with superimposed pilot sequence," in *Seamless Interconnection for Universal Services. Global Telecommunications Conference. GLOBECOM'99. (Cat. No.99CH37042)*, vol. 4, pp. 2162–2166 vol.4, 1999.

[81] J. Tugnait and W. Luo, "On channel estimation using superimposed training and first-order statistics," *IEEE Communications Letters*, vol. 7, no. 9, pp. 413–415, 2003.

[82] M. Ghogho, D. McLernon, E. Alameda-Hernandez, and A. Swami, "Channel estimation and symbol detection for block transmission using data-dependent superimposed training," *IEEE Signal Processing Letters*, vol. 12, no. 3, pp. 226–229, 2005.

[83] J. Tugnait and X. Meng, "On superimposed training for channel estimation: performance analysis, training power allocation, and frame

synchronization," *IEEE Transactions on Signal Processing*, vol. 54, no. 2, pp. 752–765, 2006.

[84] A. T. Asyhari and S. ten Brink, "Orthogonal or Superimposed Pilots? A Rate-Efficient Channel Estimation Strategy for Stationary MIMO Fading Channels," *IEEE Transactions on Wireless Communications*, vol. 16, no. 5, pp. 2776–2789, 2017.

[85] J. W. Cooley and J. W. Tukey, "An algorithm for the machine calculation of complex Fourier series," *Mathematics of computation*, vol. 19, no. 90, pp. 297–301, 1965.

[86] P. Duhamel and H. Hollmann, "Split radix'FFT algorithm," *Electronics letters*, vol. 20, no. 1, pp. 14–16, 1984.

[87] C.-H. Yang, T.-H. Yu, and D. Markovic, "Power and area minimization of reconfigurable fft processors: A 3gpp-lte example," *IEEE Journal of Solid-State Circuits*, vol. 47, no. 3, pp. 757–768, 2012.

[88] L. Zhang, A. Ijaz, P. Xiao, and R. Tafazolli, "Multi-service system: An enabler of flexible 5G air interface," *IEEE Communications Magazine*, vol. 55, no. 10, pp. 152–159, 2017.

[89] L. Zhang, A. Ijaz, P. Xiao, A. Quddus, and R. Tafazolli, "Subband Filtered Multi-Carrier Systems for Multi-Service Wireless Communications," *IEEE Transactions on Wireless Communications*, vol. 16, no. 3, pp. 1893–1907, 2017.

[90] M. Mukherjee, L. Shu, V. Kumar, P. Kumar, and R. Matam, "Reduced out-of-band radiation-based filter optimization for UFMC systems in 5G," in *2015 International Wireless Communications and Mobile Computing Conference (IWCMC)*, pp. 1150–1155, 2015.

[91] Z. Zhang, H. Wang, G. Yu, Y. Zhang, and X. Wang, "Universal filtered multi-carrier transmission with adaptive active interference cancellation," *IEEE Transactions on Communications*, vol. 65, no. 6, pp. 2554–2567, 2017.

[92] L. Zhang, A. Ijaz, P. Xiao, K. Wang, D. Qiao, and M. A. Imran, "Optimal filter length and zero padding length design for universal filtered multi-carrier (ufmc) system," *IEEE Access*, vol. 7, pp. 21687–21701, 2019.

[93] X. Wang, T. Wild, and F. Schaich, "Filter optimization for carrier-frequency- and timing-offset in universal filtered multi-carrier systems," in *2015 IEEE 81st Vehicular Technology Conference (VTC Spring)*, pp. 1–6, 2015.

[94] X. Chen, L. Wu, Z. Zhang, J. Dang, and J. Wang, "Adaptive modulation and filter configuration in universal filtered multi-carrier systems," *IEEE Transactions on Wireless Communications*, vol. 17, no. 3, pp. 1869–1881, 2018.

[95] L. R. Rabiner, J. H. McClellan, and T. W. Parks, "FIR digital filter design techniques using weighted Chebyshev approximation," *Proceedings of the IEEE*, vol. 63, no. 4, pp. 595–610, 1975.

[96] A. Omri, M. Shaqfeh, A. Ali, and H. Alnuweiri, "Synchronization Procedure in 5G NR Systems," *IEEE Access*, vol. 7, pp. 41286–41295, 2019.

[97] R. K. V. Nithya, C. P. Najlah, and S. M. Sameer, "Bit error probability analysis of ufmc systems with carrier frequency offset," in *TENCON 2019 - 2019 IEEE Region 10 Conference (TENCON)*, pp. 841–845, 2019.

[98] C.-P. Li and W.-W. Hu, "Super-Imposed Training Scheme for Timing and Frequency Synchronization in OFDM Systems," *IEEE Transactions on Broadcasting*, vol. 53, no. 2, pp. 574–583, 2007.

[99] J. Nair, "Improved superimposed training-based channel estimation method for closed-loop multiple input multiple output orthogonal frequency division multiplexing systems," *IET Communications*, vol. 5, pp. 209–221(12), January 2011.

[100] M. Rajarao, R. V. R. Kumar, D. Madhuri, and M. Latha, "Efficient channel estimation technique for lte air interface," in *2012 Asia Pacific Conference on Postgraduate Research in Microelectronics and Electronics*, pp. 214–219, 2012.

[101] B. Popovic, "Generalized chirp-like polyphase sequences with optimum correlation properties," *IEEE Transactions on Information Theory*, vol. 38, no. 4, pp. 1406–1409, 1992.

[102] J. Tao and L. Yang, "Improved Zadoff-Chu Sequence Detection in the Presence of Unknown Multipath and Carrier Frequency Offset," *IEEE Communications Letters*, vol. 22, no. 5, pp. 922–925, 2018.

[103] N. Chen and G. Zhou, "Superimposed training for OFDM: a peak-to-average power ratio analysis," *Signal Processing, IEEE Transactions on*, vol. 54, pp. 2277 – 2287, june 2006.

[104] Theodore S. Rappaport, *Wireless Communications: Principles and practice*. Prentice Hall PTR, second ed., 1996.

[105] Recommendation, "ITU-R M.1225, Guidelines for the evaluation of radio transmission technologies for IMT-2000," 1997.

[106] T. Sorensen, P. Mogensen, and F. Frederiksen, "Extension of the ITU channel models for wideband (OFDM) systems," in *Vehicular Technology Conference, 2005. VTC-2005-Fall. 2005 IEEE 62nd*, vol. 1, pp. 392 – 396, sept., 2005.

[107] M. K. C. J. D. C. V.Erceg, K.Hari, "Channel Models for Fixed Wireless Applications: IEEE 802.16 Broadband Wireless Access Working Group," July 2001.

[108] 3GPP TR 38.901, "5G; Study on channel model for frequencies from 0.5 to 100 GHz," tech. rep., 2018.

Publications from this Thesis

Journals

1. R. Manda, A. Kumar, R. Gowri, "Optimal Filter Length Selection for Universal Filtered Multicarrier Systems", International Journal of Engineering, Transactions A: Basics, Vol. 36, No. 07, (2023), 1322-1330, doi: 10.5829/ije.2023.36.07a.13 (**Published- Scopus Indexed**)

2. R. Manda, R. Gowri, "Universal Filtered Multicarrier Receiver Complexity Reduction to Orthogonal Frequency Division Multiplexing Receiver", International Journal of Engineering, Transactions A: Basics, Vol. 35, No. 04, (2022) 725-731. doi: 10.5829/ije.2022.35.04a.12, Online link: https://www.ije.ir/article_143048.html (**Published- Scopus Indexed**)

3. R. Manda, R. Gowri, "Interference Analysis in the Multi-Service Universal Filtered Multi-carrier Systems", Tianjin Daxue Xuebao (Ziran Kexue yu Gongcheng Jishu Ban)/ Journal of Tianjin University Science and Technology, vol.55 (4), pp. 651-664,2022. DOI:10.17605/OSF.IO/EKDVH, Online link: https://tianjindaxuexuebao.com/details.php?id=DOI:10.17605/OSF.IO/EKDVH (**Published- Scopus Indexed**)

4. R. Manda, A. Kumar, R. Gowri, "Computational complexity for simplified Universal Filtered Multicarrier (UFMC) wireless transmitter", National Academy Science Letters. (**under review- SCI Indexed**)

5. R. Manda, A. Kumar, R. Gowri, "An efficient Carrier Frequency Offset Estimation in UFMC-based wireless systems", Multimedia Tools and Applications (**Under review- SCI indexed**)

Conferences

1. Manda R., Gowri R. (2020) "A Method to Reduce the Effect of Inter-Sub-band Interference (ISBI) and Inter Carrier Interference (ICI) in UFMC", Intelligent Communication, Control and Devices. Advances in Intelligent Systems and Computing, vol 989. Springer, Singapore, DOI: https://doi.org/10.1007/978-981-13-8618-3_97 **(Scopus Indexed)**

2. R. Manda and R. Gowri, "Filter Design for Universal Filtered Multicarrier (UFMC) based Systems," 2019 4th International Conference on Information Systems and Computer Networks (ISCON), Mathura, India, 2019, pp. 520-523, doi: 10.1109/ISCON47742.2019.9036268. **(IEEE-Scopus Indexed)**

Author's Curriculum Vitae

Rajarao Manda is a part-time Ph.D. candidate from Department of Electrical and Electronics Engineering, School of Advanced Engineering, UPES, Dehradun. He completed his M.Tech. degree in Telecommunications System Engineering from Indian Institute of Technology Kharagpur during 2008-2010 and completed B.Tech. degree in Electronics and Communication Engineering from Bapatla Engineering College during 2003-2007.

Contact Information

Permanent Address: 3-146B, P Gudipadu, Andhra Pradesh, PIN-523212, India.
Mobile: +91-8979803148
Email: rajaec6405@gmail.com

Research Interests

Modulation waveform techniques for next-generation Wireless communication networks, Digital signal processing in wireless communications, AI and ML in wireless networks

Technical Skills:

Programming Languages: C, C++
Simulation Tools: MATLAB, Python

Education

Doctor of Philosophy (PhD)*, Electrical and Electronics Engineering
University of Petroleum & Energy Studies, Dehradun, India
Dissertation title: An Efficient Carrier Frequency Offset Compensation

Technique using Superimposed Training Sequence for Next generation (5G) Wireless Networks

Master of Technology (M.Tech), Telecommunications System Engineering (2010)

Indian Institute of Technology Kharagpur (CGPA: 8.11)

Bachelor of Technology (B.Tech), Electronics and Communication Engineering   (2007)

Bapatla Engineering College (Percentage: 76.27)

12th (percentage: 80.00) from A.P.S.W.R.Jr College, Shaikpet, Andhra Pradesh, India.

10th (percentage: 86.67) from A.P.S.W.R.School,Velugonda, Andhra Pradesh, India.

Awards

- School First in 10th SSC Public Examination.

- "PRATHIBHA" award from AP Government, and "Best student" award from A.P.S.W.R Scocity in 2000

- **Secured 1100 rank** in Electronics and Communication engineering GATE 2010.

Teaching Experience

- Worked as faculty member in Dept. of Electronics and Communication Engineering, FST, ICFAI University, Dehradun, India from July 2010 to December 2015.

- Worked as Asst. Professor (Senior Scale) in Dept. Electronics Engineering, UPES, Dehradun, India from Jan 2016 to November 2022.

- Worked as an Adhoc Faculty in Dept. Electronics Engineering, National Institute of Technology Tadepalligudem, Andhra Pradesh, India from November 2022 to May 2023.

- Presently working as an Adhoc Faculty in Dept. Electronics Engineering, National Institute of Technology Tadepalligudem, Andhra Pradesh, India from Aug. 2023 to till date.

Rajarao_thesis_plg_report

PRIMARY SOURCES

1	www.researchgate.net Internet Source	1 %
2	web.archive.org Internet Source	<1 %
3	trepo.tuni.fi Internet Source	<1 %
4	pws.npru.ac.th Internet Source	<1 %
5	downloads.hindawi.com Internet Source	<1 %
6	eprints.gla.ac.uk Internet Source	<1 %
7	hdl.handle.net Internet Source	<1 %
8	aaltodoc.aalto.fi Internet Source	<1 %
9	dokumen.pub Internet Source	<1 %

10 tel.archives-ouvertes.fr
Internet Source
<1 %

11 Tomasz P. Zieliński. "Starting Digital Signal Processing in Telecommunication Engineering", Springer Science and Business Media LLC, 2021
Publication
<1 %

12 Guangliang Ren, Yilin Chang, Huining Zhang, Hui Zhang. "An Efficient Frequency Offset Estimation Method With a Large Range for Wireless OFDM Systems", IEEE Transactions on Vehicular Technology, 2007
Publication
<1 %

13 theses.gla.ac.uk
Internet Source
<1 %

14 Zhenjin Guo, Qiang Liu, Wei Zhang, Shilian Wang. "Low Complexity Implementation of Universal Filtered Multi-Carrier Transmitter", IEEE Access, 2020
Publication
<1 %

15 "Radio Access Network Slicing and Virtualization for 5G Vertical Industries", Wiley, 2021
Publication
<1 %

16 T.C. Chen, T.T. Lin. "Low-complexity carrier frequency offset estimation for UFMC systems", Electronics Letters, 2019
<1 %

17 Jeremy Nadal, Charbel Abdel Nour, Amer Baghdadi. "Novel UF-OFDM Transmitter: Significant Complexity Reduction Without Signal Approximation", IEEE Transactions on Vehicular Technology, 2018
Publication

<1%

18 Jinesh P. Nair, Ratnam V. Raja Kumar. "Optimal Superimposed Training Sequences for Channel Estimation in MIMO-OFDM Systems", EURASIP Journal on Advances in Signal Processing, 2010
Publication

<1%

19 hal.archives-ouvertes.fr
Internet Source

<1%

20 idoc.pub
Internet Source

<1%

21 vdoc.pub
Internet Source

<1%

22 www.politesi.polimi.it
Internet Source

<1%

23 D. Huang. "Carrier Frequency Offset Estimation for OFDM Systems Using Null Subcarriers", IEEE Transactions on Communications, 5/2006
Publication

<1%

24 Malik Muhammad Usman Gul, Xiaoli Ma, Sungeun Lee. "Timing and Frequency Synchronization for OFDM Downlink Transmissions Using Zadoff-Chu Sequences", IEEE Transactions on Wireless Communications, 2015
Publication

<1%

25 Xiao Chen, Liang Wu, Zaichen Zhang, Jian Dang, Jiangzhou Wang. "Adaptive Modulation and Filter Configuration in Universal Filtered Multi-Carrier Systems", IEEE Transactions on Wireless Communications, 2018
Publication

<1%

26 www.adb.org
Internet Source

<1%

27 "Communications, Signal Processing, and Systems", Springer Science and Business Media LLC, 2019
Publication

<1%

28 d-nb.info
Internet Source

<1%

29 kar.kent.ac.uk
Internet Source

<1%

30 livrepository.liverpool.ac.uk
Internet Source

<1%

31 Gerlind Plonka, Daniel Potts, Gabriele Steidl, Manfred Tasche. "Numerical Fourier Analysis", Springer Nature, 2018
Publication
<1%

32 nectar.northampton.ac.uk
Internet Source
<1%

33 Sameh A. Fathy, Michael Ibrahim, Salah El-Agooz, Hadia El-Hennawy. "Low-Complexity SLM PAPR Reduction Approach for UFMC Systems", IEEE Access, 2020
Publication
<1%

34 Ze-Nian Li, Mark S. Drew, Jiangchuan Liu. "Fundamentals of Multimedia", Springer Science and Business Media LLC, 2021
Publication
<1%

35 repozitorium.omikk.bme.hu
Internet Source
<1%

36 scholar.uwindsor.ca
Internet Source
<1%

37 C. Yan, S. Li, Y. Tang, X. Luo, J. Fang. "A Novel Frequency Offset Estimation Method for OFDM Systems With Large Estimation Range", IEEE Transactions on Broadcasting, 2006
Publication
<1%

38 Hong Wang, Zhaoyang Zhang, Yu Zhang, Chao Wang. "Universal filtered multi-carrier
<1%

transmission with active interference cancellation", 2015 International Conference on Wireless Communications & Signal Processing (WCSP), 2015
Publication

39   Mishal Al-Gharabally, Ali. F. Almutairi, A. Krishna.. "Performance Analysis of the Two-Piecewise Linear Companding Technique on Filtered-OFDM Systems", IEEE Access, 2021
Publication   <1%

40   de.slideshare.net
Internet Source   <1%

41   Korey Cain, Vida Vakilian, Reza Abdolee. "Low-Complexity Universal-Filtered Multi-Carrier for Beyond 5G Wireless Systems", 2018 International Conference on Computing, Networking and Communications (ICNC), 2018
Publication   <1%

42   Pengfei Sun, Li Zhang. "Low complexity pilot aided frequency synchronization for OFDMA uplink transmission", IEEE Transactions on Wireless Communications, 2009
Publication   <1%

43   Xiaoqiang Ma, H. Kobayashi, S.C. Schwartz. "Joint frequency offset and channel estimation for ofdm", GLOBECOM '03. IEEE Global Telecommunications Conference (IEEE Cat. No.03CH37489), 2003

Publication

44   arxiv.org
     Internet Source   <1%

45   id.scribd.com
     Internet Source   <1%

46   "2nd International Conference on 5G for
     Ubiquitous Connectivity", Springer Science   <1%
     and Business Media LLC, 2020
     Publication

47   "Cognitive Radio Oriented Wireless Networks",
     Springer Science and Business Media LLC,   <1%
     2018
     Publication

48   theses.ncl.ac.uk
     Internet Source   <1%

49   "Communications and Networking", Springer
     Science and Business Media LLC, 2020   <1%
     Publication

50   Submitted to Jawaharlal Nehru Technological
     University   <1%
     Student Paper

51   Shruthi Koratagere Anantha Kumar, Edward
     Oughton. "Techno-Economic Assessment of   <1%
     5G Infrastructure Sharing Business Models in
     Rural Areas", Institute of Electrical and
     Electronics Engineers (IEEE), 2022
     Publication

52 Wu Yan, S. Attallah, J.W.M. Bergmans. "Blind iterative carrier offset estimation for OFDM systems", Proceedings of the Eighth International Symposium on Signal Processing and Its Applications, 2005., 2005
Publication

<1 %

53 deepai.org
Internet Source

<1 %

54 depositonce.tu-berlin.de
Internet Source

<1 %

55 ebin.pub
Internet Source

<1 %

56 eprints.usm.my
Internet Source

<1 %

57 es.scribd.com
Internet Source

<1 %

58 hal.inria.fr
Internet Source

<1 %

59 spectrum.library.concordia.ca
Internet Source

<1 %

60 www.hasanbalik.com
Internet Source

<1 %

61 www.qucosa.de
Internet Source

<1 %

www.semanticscholar.org

62 Internet Source <1%

63 "Big Data and Smart Digital Environment", Springer Nature, 2019
Publication <1%

64 "Handbook of Cognitive Radio", Springer Science and Business Media LLC, 2019
Publication <1%

65 Submitted to Old Dominion University
Student Paper <1%

66 peng wei, Xiang-Gen Xia, Yue Xiao, Shaoqian Li. "Fast DGT Based Receivers for GFDM in Broadband Channels", IEEE Transactions on Communications, 2016
Publication <1%

67 tud.qucosa.de
Internet Source <1%

68 www.keysight.com
Internet Source <1%

69 Adarsh B. Narasimhamurthy, Mahesh K. Banavar, Cihan Tepedelenlioğlu. "OFDM Systems for Wireless Communications", Springer Science and Business Media LLC, 2010
Publication <1%

70   Sassan Ahmadi. "New Radio Access Physical Layer Aspects (Part 2)", Elsevier BV, 2019
Publication
   <1 %

71   "2011 International Conference in Electrics, Communication and Automatic Control Proceedings", Springer Science and Business Media LLC, 2012
Publication
   <1 %

72   Lei Zhang, Ayesha Ijaz, Pei Xiao, Rahim Tafazolli. "Multi-Service System: An Enabler of Flexible 5G Air Interface", IEEE Communications Magazine, 2017
Publication
   <1 %

73   Submitted to Staffordshire University
Student Paper
   <1 %

74   Tsui-Tsai Lin, Fuh-Hsin Hwang. "Design of a Blind Estimation Technique of Carrier Frequency Offset for a Universal-Filtered Multi-carrier System over Rayleigh Fading", IEEE Wireless Communications Letters, 2022
Publication
   <1 %

75   Vikas Kumar, Mithun Mukherjee, Jaime Lloret. "Reconfigurable Architecture of UFMC Transmitter for 5G and Its FPGA Prototype", IEEE Systems Journal, 2020
Publication
   <1 %

76   www.gcekjr.ac.in

Internet Source

<1 %

77 K.R. Rao, D.N. Kim, J.-J. Hwang. "Fast Fourier Transform - Algorithms and Applications", Springer Science and Business Media LLC, 2010
Publication

<1 %

78 Submitted to Metropolia Ammattikorkeakoulu
Student Paper

<1 %

79 Submitted to University of Newcastle upon Tyne
Student Paper

<1 %

80 creativecommons.org
Internet Source

<1 %

81 mafiadoc.com
Internet Source

<1 %

82 V. Boriakoff. "FFT computation with systolic arrays, a new architecture", IEEE Transactions on Circuits and Systems II: Analog and Digital Signal Processing, 1994
Publication

<1 %

83 www.ece.mcgill.ca
Internet Source

<1 %

84 www.yunzhan365.com
Internet Source

<1 %

85   **5gnow.eu**
Internet Source   <1 %

86   Al-Dweik, A., S. Younis, A. Hazmi, C.
Tsimenidis, and B. Sharif. "Efficient OFDM   <1 %
Symbol Timing Estimator Using Power
Difference Measurements", IEEE Transactions
on Vehicular Technology, 2012.
Publication

87   Jianhua Lu. "Reduced complexity carrier
frequency offset estimation for OFDM   <1 %
systems", 2004 IEEE Wireless Communications
and Networking Conference (IEEE Cat No
04TH8733), 2004
Publication

88   Qixun Zhang, Huiqing Sun, Zhiyong Feng, Hui
Gao, Wei Li. "Data-Aided Doppler Frequency   <1 %
Shift Estimation and Compensation for UAVs",
IEEE Internet of Things Journal, 2020
Publication

89   Shashank Tiwari, Sourav Chatterjee, Suvra
Sekhar Das. "Comparative analysis of   <1 %
waveforms for fifth generation mobile
networks", 2016 IEEE International
Conference on Advanced Networks and
Telecommunications Systems (ANTS), 2016
Publication

90 Young-Hwan You, Hyoung-Kyu Song. "Sequential Detection of Cyclic Prefix Mode, Sidelink Synchronization Signal, and Frequency Offset for LTE Device-to-Device Networks", IEEE Transactions on Industrial Informatics, 2021
Publication

<1 %

91 diglib.tugraz.at
Internet Source

<1 %

92 dspace.aus.edu:8443
Internet Source

<1 %

93 jwcn-eurasipjournals.springeropen.com
Internet Source

<1 %

94 mj emadi, Sha Hu, Hao Wang. "Precise Positioning: When OTFS Meets Distributed Cooperative Positioning", Institute of Electrical and Electronics Engineers (IEEE), 2023
Publication

<1 %

95 www.ericsson.com
Internet Source

<1 %

96 "Soft Computing and Signal Processing", Springer Nature, 2019
Publication

<1 %

97 Preksha Jain, Akhil Gupta, Neeraj Kumar. "A vision towards integrated 6G communication networks: Promising technologies,

architecture, and use-cases", Physical
Communication, 2022
Publication

98   Rajendran K V Nithya, C P Najlah, S M Sameer.
"Bit Error Probability Analysis of UFMC
Systems with Carrier Frequency Offset",
TENCON 2019 - 2019 IEEE Region 10
Conference (TENCON), 2019
Publication

                                                  <1 %

99   Rongkun Jiang, Zesong Fei, Shan Cao,
Chengbo Xue, Ming Zeng, Qingqing Tang,
Shiwei Ren. "Deep Learning-Aided Signal
Detection for Two-Stage Index Modulated
Universal Filtered Multi-Carrier Systems", IEEE
Transactions on Cognitive Communications
and Networking, 2022
Publication

                                                  <1 %

100   Said Lmai, Arnaud Bourre, Christophe Laot,
Sebastien Houcke. "An Efficient Blind
Estimation of Carrier Frequency Offset in
OFDM Systems", IEEE Transactions on
Vehicular Technology, 2014
Publication

                                                  <1 %

101   Yang, Shih-Jen, Yung-Yi Wang, and Wei-Wei
Chen. "A vector coding scheme with improved
spectral efficiency for OFDM with frequency
error", Journal of the Franklin Institute, 2016.
Publication

                                                  <1 %

102   Yang, Tiejun, and Lei Hu. "An improved frequency offset estimation algorithm for OFDM system", 2010 International Conference on Information Networking and Automation (ICINA), 2010.
Publication   <1 %

103   dspace.cc.tut.fi
Internet Source   <1 %

104   etd.aau.edu.et
Internet Source   <1 %

105   go.gale.com
Internet Source   <1 %

106   jungwon.comoj.com
Internet Source   <1 %

107   repo.pw.edu.pl
Internet Source   <1 %

108   repository.kulib.kyoto-u.ac.jp
Internet Source   <1 %

109   sarl.ece.gatech.edu
Internet Source   <1 %

110   usir.salford.ac.uk
Internet Source   <1 %

111   "5G New Radio", Wiley, 2020
Publication   <1 %

112 "Practical Guide to LTE - A, VoLTE and IoT", Wiley, 2018
Publication
<1%

113 5g-range.eu
Internet Source
<1%

114 Ahmed Hammoodi, Lukman Audah, Montadar Abas Taher. "Green Coexistence for 5G Waveform Candidates: A Review", IEEE Access, 2019
Publication
<1%

115 Anutusha Dogra, Rakesh Kumar Jha, Shubha Jain. "A Survey on beyond 5G network with the advent of 6G: Architecture and Emerging Technologies", IEEE Access, 2020
Publication
<1%

116 B. Ai, Z. Yang, C. Pan, J. Ge, Y. Wang, Z. Lu. "On the Synchronization Techniques for Wireless OFDM Systems", IEEE Transactions on Broadcasting, 2006
Publication
<1%

117 D. Huang, K.B. Letaief. "An Interference-Cancellation Scheme for Carrier Frequency Offsets Correction in OFDMA Systems", IEEE Transactions on Communications, 2005
Publication
<1%

118 H. Wang, Q. Yin, Y. Meng, K. Deng. "Adaptive Joint Estimation of Symbol Timing and Carrier
<1%

Frequency Offset for OFDM Systems", 2007
IEEE International Conference on
Communications, 2007
Publication

119 Hachim Azzahhafi, Moussa El Yahyaoui, Ali El
Moussati. "Performance Analysis of
Frequency Spreading FBMC in Mobile Radio
Channel", 2018 International Symposium on
Advanced Electrical and Communication
Technologies (ISAECT), 2018
Publication

<1%

120 Hamed Abdzadeh-Ziabari, Wei-Ping Zhu,
M.N.S. Swamy. "A Marginalized Particle
Filtering-Based Approach for Carrier
Frequency Offset and Doubly Selective
Channel Estimation in OFDM Systems", 2018
IEEE Canadian Conference on Electrical &
Computer Engineering (CCECE), 2018
Publication

<1%

121 Hmaied Shaiek, Rafik Zayani, Yahia Medjahdi,
Daniel Roviras. "Analytical analysis of SER for
beyond 5G post-OFDM Waveforms in
presence of High Power Amplifiers", IEEE
Access, 2019
Publication

<1%

122 Imadur Rahman, Sara Modarres Razavi, Olof
Liberg, Christian Hoymann et al. "5G Evolution
Toward 5G Advanced: An overview of 3GPP

<1%

releases 17 and 18", Ericsson Technology Review, 2021
Publication

123   Imran Baig, Umer Farooq, Najam Ul Hasan, Manaf Zghaibeh, Varun Jeoti. "A Multi-Carrier Waveform Design for 5G and beyond Communication Systems", Mathematics, 2020
Publication   <1 %

124   Ivo Bizon Franco de Almeida, Luciano Leonel Mendes, Joel J. P. C. Rodrigues, Mauro A. A. da Cruz. "5G Waveforms for IoT Applications", IEEE Communications Surveys & Tutorials, 2019
Publication   <1 %

125   Jiang, Yufei, Xu Zhu, Eng Gee Lim, Yi Huang, and Hai Lin. "Low-complexity frequency synchronization for ICA based semi-blind CoMP systems with ICI and phase rotation caused by multiple CFOs", 2014 IEEE International Conference on Communications (ICC), 2014.
Publication   <1 %

126   John Cosmas. "4. Towards Joint Communication and Sensing", Now Publishers, 2023
Publication   <1 %

127   Jose A. del Peral-Rosado, Jose A. Lopez-Salcedo, Sunwoo Kim, Gonzalo Seco-   <1 %

Granados. "Feasibility study of 5G-based localization for assisted driving", 2016 International Conference on Localization and GNSS (ICL-GNSS), 2016
Publication

128 Lu Miaomiao, A. Nallanathan, T.T. Tjhung. "Decoupled maximum likelihood blind carrier offset estimator for OFDM systems", IEEE 60th Vehicular Technology Conference, 2004. VTC2004-Fall. 2004, 2004
Publication

<1%

129 Malik Muhammad Usman Gul, Sungeun Lee, Xiaoli Ma. "Carrier frequency offset estimation for OFDMA uplink using null sub-carriers", Digital Signal Processing, 2014
Publication

<1%

130 Morteza Rajabzadeh, Mohammad Towliat, Seyyed Mohammad Javad Asgari Tabatabaee, Heidi Steendam. "Uplink transceiver design for coded GFDMA systems", Signal Processing, 2021
Publication

<1%

131 Nour Kousa, Mohamed El-Tarhuni. "Pilot-aided double-dwell frequency synchronization in OFDM systems", 2015 7th International Conference on Information Technology and Electrical Engineering (ICITEE), 2015
Publication

<1%

132 Qinjuan Zhang, Muqing Wu, Qilin Guo, Tingting Zhang, Rui Zhang. "Carrier frequency offset estimation based on data-dependent superimposed training for OFDM systems", 2012 19th International Conference on Telecommunications (ICT), 2012
Publication

<1 %

133 Rong Wang, Jingye Cai, Xiang Yu, Sirui Duan. "Compressive channel estimation for universal filtered multi-carrier system in high-speed scenarios", IET Communications, 2017
Publication

<1 %

134 Tewelgn Kebede, Yihenew Wondie, Johannes Steinbrunn, Hailu Belay Kassa, Kevin T. Kornegay. "Multi-Carrier Waveforms and Multiple Access Strategies in Wireless Networks: Performance, Applications, and Challenges", IEEE Access, 2022
Publication

<1 %

135 Tsui-Tsai Lin, Tung-Chou Chen, Fuh-Hsin Hwang. "Design of Universal Filtered Multicarrier Receivers with High Efficiency and Low Complexity for Cancelling Residual Carrier Frequency Offset", Journal of Communications Technology and Electronics, 2022
Publication

<1 %

136 Xiaohu You, Cheng-Xiang Wang, Jie Huang, Xiqi Gao et al. "Towards 6G wireless communication networks: vision, enabling technologies, and new paradigm shifts", Science China Information Sciences, 2020
Publication

<1 %

137 Yinsheng Liu, Xia Chen, Zhangdui Zhong, Bo Ai, Deshan Miao, Zhuyan Zhao, Jingyuan Sun, Yong Teng, Hao Guan. "Waveform Design for 5G Networks: Analysis and Comparison", IEEE Access, 2017
Publication

<1 %

138 Yufei Jiang, , Xu Zhu, Eng Gee Lim, Hai Lin, and Yi Huang. "Semi-blind MIMO OFDM systems with precoding aided CFO estimation and ICA based equalization", 2013 IEEE Global Communications Conference (GLOBECOM), 2013.
Publication

<1 %

139 acikbilim.yok.gov.tr
Internet Source

<1 %

140 archive.org
Internet Source

<1 %

141 biblio.univ-annaba.dz
Internet Source

<1 %

142 digitalcommons.du.edu
Internet Source

<1 %

143 discovery.ucl.ac.uk
Internet Source
<1%

144 doku.pub
Internet Source
<1%

145 doras.dcu.ie
Internet Source
<1%

146 dr.ntu.edu.sg
Internet Source
<1%

147 dro.dur.ac.uk
Internet Source
<1%

148 ds.amu.edu.et
Internet Source
<1%

149 dspace.library.uvic.ca:8080
Internet Source
<1%

150 e-archivo.uc3m.es
Internet Source
<1%

151 eprints.soton.ac.uk
Internet Source
<1%

152 era.library.ualberta.ca
Internet Source
<1%

153 escholarship.org
Internet Source
<1%

154 espace.inrs.ca
Internet Source
<1%

155 etheses.whiterose.ac.uk
Internet Source
<1 %

156 export.arxiv.org
Internet Source
<1 %

157 lib.tkk.fi
Internet Source
<1 %

158 opus4.kobv.de
Internet Source
<1 %

159 publications.aston.ac.uk
Internet Source
<1 %

160 pure.manchester.ac.uk
Internet Source
<1 %

161 s3.eu-central-1.amazonaws.com
Internet Source
<1 %

162 smartech.gatech.edu
Internet Source
<1 %

163 sun.ti.rwth-aachen.de
Internet Source
<1 %

164 theses.eurasip.org
Internet Source
<1 %

165 theses.hal.science
Internet Source
<1 %

166 wnt.sjtu.edu.cn
Internet Source
<1 %

167	www.anchor-publishing.com Internet Source	<1 %
168	www.coursehero.com Internet Source	<1 %
169	www.freepatentsonline.com Internet Source	<1 %
170	www.itu.int Internet Source	<1 %
171	www.scilit.net Internet Source	<1 %
172	www.scribd.com Internet Source	<1 %

Exclude quotes   On   Exclude matches   < 8 words
Exclude bibliography On